# Catalytic Activation of Alkanes on Noble Metal-loaded Zeolites: Experimental Studies and Simulation of the Dehydroalkylation of Toluene with Ethane

Von der Fakultät Energie-, Verfahrens- und Biotechnik der Universität Stuttgart
genehmigte Abhandlung zur Erlangung des akademischen
Grads eines Doktor-Ingenieurs (Dr.-Ing.)

Vorgelegt von

Alireza Rezai

aus Teheran

| | |
|---|---|
| Hauptberichter: | Prof. Dr.-Ing. Jens Weitkamp |
| Mitberichter: | Prof. Dr.-Ing. Ulrich Nieken |

Tag der mündlichen Prüfung: 02.04.2012

Institut für Technische Chemie der Universität Stuttgart

2012

*Dedicated to my loving mother*

# Acknowledgements

The Ph.D. work presented in this thesis was carried out at the Institute of Chemical Technology, University of Stuttgart, from September 2005 to March 2008.

I would like to express my thanks to Prof. Dr.-Ing. Ulrich Nieken for examining my thesis. I would also like to thank Prof. Dr.-Ing. Jens Weitkamp for his support and insightful advice. The many opportunities he presented to me are appreciated. I would like to thank the Deutscher Akademischer Austauschdienst for financial support and Michael Baumgardt for his support.

I would like to thank Dr. Yvonne Traa for help and giving me so much of her time, but also for her direction and critical approach during the course of my work. I am thankful to Prof. Klaus Möller for his long-distance help regarding the finer points of FORTRAN. Dr. Frank Bauer is acknowledged for his co-operation on mechanistic studies. I would also like to acknowledge Ute Albrecht, Ingo Nägele, Barbara Gehring, Heike Fingerle, Andreas Stieber, and Walter Röhm for help with administrative matters, broken apparatus, and characterization of my catalyst. Dirk Singer, Bongani Mtombeni, Jasper Dick, Senzo Xulu, Nicole Weiß and Ines Kley are acknowledged for their help with experimental and modeling work. Special thanks go to Dr. Daniela Pufky-Heinrich and Elena Stefanova for proofreading my thesis.

I would like to thank Prof. Dr. Michael Hunger, Dr. Yijiao Jiang, Jun Huang, and especially Reddy Marthala for informal discussions and help with NMR measurements. I would also like to mention Dr. Thomas Donauer, Dr. Stefan Altwasser, Dr. Patrizia de Cola, Dr. Christine Berger, Tino Schreiber, Fanny Schurz, Frank Salzbauer, Sandra Rabl and all other institute members for their companionship.

I would finally like to thank my family and friends, especially my mother, Behdokht Jamshidi and father Saeyd Rezai for their everlasting, unconditional support in every endeavor I have undertaken. I am proud to dedicate this work to you mom!

# Table of contents

# Nomenclature

## *List of symbols*

| Symbol | Unit | Description |
|---|---|---|
| $a$ | $Pa \cdot m^6 \cdot mol^{-2}$ | PR attraction coefficient |
| $a_i$ | - | Activity of species i |
| $A$ | - | PR dimensionless attraction coefficient |
| $A_i$ | Vs or As | GC peak area of species i |
| $A_{i,corrected}$ | Vs or As | Corrected GC peak area of species i |
| $A_{reactor}$ | $m^2$ | Cross-sectional area of reactor |
| $b$ | $m^3 \cdot mol^{-1}$ | PR volumetric coefficient |
| $B$ | - | PR dimensionless volumetric coefficient |
| $B_i$ | - | First vapor pressure constant |
| $C_i$ | K | Second vapor pressure constant |
| $Cp_i$ | $J \cdot mol^{-1} \cdot K^{-1}$ | Heat capacity of species i |
| $CT$ | h | Contact time |
| $D_i$ | - | Third vapor pressure constant |
| $d_p$ | m | Particle diameter |
| $Ea_i$ | $J \cdot mol^{-1}$ | Permeation activation energy for species i |
| $E_i$ | - | Fourth vapor pressure constant |
| $F$ | - | Alkane to aromatic molar feed ratio |
| $F_i$ | - | Fifth vapor pressure constant |
| $f_{i,j}$ | - | Response factor for species i from detector j |
| $f_i$ | Pa or bar | Pure fugacity coefficient of species i |
| $\bar{f}_i$ | Pa or bar | Fugacity of species i in the mixture |
| $j_D$ | - | Chilton-Colburn factor |
| $J_i$ | $mol \cdot s^{-1} \cdot m^{-2}$ | Permeance of species i |
| $k_j$ | $mol \cdot g^{-1} \cdot s^{-1}$ | Rate constant for reaction j |
| $k_{mt}$ | $m \cdot s^{-1}$ | Mass-transfer coefficient |
| $k_{perm}$ | $mol \cdot s^{-1} \cdot m^{-1} \cdot Pa^{-0.5}$ | Sieverts' law rate constant |
| $K_j$ | - | Equilibrium constant for reaction j |

| | | |
|---|---|---|
| $K_{\lambda,j}$ | - | Product of fugacity coefficients for reaction j |
| $\dot{m}_i$ | $kg \cdot s^{-1}$ | Mass flow rate of species i |
| $m_{catalyst}$ | kg or g | Mass of catalyst |
| $M_i$ | $kg \cdot mol^{-1}$ | Molar mass of species i |
| $\dot{n}_i$ | $mol \cdot s^{-1}$ | Molar flow rate of species i |
| $n_i$ | mol | Molar amount of species i |
| $N_{Re}$ | - | Reynolds number |
| $N_{Sc}$ | - | Schmidt number |
| $N_{Sh}$ | - | Sherwood number |
| $p_i$ | Pa or bar | Partial pressure of species i |
| $P$ | Pa or bar | Pressure |
| $P_C$ | bar | Critical pressure |
| $P_R$ | - | Reduced pressure |
| $P_{atm}$ | Pa or bar | Atmospheric pressure |
| $p_i^{vap}$ | Pa or bar | Vapor pressure of species i |
| $Pe_i$ | $mol \cdot s^{-1} \cdot m^{-1} \cdot Pa^{-0.5}$ | Permeation pre-exponential factor of species i |
| $r$ | m | Reactor radius |
| $r_{i,j}$ | $mol \cdot kg^{-1} \cdot s^{-1}$ | Rate of reaction of species i in reaction j |
| $r_R$ | m | Ratio of reactor volume to membrane area |
| $R$ | $8.31\ J \cdot K^{-1} \cdot mol^{-1}$ | Ideal gas law constant |
| $S_i$ | - | Selectivity to species i |
| $SR$ | - | Sweep gas to alkane molar feed ratio |
| $S_{equilibrium}$ | - | Selectivity at equilibrium |
| $t_{ret}$ | min | Retention time |
| $T$ | K or ° C | Temperature |
| $T_C$ | K | Critical temperature |
| $T_R$ | - | Reduced temperature |
| $T_{sat}$ | K | Saturator temperature |
| $T_{ref}$ | K | Reference temperature (1 K) |
| $TOS$ | min or h | Time on stream |
| $V$ | $m^3$ or $cm^3$ | Volume |
| $\overline{V}$ | $m^3 \cdot mol^{-1}$ | Molar volume |
| $\dot{V}_{BFM}$ | $m^3 \cdot s^{-1}$ | Volumetric flow rate measured at a bubble flow meter |

| | | |
|---|---|---|
| $\dot{V}_{super}$ | $m \cdot s^{-1}$ | Volumetric superficial velocity |
| $\dot{V}_{total}$ | $mol \cdot s^{-1}$ | Total volumetric flow rate |
| $WHSV$ | $h^{-1}$ | Weight hourly space velocity |
| $x_i$ | - | Mole fraction |
| $X_i$ | - | Conversion of species i |
| $X_{equilibrium}$ | - | Conversion at equilibrium |
| $Y_i$ | - | Yield of species i |
| $z$ | m | Length of reactor |
| $Z$ | - | Compressibility factor of species i |
| | | |
| $\alpha$ | - | PR scaling factor |
| $\wp$ | $m \cdot s^{-2}$ | Diffusivity |
| $\delta$ | m | Membrane thickness |
| $\Delta G_j^{rxn}$ | $J \cdot mol^{-1}$ | Change of standard Gibbs free energy of reaction j |
| $\Delta H_j^{rxn}$ | $J \cdot mol^{-1}$ | Change in standard enthalpy of reaction j |
| $\Delta T$ | K | Temperature difference |
| $\varepsilon$ | - | Catalyst bed porosity |
| $\phi$ | - | Thiele modulus |
| $\kappa$ | - | Characteristic factor |
| $\mu$ | Pa·s | Viscosity |
| $\omega$ | - | Acentric factor |
| $\rho$ | $kg \cdot m^{-3}$ | Density |
| $\rho_{bed}$ | $kg \cdot m^{-3}$ | Catalyst bed density |
| $\sigma$ | - | Variance |
| $\theta_i$ | - | Surface coverage of species i |
| $\theta$ | ° | Diffraction angle |
| $\nu_{ij}$ | - | Stoichiometric coefficient of species i in reaction j |

## *List of abbreviations*

| Abbreviation | Description |
|---|---|
| BET | Brunauer-Emmet-Teller |
| BFM | Bubble flow meter |
| BREST | Bifunctional reaction step |
| DCC | Deep catalytic cracking |
| DHA | Dehydroalkylation |
| FCC | Fluid catalytic cracking |
| FID | Flame ionization detector |
| FT-IR | Fourier transform infrared spectroscopy |
| GC | Gas chromatography |
| HDA | Hydrodealkylation |
| ICP/OES | Inductively coupled plasma optical emission spectroscopy |
| IZA | International Zeolite Association |
| LMA | Levenberg-Marquardt algorithm |
| LSODE | Livermore solver for ordinary differential equations |
| MAS | Magic angle spinning |
| MS | Mass spectrometry |
| MT | Mass-transfer |
| MTG | Methanol to gasoline |
| NMR | Nuclear magnetic resonance |
| PPCP | Protonated pseudo-cyclopropane |
| PR | Peng-Robinson equation of state |
| PSSH | Pseudo-steady-state hypothesis |
| SNOW | Snamprogetti and Dow |
| SSR | Sum of squares residual |
| TCD | Thermal conductivity detector |
| TDP | Toluene disproportionation |
| TND | Total number of data points |
| UOP | Universal Oil Products |
| XRD | X-ray diffraction |
| ZSM | Zeolite Socony Mobil |

## List of zeolite nomenclature

| IZA code | Zeolite name |
|---|---|
| CLO | Cloverite |
| LTA | Linde Type A |
| FAU | Faujasite |
| MFI | ZSM-5 |
| MWW | MCM-22 |

## List of hydrocarbon nomenclature

| Symbol | Hydrocarbon |
|---|---|
| Bz | Benzene |
| E-Bz | Ethylbenzene |
| E-To | Ethyltoluene |
| To | Toluene |
| Xy | Xylene |
| *i*- | iso |
| *m*- | meta |
| *n*- | normal |
| *o*- | ortho |
| *p*- | para |

## Catalyst nomenclature

In the following work, the catalyst is defined as follows: *x*M/zeolite. The *x* represents the amount of metal determined by AES/ICP analysis in wt.-% of the dry zeolite. The M represents the type of metal loaded onto the zeolite, by ion exchange. For example: 0.9Pd/H-MCM-22 is a palladium-exchanged zeolite MCM-22 (in the acidic form) with a palladium metal content of 0.9 wt.-%.

# Zusammenfassung

Jüngste Fortschritte in der Reaktortechnik sowie die Entwicklung aktiver, multifunktionaler Katalysatoren ermöglichten die Aktivierung der relativ inerten leichten Alkane. Die Nutzung von kurzkettigen Alkanen, insbesondere von Methan und Ethan, als Ausgangsstoffe für die chemische Industrie bietet eine attraktive Alternative zu den herkömmlich verwendeten Alkenen. Beträchtliche Mengen an Alkanen findet man in Form von Erdgas, wogegen Alkene ausschließlich durch chemische Umsetzung gewonnen werden können. Die Aktivierung von Alkanen kann entweder oxidativ oder nicht oxidativ erfolgen. Die oxidative Aktivierung ist thermodynamisch begünstigt, führt jedoch zur Bildung der wertlosen und unerwünschten Nebenprodukte Wasser und Kohlendioxid. Dagegen kann bei der nicht oxidativen Aktivierung Wasserstoff als wertvolles Nebenprodukt gewonnen werden. Die Umsätze nicht oxidativer Reaktionen sind jedoch sehr gering. Durch das Verschieben des Gleichgewichts der Reaktion, z.B. durch Entfernen eines Reaktionsproduktes, können diese Nachteile abgemildert werden.

Die Alkylierung von Aromaten mit Alkanen bietet eine neuartige Möglichkeit zur Herstellung wichtiger Grundchemikalien wie n-Propylbenzol, Cumol, Ethyltoluol und Ethylbenzol. Laut aktuellen Schätzungen beläuft sich die derzeitige Produktionskapazität von Ethylbenzol und Cumol, den beiden wichtigsten durch Alkylierung von Aromaten hergestellten Chemikalien, auf $25 \cdot 10^6$ $t \cdot a^{-1}$ bzw. $10 \cdot 10^6$ $t \cdot a^{-1}$ [1]. Herkömmliche Alkylierungsmittel, wie Alkene, Alkohole und Alkylhalogenide, müssen dabei in einem zusätzlichen Prozessschritt synthetisiert werden. Die direkte Alkylierung von Aromaten mit *Alkanen* würde daher zu einer erheblichen Kostensenkung und Prozessintensivierung führen, da Alkane preiswerter und leicht verfügbar sind und dadurch ein zusätzlicher Syntheseschritt vermieden werden kann. Aus diesem Grund wurde in der hier vorliegenden Arbeit die direkte Anwendung von Ethan als Alkylierungsmittel in der Dehydroalkylierung von Toluol zu Ethyltoluol an edelmetallhaltigen Zeolithen untersucht.

Ethan befindet sich in einer thermodynamischen Senke. Die gewünschte Reaktion ist daher stark thermodynamisch limitiert. Experimentelle Untersuchungen verbunden mit theoretischen Berechnungen wurden durchgeführt, um die Reaktion besser zu verstehen und folglich die Ausbeuten in der untersuchten Reaktion zu verbessern. Die Druckabhängigkeit wurde anhand eines Modells mit thermodynamischen Berechnungen und kinetischen Annahmen simuliert. Die Werte des Modells stimmen bei 300 °C mit den experimentellen

Daten überein. Bei 350 °C erhält man jedoch Umsätze, die weit über den berechneten Werten liegen. Dies wird vermutlich durch die Bildung von wasserstoffreichem Methan hervorgerufen, welches als „Wasserstoffsenke“ fungiert. Dadurch wird das Gleichgewicht in Richtung der Ethyltoluole verschoben.

Da Methan hauptsächlich aus Wasserstoff in einer Folgereaktion gebildet wird, wurde die Raumgeschwindigkeit verändert, um die Selektivität zur Wunschreaktion zu verbessern. Bei hohen Raumgeschwindigkeiten kann die Bildung von Methan vermieden werden. Auch die Disproportionierung von Toluol wird in diesem Fall nicht beobachtet, was zu einer 100%-igen Selektivität zu Ethyltoluolen und Wasserstoff führt. Das Absenken der Raumgeschwindigkeit resultiert in einem Anstieg des Umsatzes sowie der Ausbeute an Ethyltoluolen. Erhöhte Umsätze führen jedoch zu schlechteren Selektivitäten zu den Ethyltoluolen, da die Disproportionierung von Toluol parallel zur Dehydroalkylierung ablaufen kann. Mit steigendem Umsatz wird zudem die Bildung von $C_1$- bis $C_4$-Alkanen und anderen Aromaten, wie z.B. Benzol, Xylolen und Ethylbenzol, beobachtet. Die größte Ausbeute an Ethyltoluolen erhält man bei einem Umsatz von 13 % bei 90 h Laufzeit und einer mittleren Raumgeschwindigkeit. Dieses Maximum könnte durch Folgereaktionen der Ethyltoluole bedingt sein. Hydrocracking-Experimente haben bestätigt, dass Methan vornehmlich aus Folgereaktionen der Edukte und Produkte gebildet wird.

Ein Dehydroalkylierungskatalysator mit guter Aktivität enthält ein Edelmetall als aktives Zentrum. Dieses Edelmetall kann jedoch zu unerwünschten Folgereaktionen führen, wie Hydrocracking/Hydrogenolyse sowie zu Hydrodealkylierung von Edukten und Produkten. Obwohl Pt/H-ZSM-5 als Katalysator den höchsten Umsatz an Toluol aufweist, besitzt Pd/H-ZSM-5 die höchste Aktivität für die Dehydroalkylierung von Toluol und führt zu den größten Ausbeuten an Ethyltoluolen, hervorgerufen durch die geringere Aktivität von Pd gegenüber Hydrodealkylierungsreaktionen.

Neben der hohen Selektivität zu den gewünschten Produkten standen die Erhöhung des Umsatzes an Toluol und damit bessere Ausbeuten im Mittelpunkt weiterer Untersuchungen. Diese Ziele können durch Verwendung eines Membranreaktors erreicht werden, da das Produkt Wasserstoff selektiv entfernt und damit das Gleichgewicht in Richtung der Produkte verschoben wird. Vor der Durchführung katalytischer Experimente wurde ein thermodynamisches Modell entwickelt, welches unter Berücksichtigung der selektiven

Entfernung des Wasserstoffs im Membranreaktor die maximal erreichbare Verschiebung des chemischen Gleichgewichts simuliert. Dem Modell liegen sowohl das chemische Gleichgewicht der Reaktion als auch der Wasserstoffgradient innerhalb des Reaktors zugrunde. Der Stoffmengenstrom des Trägergases muss 10-mal größer sein als der Stoffmengenstrom des Alkans, um ausreichend Wasserstoff gewinnen zu können. Die optimale Verschiebung des chemischen Gleichgewichts wird durch maximale Verdünnung des Wasserstoffs an der Permeatseite erreicht. Im Membranreaktor zeigen Dehydroalkylierungsreaktionen gegenüber Dehydrierungen Vorteile. Da Dehydrierungsreaktionen einen Anstieg der Stoffmenge zur Folge haben, begünstigt ein niedriger Druck die Reaktion. Bei Dehydroalkylierungsreaktionen bleibt die Stoffmenge jedoch gleich. In einem Membranreaktor beobachtet man daher höhere Ausbeuten bei erhöhtem Druck, da mehr Wasserstoff durch die Membran permeieren kann. Es gibt jedoch einen Grenzwert, bis zu welchem das chemische Gleichgewicht verschoben werden kann, abhängig von der Thermodynamik der untersuchten Reaktion. Das hier entwickelte Modell kann daher angewendet werden, um die optimalen Bedingungen zur Verschiebung des chemischen Gleichgewichts für Reaktionen im Membranreaktor zu berechnen. Die Modellrechnungen wurden durch experimentelle Untersuchungen bestätigt.

Dabei wurde gezeigt, dass die Dehydroalkylierung von Toluol mit Ethan in einem Membranreaktor erfolgreich durchgeführt werden kann. Da die Reaktionsbedingungen sehr mild gehalten werden können, ist das Laufzeitverhalten des Katalysators während der Reaktion stabil. Eine Erhöhung des Druckes während der Reaktion hat einen positiven Einfluss auf die Umsätze, da sich die Fugazitätfaktoren während der Reaktion nicht ändern. Bei erhöhtem Druck ist jedoch die Disproportionierung von Toluol vorherrschend. Kurze Kontaktzeiten - um die Toluoldisproportionierung zu vermeiden - wären jedoch hier nicht möglich, da der entstehende Wasserstoff aus dem Reaktionsraum herausgetragen würde, bevor er durch die Membran diffundieren kann. Eine weitere Optimierung des Katalysators und der Reaktionsbedingungen im Membranreaktor sind daher notwendig, bevor industriell bedeutsame Ausbeuten erreicht werden können.

# Abstract

With the recent progress in chemical reaction engineering and highly active, multi-functional catalysts, the activation of relatively inert alkanes may be achieved. The direct use of short-chain alkanes, especially methane and ethane, as basic chemical feedstocks represents an attractive alternative to alkenes. Significant reserves of alkanes are found in nature in the form of wet natural gas, whereas alkenes have to be synthesized via other chemical reactions. The activation of alkanes can be achieved by oxidative and non-oxidative methods. Reactions of oxidative activation are often thermodynamically favored, e.g., due to formation of the stable but economically unattractive by-products water and/or carbon dioxide. In contrast, reactions of non-oxidative activation may produce hydrogen as a valuable by-product, but the equilibrium conversions of such reactions are generally low, and thus, measures have been taken to improve this situation, e.g., shifting equilibrium by removing a product.

The alkylation of aromatics with alkanes, in particular, represents a potential new route for the synthesis of important feedstock chemicals such as *n*-propylbenzene and cumene, ethyltoluenes, and ethylbenzene. Estimates for current worldwide annual production capacities of ethylbenzene and cumene, the two most important chemicals produced by alkylation of aromatics, amount to $25 \cdot 10^6$ t·a$^{-1}$ and $10 \cdot 10^6$ t·a$^{-1}$[1], respectively. Conventional alkylating agents, including alkenes, alcohols and alkyl halides, have to be pre-synthesized via other processes, typically from an alkane feedstock. Alternatively, the direct alkylation of aromatics with *alkanes* may result in reduced costs and process intensification, since alkanes are much cheaper than other typical alkylating agents, abundantly available and pre-synthesis steps can be avoided. Therefore, the focus of the present work has been the heterogeneously catalyzed activation of ethane by direct application of ethane as an alkylating agent during toluene dehydroalkylation to ethyltoluenes on noble metal-loaded zeolite catalysts.

Due to the thermodynamic stability of ethane, the desired reaction is strongly limited by equilibrium. Therefore, during the present work efforts were concentrated on experimental work in conjunction with theoretical modeling in order to better understand and hence improve the yield to the title reaction. The effect of pressure was investigated by a non-ideal gas model complemented by kinetic assumptions. At 300 °C, the thermodynamic model is in agreement with experimental results. However, at 350 °C conversions are well over the expected values calculated from the same model. The “supra-equilibrium” may be due to the

formation of hydrogen-rich methane, acting as a hydrogen sink, hence shifting equilibrium towards the formation of ethyltoluenes. This was attributed to the consumption of hydrogen as a result of methane formation.

Since methane is mainly formed by consumption of hydrogen, i.e., it is a secondary reaction, the space velocity was varied to improve selectivity to the title reaction. At a high space velocity, the formation of methane can be entirely avoided. Furthermore, the disproportionation of toluene is also absent, resulting in 100 % selectivity to ethyltoluenes and hydrogen. Decreasing the space velocity results in an increase in conversions as well as the yield of ethyltoluenes. However, at space velocities lower than about 3.0 $h^{-1}$, the selectivity to ethyltoluenes decreases since the toluene disproportionation reaction can compete with the dehydroalkylation reaction. With increasing conversion, $C_1$ to $C_4$ alkanes are also formed to a larger extent, as well as other aromatics including benzene, xylenes, and ethylbenzene. A maximum yield of ethyltoluenes is observed at a conversion of 13 % at 90 h on stream and medium space velocities. It is suggested that this maximum is a result of secondary reactions of ethyltoluenes. Hydrocracking experiments confirm that methane forms mainly from secondary reactions of products or reactants.

A noble metal is required for a dehydroalkylation catalyst with good activity. However, the noble metal can also promote undesired side reactions including hydrocracking or hydrogenolysis and, mainly, the hydrodealkylation of the reactants and products. Although on Pt/H-ZSM-5 catalysts the highest toluene conversion is observed, on Pd/H-ZSM-5 the highest yields to ethyltoluenes can be achieved. This is as a result of Pd being less active for hydrodealkylation. Hence, further experiments in the membrane reactor were carried out using a Pd/H-ZSM-5 catalyst.

Since high selectivity to the desired products can be achieved, the ultimate goal of increased yields can be achieved by improving conversion. This was attempted by application of a membrane reactor, which may improve yields by selectively removing a product and hence shifting equilibrium. Prior to catalytic experiments in a membrane reactor, a model was developed applying fundamental thermodynamics in order to gauge the maximum attainable shift in equilibrium by the selective removal of hydrogen in a membrane reactor. The model considers chemical reaction equilibrium and simultaneously the hydrogen partial pressure equilibrium across the membrane. From the viewpoint of hydrogen recovery, the molar flow

of the sweep gas must be about 10 times higher than the molar flow of the alkane to ensure a high hydrogen recovery from the reactor. Under these conditions, an optimum shift in equilibrium can be achieved with a minimum dilution of the hydrogen on the sweep side.

Dehydroalkylation reactions show interesting advantages in comparison to, more widely studied, dehydrogenation reactions. Since dehydrogenation reactions typically result in a net increase in the number of moles, low pressure is favored. However, for the membrane reactor, removal of hydrogen means that high conversions can still be maintained at high pressure. However, in the case of dehydroalkylation of toluene with ethane, the number of moles does not change. Thus, in a membrane reactor an increase in conversion can be achieved at higher pressures since more hydrogen can permeate at higher pressure. However, there is a limit to which the equilibrium can be shifted, depending on the thermodynamics of the given reaction. The model suggested here may be applied to simply estimate optimum conditions for specific reactions in order to achieve the highest attainable conversions when applying membrane reactors. The modeling results are confirmed by experimental results.

Experiments show that the dehydroalkylation of toluene with ethane can be successfully performed in a membrane reactor. Since the reaction is taking place under mild conditions, the catalytic performance of the bifunctional zeolite in the membrane reactor is stable with time on stream. Experiments demonstrate large improvements with tripled conversion and almost tripled yield to the desired ethyltoluenes by increasing the sweep gas flow rate and the pressure on the reaction side. Selectivity to methane and ethylbenzene, formed from hydrodealkylation reactions that consume hydrogen, is reduced. Increasing pressure has a positive effect on conversion since the net number of moles does not change during this reaction. However, at high pressure, the toluene disproportionation reaction is dominant. Unfortunately, choosing a low contact time to successfully eliminate the toluene disproportionation is not possible here, since under such conditions the produced hydrogen is swept out of the reaction zone before it can permeate. Hence, a careful optimization of the catalyst and the reaction conditions in the membrane reactor is needed in order to achieve industrially relevant yields.

# 1 Introduction

## 1.1 Background

The activation of alkanes, of which huge reserves exist worldwide, is among the great challenges of modern catalysis research [2]. With the recent progress in chemical reaction engineering and highly active, multi-functional catalysts, the activation of relatively inert alkanes may now be achieved. The direct use of short-chain alkanes, especially methane and ethane, as basic chemical feedstocks represents an attractive alternative to alkenes. Significant reserves of alkanes are found in nature in the form of wet natural gas, whereas alkenes have to be synthesized via other chemical reactions. The activation of alkanes may be achieved by oxidative or non-oxidative methods. Reactions of oxidative activation are often thermodynamically favored, e.g., due to formation of the stable but economically unattractive by-products water and/or carbon dioxide [3]. In contrast, reactions of non-oxidative activation may produce hydrogen as a valuable by-product, however, the equilibrium conversions of such reactions are generally low. The alkylation of aromatics with alkanes, in particular, represents a potential new route for the synthesis of important feedstock chemicals such as *n*-propylbenzene and cumene [4-6], ethyltoluenes [2, 7], and ethylbenzene [8-10].

Figure 1.1 shows the various possible strategies that may be followed to chemically activate alkanes. The two major routes include catalytic and non-catalytic activation. Non-catalytic activation includes combustion for heating purposes or thermal decomposition forming coke and hydrogen. In contrast, the focus of the catalytic route is to functionalize the alkane, yielding more valuable chemicals. Alkane activation using a variety of enzymes (biocatalysis) and transition-metal centers (homogeneous catalysis) has been extensively reported, often under remarkably mild conditions and with high selectivity [11]. However, there are usually other obstacles for large-scale realization of homogeneously catalyzed processes. Heterogeneously catalyzed processes are currently preferred for the industrial-scale production of bulk chemical intermediates. There are four possibilities for heterogeneously catalyzed alkane activation, namely by acids, bases, on soft electrophiles, or via radicals in the presence of oxygen or light. The aim of this work is to investigate catalytic activation of alkanes on solid acid catalysts.

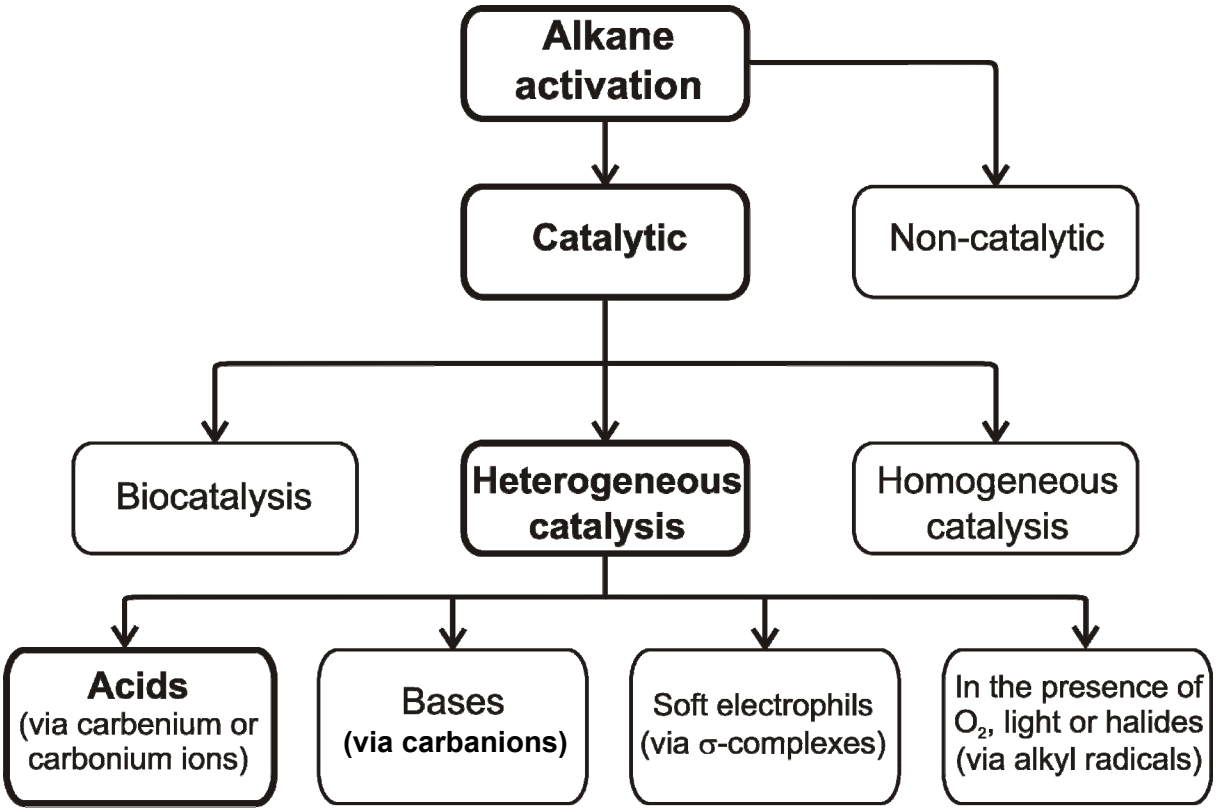


Fig. 1.1: Various strategies that may be followed for the activation of alkanes, adapted from [12].

## *1.2 Objectives*

The production of alkyl aromatics as chemical intermediates is carried out on a very large scale. Estimates for current worldwide annual production capacities of ethylbenzene and cumene, the two most important chemicals produced by alkylation of aromatics, amount to $25 \cdot 10^6$ t·a$^{-1}$ and $10 \cdot 10^6$ t·a$^{-1}$, respectively [1]. Conventional alkylating agents, including alkenes, alcohols and alkyl halides, have to be pre-synthesized via other processes, typically from an alkane feedstock. Alternatively, the direct alkylation of aromatics with *alkanes* may result in reduced costs and process intensification, since alkanes are much cheaper than other typical alkylating agents, abundantly available and pre-synthesis steps can be avoided [3].

The main objective in the following work is to investigate the feasibility of replacing conventional alkylating agents with alkanes (cf. Figure 1.2). Since the reaction is endothermic and endergonic (cf. Figure 1.2), improving conversion, at high selectivity, is of utmost

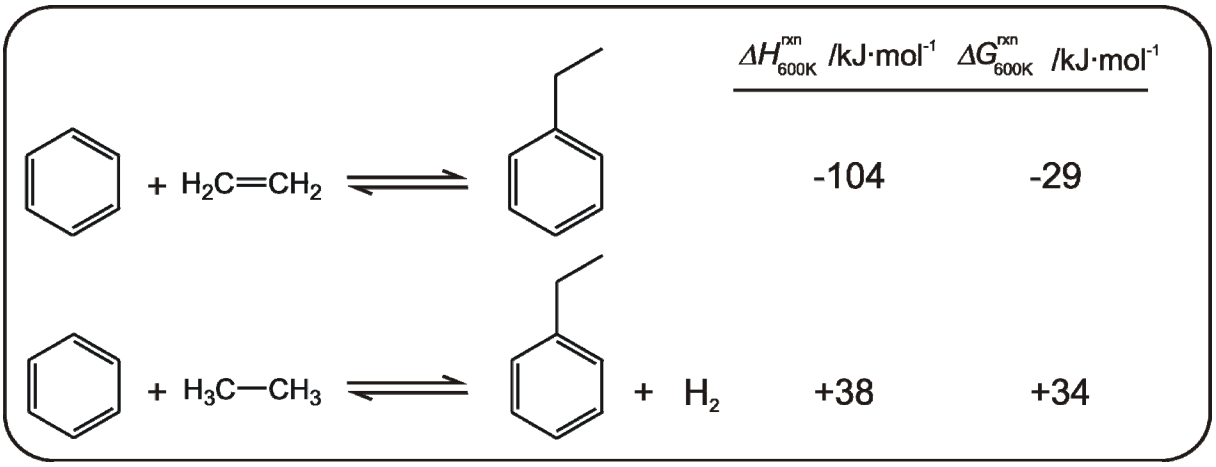


Fig. 1.2: Conventional (top) and alternative (bottom) routes to ethylbenzene and the corresponding standard enthalpy of reaction and standard Gibbs free energy of reaction [13, 14].

importance. The aims are threefold:

- To optimize the catalyst and reaction conditions in order to achieve high selectivity,
- To improve the yield of the reaction, and
- To improve the understanding of critical reaction parameters by mathematical models which adequately describe the system.

## *1.3 Scope and limitations*

To pursue the objectives of this work, a model reaction was chosen, namely the dehydroalkylation of toluene with ethane to the isomeric ethyltoluenes and hydrogen. The product of this direct alkylation contains an ethyl group on the aromatic ring, and hence, is easily distinguishable from the toluene disproportionation products benzene and xylenes. In addition, the reaction is industrially relevant: Dehydrogenation of *p*-ethyltoluene gives *p*-methylstyrene, a useful monomer yielding polymers with improved properties relative to polystyrene, such as higher flash-point and glass transition temperature [15, 16].

The synthesis of the membrane is beyond the scope of this work. Extensive characterization of the membrane is not allowed, in agreement with the provider of the membrane reactor (REB Research & Consulting, Ferndale, MI, USA).

# 2 Literature review

The following section will give an overview of the relevant literature in the field of alkanes as alkylating agents for aromatics as well as membrane reactors and specifically hydrogen-selective membrane reactors and their application for the dehydrogenation of alkanes.

## *2.1 Zeolites*

### 2.1.1 Background

Zeolites have been defined [17] as *crystalline* substances with a structure characterized by a *framework of linked tetrahedra* each consisting of four oxygen anions surrounding a cation. This framework contains *open cavities* in the form of channels and cages. These are usually occupied by water molecules and extra-framework cations that are commonly exchangeable. The channels are large enough to *allow the passage of guest species*. In the hydrated phases, reversible dehydration occurs at temperatures above 400 °C.

It has been established that there are exactly 9, 117 and 926 topological types of, respectively, 4-connected uninodal, binodal and trinodal possible networks [18]. The Structure Commission of the International Zeolite Association (IZA) [19] is responsible for verifying new structures and assigning a three-letter code accordingly. Of the more than 1000 possible structures, Figure 2.1 shows the crystallographic pore diameters, of the largest pore, for the 186 currently known zeolite structures as function of the number of tetrahedra in the ring [20]. More than three-quarters of the known structures have 8 to 12 tetrahedra in the largest ring with a pore diameter in the range of 0.3 to 1.0 nm. The largest-pore zeolite (cloverite, CLO) has a pore diameter of 1.3 nm made up of a 20-tetrahedra ring.

Natural and synthetic zeolites have many commercial and domestic applications [21]. Natural zeolites are used as fillers in construction, and in the agricultural sector for soil treatment and as an additive for animal feedstock. Synthetic zeolites have more industrially relevant applications, the most important being as ion-exchangers, adsorbents and catalysts. The interests for application of zeolites in catalysis are due to their high surface area, high adsorption capacity, and molecular range dimensions of the pores [22]. Of the vast structure base, only a handful of these are produced and used industrially, including zeolite A (LTA), e.g., as ion-exchange medium in detergents, zeolite Y (FAU), e.g., in fluid catalytic cracking

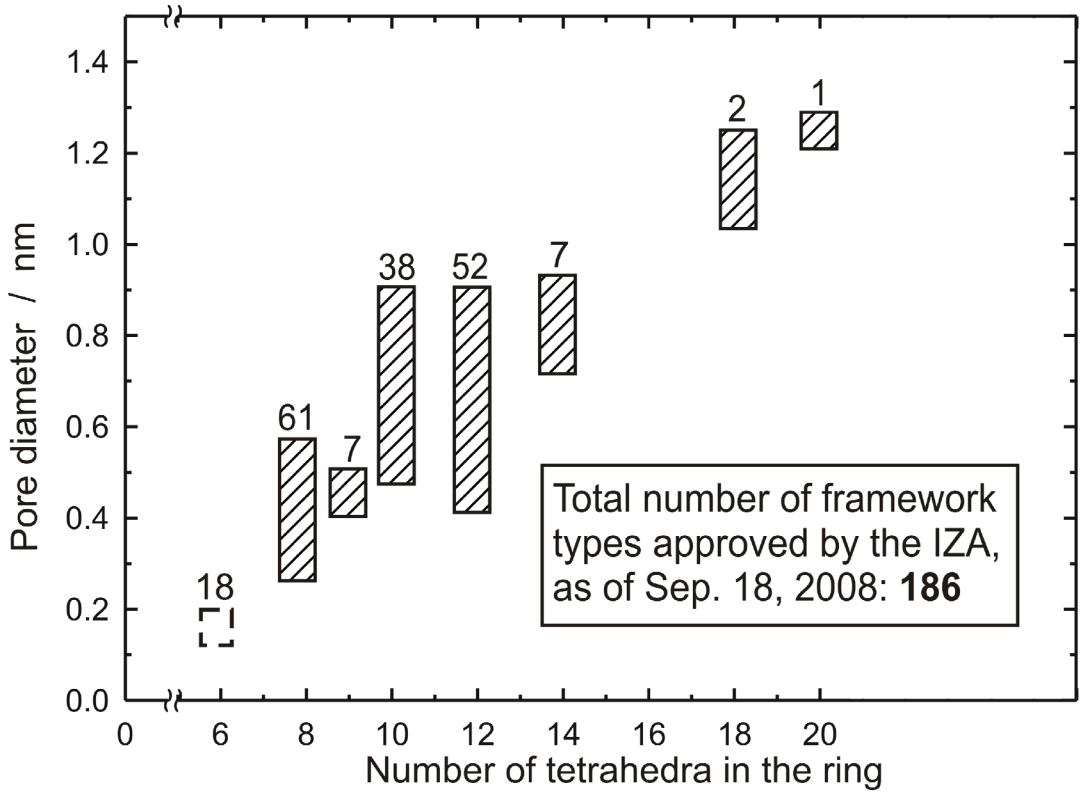


Fig. 2.1: Representing the pore diameter of all known zeolite framework types as a function of the number of tetrahedra in the ring [20], updated from [19].

(FCC) of petroleum fractions, ZSM-5 (MFI), e.g., in deep catalytic cracking (DCC), MCM-22 (MWW), e.g., for ethylbenzene production [23].

## 2.1.2 Zeolite ZSM-5 (MFI)

To date, ZSM-5 (MFI) is one of the most important and industrially most widely applied zeolites. It was discovered in 1976 by Mobil Oil Corporation [24]. Figure 2.2 shows the MFI framework structure. The zigzag channels (running along the crystal a-axis) have pore dimensions of 0.55 x 0.51 nm, and the straight channels (running along the crystal b-direction) have pore dimensions of 0.56 x 0.53 nm. One advantage of the MFI-type zeolites is that the aluminum content of the MFI structure can be controlled over a wide range. Silicalite-1 is the aluminum-free analogue to ZSM-5. Synthesis is commonly carried out under hydrothermal conditions, and with or without the aid of a structure-directing agent (template) depending on the desired aluminum content. However, this template remains in the pores of the zeolite after synthesis and must be removed to render the microporous structure

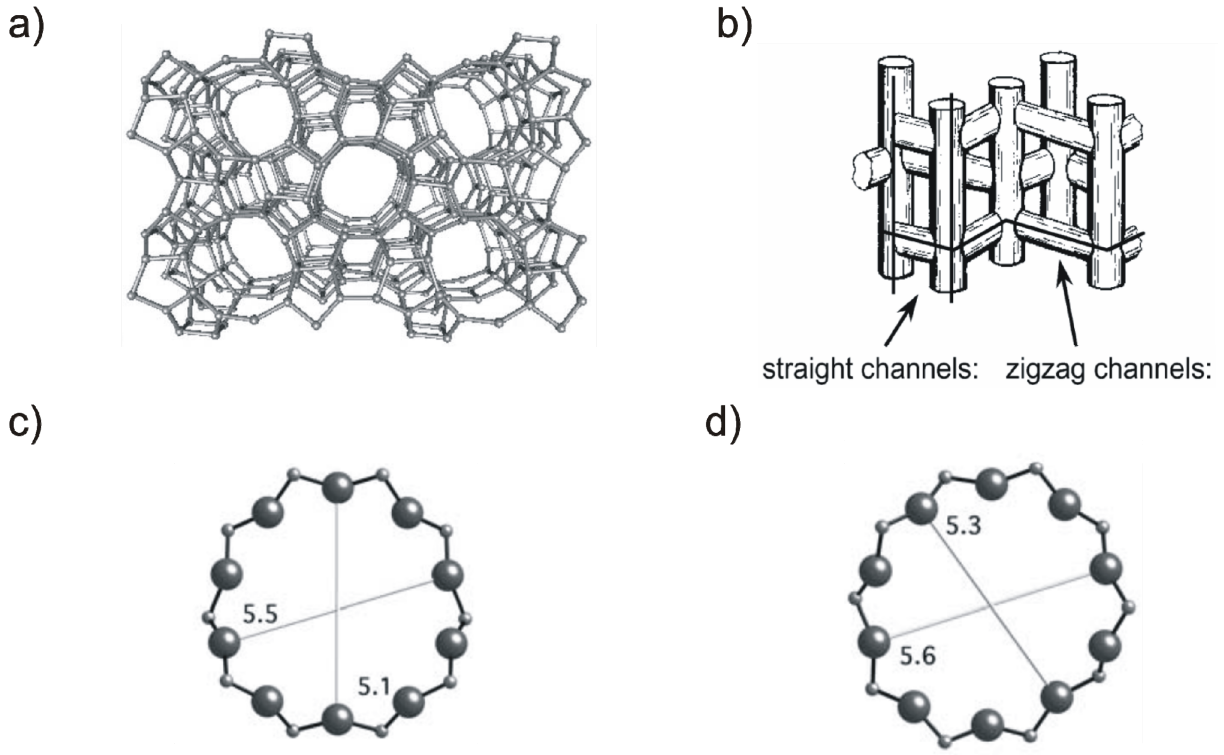


Fig. 2.2: MFI structure, using a stick model (a) [25], the channels configuration (b), i.e. straight and zigzag channels, pore dimensions, along the a-axis (c) [19], and along the b-axis (d). Pore dimensions are in Å (1 Å = 0.1 nm).

accessible for molecules. Zeolite ZSM-5, as a catalyst, has a wide range of industrial applications including dewaxing, hydrocracking, ethylbenzene production (Mobil-Badger), xylene isomerization, methanol to gasoline (MTG), catalytic aromatization, toluene disproportionation, and as an additive to the FCC catalyst [23].

### 2.1.3 Zeolites for alkylation of aromatics

Historically, the production of alkyl aromatics for chemical intermediates has been an important process for the production of a range of polystyrenes as well as phenol [26, 27]. Estimates for current total worldwide annual production capacities for the alkylation of aromatics amount to over $35 \cdot 10^6$ t·a$^{-1}$ [1] with an annual projected growth rate of over 4 % [27]. Table 2.1 shows the historical development of the ethylbenzene process. Prior to 1970, the Friedel-Crafts alkylation process prevailed. However, due to the operating costs associated with the corrosivity of $AlCl_3$ and problems with safe handling, disposal, and the environmentally unfriendly nature of such catalysts, process technologies have been moving away from conventional Friedel-Crafts catalyzed alkylation toward zeolite-based processes.

Table 2.1: Historical ethylbenzene process development [27, 28].

| Year | Catalyst | Process | $T$ / °C | Phases | Remarks |
|---|---|---|---|---|---|
| 1930s | $AlCl_3$ | Dow | <130 | liquid/ solid | Single reactor; processes by BASF, Dow, Monsanto etc. |
| 1960s | $BF_3/AlCl_3$ | Alkar (UOP) | 300 | gas/ solid | Single reactor; pure or dilute ethene; severe corrosion |
| 1970s | H-ZSM-5 | Mobil-Badger | >400 | gas/ solid | Non-corrosive; no waste water; many by-products including methyl- and high-boiling aromatics |
| 1990s | H-MCM-22 | EBMax | 170-240 | liquid/ solid | Much less by-products, very little (4 $kg \cdot t^{-1}$) high-boiling aromatics, very low excess of benzene over ethene possible |
| late 1990s | H-Y | CDTech | <270 | liquid/ solid | Catalytic distillation; Reduced coke formation, long catalyst life; high product selectivity can be achieved |
| 2000s | $Ga_2O_3$-Pt/ $\delta$-$Al_2O_3$ | SNOW | 450-650 | gas/ solid | Circulating fluidized bed; ethane or ethene; direct styrene production, no dilution with steam required |

In 1976, the Mobil-Badger process was introduced, using an H-ZSM-5 catalyst, and is still the most widely used zeolite-catalyzed process for ethylbenzene production. A third-generation process, EBMax, was first commercialized in 1995, primarily using an H-MCM-22 catalyst. The main features of the EBMax process are much milder reaction conditions due to the high activity of H-MCM-22 as well as lower yields of by-products. Another potential process is the CDTech process applying catalytic distillation with an H-Y catalyst. More interesting are the likely future process developments. There seems to be a move towards using dilute ethene streams (e.g., from FCC) instead of pure ethene. A very recent development, the SNOW process from Snamprogetti and Dow [28], applies a circulating fluidized bed with a regenerator. Pure ethane and benzene can be converted to styrene by using the same unit for dehydrogenation of ethylbenzene to styrene and for production of ethene which is then led to the alkylation unit. The process eliminates the need for upstream investment in ethene production at a steam cracker, and the catalyst is said to be so active that only very short contact times are required. Furthermore, the catalyst is claimed to be so selective that no steam dilution is required [28].

## 2.2 Alkanes as alkylating agents for aromatics

Alkanes as alkylating agents for the production of alkyl aromatics have enjoyed increasing interest from industry and academia since the turn of the new millennium. Scheme 2.1 represents the general equation for the dehydroalkylation reaction. Studies have mainly focused on propane and ethane as alkylating agents, with a few studies on methane as alkylating agent. Primarily benzene or toluene were used as substrates for dehydroalkylation to cumene, ethylbenzene or ethyltoluenes, respectively.

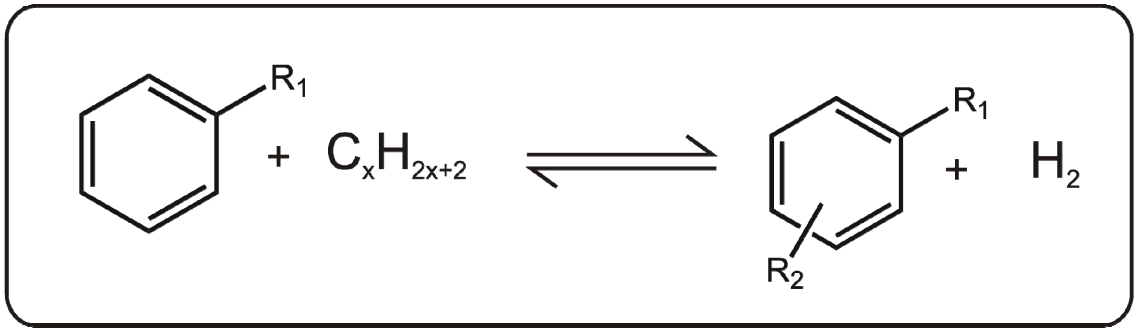


Scheme 2.1: General form of the dehydroalkylation reaction of aromatics with alkanes, with x = 1 to 3, $R_1$ = H or $CH_3$, $R_2$ = $CH_3$, $C_2H_5$ or $C_3H_7$.

Figure 2.3 shows the equilibrium conversions for typical dehydroalkylation reactions reported in literature under mild and severe conditions, with a feed ratio $\dot{n}_{\text{alkane}} / \dot{n}_{\text{aromatic}} = 1$. At 600 K, benzene dehydroalkylation with propane yields almost 5 % *n*-propylbenzene, the highest achievable conversion within the given reactions. Conversion to cumene (for phenol production) is lower, at about 3 %. Reactions of benzene dehydroalkylation with ethane to ethylbenzene (4 %) and of toluene with ethane to *m*-ethyltoluene (2 %) generally give lower conversions than with propane. Meanwhile, conversion for benzene dehydroalkylation with methane to xylenes is negligible at 600 K. At a more severe reaction temperature of 1000 K, all equilibrium conversions are significantly higher, since the reactions are endothermic. The conversion to *n*-propylbenzene is about 17 %, whereas a conversion to ethylbenzene of about 15 % can be achieved at 1000 K. However, it must be noted that although these high temperatures seem to be attractive, it should be kept in mind that thermal reactions can dominate under these conditions, hence reducing selectivity to the desired products. Furthermore, coke formation is strongly promoted at such high temperatures, significantly reducing catalyst activity and lifetime.

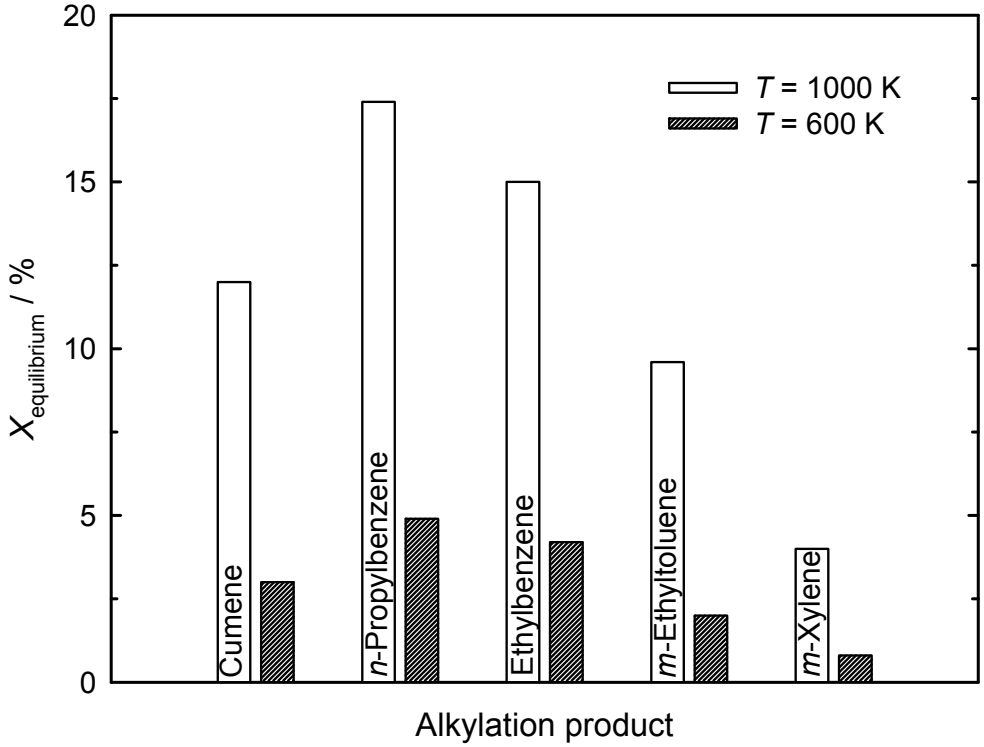


Fig. 2.3: Equilibrium conversion for dehydroalkylation of benzene with propane to cumene or *n*-propylbenzene, benzene with ethane to ethylbenzene, toluene with ethane to *m*-ethyltoluene and toluene with methane to *m*-xylene under mild, 600 K, and severe, 1000 K, conditions and $\dot{n}_{alkane} / \dot{n}_{aromatic} = 1$ [13]. In the case where more than one isomer is formed results are for the most favored isomer.

## 2.2.1 Mechanisms of alkane activation

Effort has been spent in the open literature on the investigation of various mechanisms of alkane activation, with the major focus on activation of propane, mainly on noble metal- or Ga-modified zeolites. Besides catalytic experiments, $^{13}C$ MAS-NMR- and FT-IR-spectroscopy have been used to study the dehydroalkylation reaction. For a bifunctional Ga/H-ZSM-5 catalyst [29-31], initially propane is protonated forming a protonated pseudo-cyclopropane (PPCP) intermediate. The formation of the PPCP is believed to be a result of a bifunctional reaction step (BREST) which requires a $Ga^{3+}$ ion closely associated with a Brønsted acid site of the zeolite. Decomposition of the PPCP intermediate can yield $H_2$, $CH_4$ or $C_2H_6$, and propyl, ethyl, or methyl cations, respectively. Alkylation of benzene with these cations forms the corresponding cumene, ethylbenzene and toluene, respectively. On a Pt/H-ZSM-5 catalyst [4], propane activation is achieved via the dehydrogenation of propane

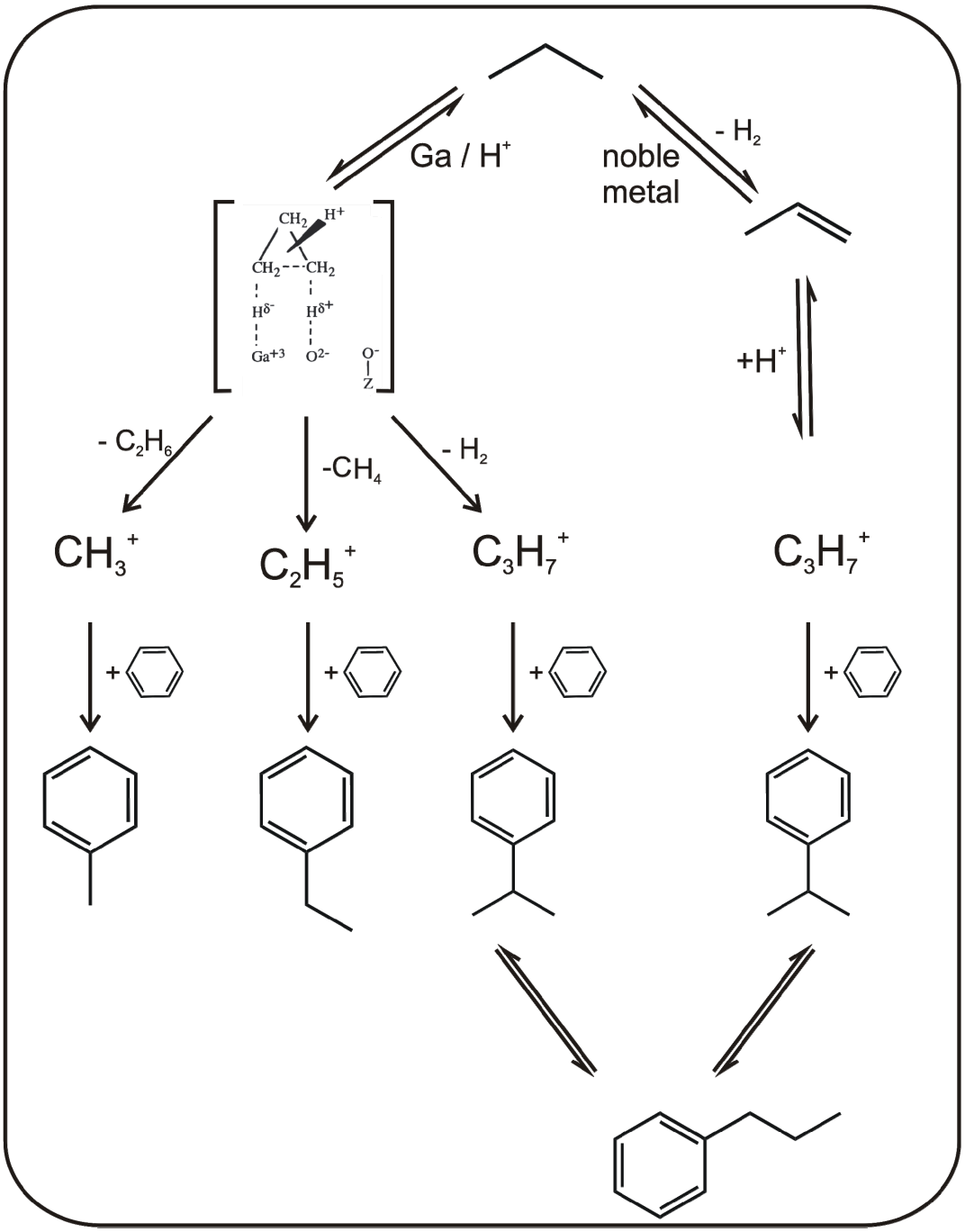


Fig. 2.4: Proposed pathways for propane activation on bifunctional catalysts. On Ga-modified catalysts, initially a protonated pseudo-cyclopropane (PPCP) intermediate is formed. Benzene alkylation with decomposition products of the PPCP then results in cumene, ethylbenzene, or toluene. On noble metal-modified catalysts, propane is dehydrogenated to propene first on the metal. Benzene alkylation with propene then follows, on the acid sites. Thereafter, isomerization of cumene to *n*-propylbenzene may take place. Adapted from [4, 29, 32].

on the metal first, followed by protonation of propene on acid sites and finally alkylation of benzene. This route is more selective for the formation of cumene since the PPCP is avoided, however, on Pt/H-ZSM-5 still large amounts of side products are observed, possibly due to the high activity of Pt for hydrogenolysis/ hydrocracking. Finally, Abasov *et al.* using a Pt-Re/$Al_2O_3$ H-Y mixed catalyst [33] have proposed the formation of aromatic carbocations on acidic sites which are alkylated with propane. Formation of *n*-propylbenzene may happen as a result of monomolecular isomerization of cumene or, to a smaller extent, of bimolecular isomerization of cumene [34].

Ethane, being more symmetric and forming less stable cationic intermediates, is less reactive than propane. Cracking of ethane under moderate or mild conditions is unlikely since only unstable ethyl cations can be formed. Therefore, the proposed route for ethane activation is similar to the one on the noble metal catalyst in Figure 2.4 and is shown in Figure 2.5. The mechanism is a two-step model, first the dehydrogenation of ethane to ethene, then transfer of ethene to the acid sites and alkylation of the aromatic with ethene [7, 32]. Although alkylation of benzene with ethane has been attempted on Ga/H-ZSM-5, very low conversions were obtained [8]. This may be due to the PPCP intermediate not being possible in the case of ethane. Since the reaction can only take place by dehydrogenation of the alkane, and Ga is not as active for dehydrogenation as Pt, conversions are poor.

Methane seems to be even less reactive [35-37]. Reactions of methane seem to only be possible via impurities in the feed. During the methylation of benzene, toluene could be formed as a result of other hydrocarbon impurities in the feed. Using a Co/H-ZSM-5 catalyst at 400 °C, with ultra-high purity methane (>99.97 %), Adebajo *et al.* [35] achieved 4 % benzene conversion with 90 % selectivity to the primary product, toluene. With chemically pure methane (>99.0 %), the conversion doubled, however, selectivity to toluene almost dropped by one half. Therefore, the yield of toluene remains almost the same. Addition of small amounts of ethane or ethene resulted in much improved conversions, but it appeared again that it is not the methane that reacts. During methylation of toluene with methane [36] in the presence or absence of air on an H-ZSM-5 catalyst, it was observed that the activation of methane can only be achieved in air via formation of methanol [36]. When air was replaced with nitrogen, disproportionation of toluene was the only pathway for conversion of toluene. Given that methane activation seems to be currently almost impossible under mild conditions due to the thermodynamic limitations (cf. Figure 2.3), it will not be discussed further.

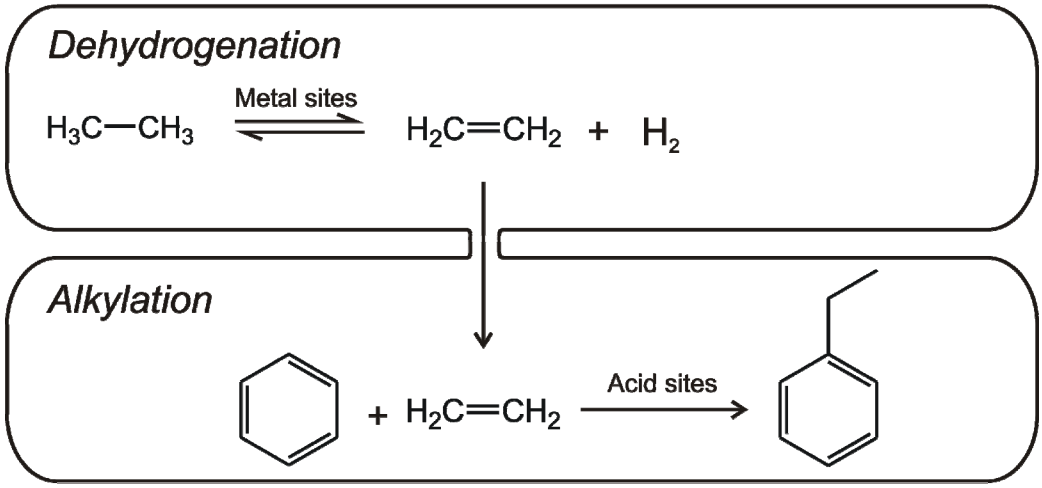


Fig. 2.5: Proposed mechanism for ethane activation on a bifunctional catalyst. First ethane is dehydrogenated on the metal sites, followed by migration of ethene to the acid sites, and finally alkylation takes place on the acid sites [7, 32].

### 2.2.2 Catalyst optimization

The alkylation of aromatics with alkanes has been studied on several types of bifunctional zeolites. The pore structure of the zeolite plays an important role both in terms of conversion as well as selectivity. Zeolites that have been tested include zeolite Y and ZSM-22 [2, 33], mordenite and MCM-22 [8], ZSM-11 [34], and ZSM-5 [2, 4, 38]. Table 2.2 shows toluene conversion and product selectivity during dehydroalkylation of toluene with ethane to ethyltoluenes for three different pore geometries. On a 0.3Pd/H-Y catalyst, relatively high conversions can be achieved [2]; however, the concentration of the desired ethyltoluenes was below the detection limit. Since the pores of zeolite Y are large, the disproportionation of toluene to xylenes and benzene dominated. On 0.7Pd/H-ZSM-22 with significantly smaller pores, the selectivity of xylenes and benzene was much lower. However, selectivity to the desired ethyltoluenes was also moderate. Hindered toluene accessibility to the acid sites inside the pores may result in lower activity; this is confirmed by the apparently low toluene conversion. 0.9Pd/H-ZSM-5 seems to be almost perfectly suited with almost as high conversions as zeolite Y, yet the selectivity to the desired ethyltoluenes is over 50 %. Similar trends have been repeatedly observed, confirming that bifunctional H-ZSM-5 catalysts are the best choice for dehydroalkylation of aromatics with alkanes.

Table 2.2: Toluene conversion and product selectivity during dehydroalkylation of toluene with ethane at 350 °C and 1 bar on various zeolites [2].

| Catalyst | 0.3Pd/H-Y | 0.9Pd/H-ZSM-5 | 0.7Pd/H-ZSM-22 |
|---|---|---|---|
| Pore system (largest pore) / nm | 0.74 x 0.74 | 0.53 x 0.56 | 0.46 x 0.57 |
| $X_{toluene}$ / % | 5.8 | 4.5 | 0.3 |
| $S_{hydrogen}$ / wt.-% | 2.9 | 1.8 | d.l.[1] |
| $S_{ethene}$ / wt.-% | d.l.[1] | d.l.[1] | 9.0 |
| $S_{propane}$ / wt.-% | d.l.[1] | 1.8 | d.l.[1] |
| $S_{benzene}$ / wt.-% | 48.4 | 17.9 | 12.2 |
| $S_{ethylbenzene}$ / wt.-% | d.l.[1] | 4.8 | 24.0 |
| $S_{xylenes}$ / wt.-% | 48.7 | 19.7 | 27.2 |
| $S_{ethyltoluenes}$ / wt.-% | d.l.[1] | 51.5 | 27.6 |

[1] below detection limit

Other factors of significance for catalyst optimization are the amount and type of the metal used. As already discussed, Ga has been used for alkylation of aromatics with propane, however, with ethane the attained conversions are very low [8]. Pt and Pd have also been used for alkylation with both propane and ethane. Sealy *et al.* [7] concluded that the type of metal does not significantly influence conversion or selectivity under their reaction conditions. These authors also studied the effect of varying the amount of metal and observed an increase in both conversion and selectivity with increasing metal content up to 1.0 wt.-% with little improvements above these metal contents. Todorova and Su [5] investigated the influence of the metal content for Ga/H-ZSM-5 and bimetallic Ga-Pt/H-ZSM-5, observing that addition of Pt improves both activity and selectivity. They explained this by reasoning that with the introduction of Pt the reaction mechanism shifts more towards dehydrogenation of propane. Furthermore, they observed that the bimetallic catalyst prevented or moderated coke deposition, since Pt enables hydrogen spillover from the noble metal to the zeolite surface.

The effect of the acid site density has also been reported for both propane and ethane as alkylating agents [4, 39]. Smirnov *et al.* [4] reported a propane conversion of 6.6 % on a 0.3Pt/H-ZSM-5 catalyst with an $n_{Si} / n_{Al}$ ratio of 325 (cf. Table 2.3), with 60 % selectivity to the desired cumene/*n*-propylbenzene. With an increase in the acid site density at an $n_{Si} / n_{Al}$ ratio of 51, conversion increased to 44.6 %, but the product selectivity shifted towards light alkanes and toluene, indicating severe cracking of reactants/products. Bressel *et al.* [39] proposed that, in the dehydroalkylation of toluene with ethane, bridging SiOHAl groups are

Table 2.3: Propane conversion and product selectivity during dehydroalkylation of benzene with propane on 0.3Pt/H-ZSM-5 with various $n_{Si} / n_{Al}$ ratios [4].

| $n_{Si} / n_{Al}$ | 325 | 104 | 51 |
|---|---|---|---|
| $X_{propane}$ / % | 6.6 | 23.0 | 44.6 |
| $S_{methane}$ / % | 0.4 | 8.5 | 4.4 |
| $S_{ethane}$ / % | 4.9 | 13.0 | 27.8 |
| $S_{propene}$ / % | 13.6 | 2.2 | 0.4 |
| $S_{toluene}$ / % | 1.3 | 4.3 | 19.6 |
| $S_{ethylbenzene}$ / % | 0.9 | 2.3 | 1.4 |
| $S_{cumene}$ / % | 23.3 | 8.5 | 1.6 |
| $S_{n\text{-propylbenzene}}$ / % | 36.6 | 16.9 | 3.2 |
| $S_{other}$ / % | 19.0 | 44.3 | 41.6 |

the active sites for the alkylation of toluene with *ethene* produced as an intermediate from the ethane reactant. With decreasing $n_{Si} / n_{Al}$ ratio, the concentration of bridging SiOHAl groups increases, promoting the alkylation with the intermediate *ethene*. However, the activity for toluene disproportionation also increases with decreasing $n_{Si} / n_{Al}$ ratio. Therefore, the authors suggest that for the dehydroalkylation of toluene with ethane to the isomeric ethyltoluenes, catalysts with intermediate concentrations of SiOHAl groups appear most promising. Bressel *et al.* [39] also report that a high crystallinity of the zeolite is beneficial for the catalytic performance in the dehydroalkylation of toluene with ethane. Lower crystallinities result in a reduced time-on-stream stability of the catalyst.

### 2.2.3 Influence of reaction conditions

As it has previously been shown dehydroalkylation reactions are endothermic and endergonic reactions. Therefore, higher temperatures would seem to favor such reactions. Some work has been done on the effects of temperature. During the dehydroalkylation of benzene with propane, Todorova and Su [38] varied the temperature from 400 to 600 °C. At 400 °C, conversion was negligible, below 1 %, however, they reported cumene and *n*-propylbenzene as the major products. With increasing temperature to 600 °C, conversion increased to 11 %, however, selectivity was sacrificed, with a product distribution including 35 % cumene and *n*-propylbenzene, with toluene, ethylbenzene, xylenes and polyaromatics formed as major by-products. During dehydroalkylation of benzene with propane, Smirnov *et al.* [4] observed

similar trends investigating the effect of temperature between 300 to 550 °C. At low temperatures, benzene conversion was very low, but with a reasonably good selectivity to cumene and *n*-propylbenzene. At the higher temperatures, a propane conversion over 60 % was observed. However, under these conditions the cracking of propane was prevalent. Sealy and Traa [2] also concluded that, in the dehydroalkylation of toluene with ethane, a mild reaction temperature of 350 °C is most suitable, above which too many side reactions take place.

Although the net change in number of moles is zero for the general dehydroalkylation reaction, the effect of pressure has been investigated for the dehydroalkylation of toluene with ethane [3]. According to Le Chatelier's principle, assuming ideal gas law behavior, no change in equilibrium is expected with increasing pressure. Table 2.4 represents the effect of pressure at 350 °C reported by Singer *et al.* [3]. At 350 °C and 1 bar, toluene conversion is approximately 6 %. With increasing pressure a maximum toluene conversion of 27 % is observed at a total pressure of 50 bar. Further increasing pressure results in a decrease in conversion, at 95 bar the toluene conversion is 19 %. At 1 bar, the yield of ethyltoluene isomers is 3.4 % increasing to a maximum of 7.8 % at 50 bar. The hydrogen yield is more constant, between 2 and 3 % over the entire pressure range, whereas it would be expected that hydrogen should follow the same trend as the ethyltoluenes, since hydrogen and ethyltoluenes

Table 2.4: Ethane and toluene conversion and yields during dehydroalkylation of toluene with ethane at 350 °C on 1.0Pd/H-ZSM-5 as a function of pressure (residence time was allowed to vary with pressure) and $\dot{n}_{\text{ethane}} / \dot{n}_{\text{toluene}}$ feed ratio of 6 [3].

| Pressure / bar | 1 | 10 | 30 | 50 | 68 | 95 |
|---|---|---|---|---|---|---|
| $X_{\text{ethane}}$ / % | 1.2 | 1.1 | 1.3 | 2.3 | 1.6 | 2.1 |
| $X_{\text{toluene}}$ / % | 6.2 | 9.6 | 16.2 | 27.1 | 20.5 | 19.2 |
| $Y_{\text{hydrogen}}$ / % | 2.6 | 2.2 | 3.3 | 2.5 | 2.4 | 2.5 |
| $Y_{\text{methane}}$ / % | 0.2 | 1.4 | 1.7 | 6.7 | 3.9 | 4.8 |
| $Y_{\text{propane}}$ / % | d.l.[1] | 0.3 | 0.6 | 0.8 | 0.8 | 0.7 |
| $Y_{\text{benzene}}$ / % | 0.4 | 1.0 | 2.1 | 4.2 | 3.5 | 2.8 |
| $Y_{\text{xylenes}}$ / % | 0.3 | 0.8 | 2.0 | 4.0 | 3.4 | 3.1 |
| $Y_{\text{ethylbenzene}}$ / % | 0.1 | 0.3 | 0.4 | 0.9 | 0.7 | 0.6 |
| $Y_{\text{ethyltoluenes}}$ / % | 3.4 | 4.0 | 4.9 | 7.8 | 5.2 | 4.4 |

[1] below detection limit

are formed in stoichiometric amounts. Furthermore, although the methane yield is very low at 1 bar, it increases to 6.7 % at 50 bar, a significant yield as methane is formed in amounts similar to ethyltoluenes at high pressure. The authors explain the low hydrogen yields by its consumption in secondary reactions, i.e., hydrogenation of coke precursors or carbonaceous deposits or toluene demethylation with hydrogen to form benzene and methane. They also report improved catalyst stability with increased conversion reasoning that at higher pressure hydrogenation of coke precursors may be improved. High pressure also has the advantage that high reactant concentrations may translate to high rates of reaction, which is industrially attractive.

## *2.3 Membrane reactors*

### 2.3.1 Background

A membrane may generally be defined as a *permselective barrier* between two phases. A permselective membrane allows the selective transport of certain species from one side of the membrane to the other. Biological membranes are often found in nature, and play a fundamental role in homeostasis (the regulation of an internal environment). Permselective membranes, in the form of polymeric membranes, have been extensively applied for water purification for decades. However, polymeric membranes are not suitable for chemical processes as often they cannot operate under the desired condition of typical chemical processes. Inorganic membrane reactors, however, are of special interest for the chemical process industry since they can withstand the harsh chemical and thermal conditions that are required and have been extensively studied over the past 3 decades [40-45]. However, membrane reactors are as yet not applied for large scale chemical processes mainly due to limitations that will be discussed shortly. Figure 2.6 shows a schematic representation of one possible setup for a membrane reactor. Catalysts may be packed outside (or alternatively inside) the permselective membrane. Feed gas is fed over the catalyst with a reaction product (e.g. $H_2$) permeating to the sweep side where it is extracted by a sweep gas (or alternatively a vacuum). The flow of the feed and sweep gases may be co- or countercurrent. The membrane is typically inert only acting as a barrier but it is possible that the membrane itself is also catalytically active, e.g., acidic-form zeolite membranes. Given that hydrogen is formed during the dehydroalkylation of toluene with ethane, the title reaction of this work, further discussions will primarily focus on $H_2$-selective membranes applied to dehydrogenative-type reactions. However, besides dehydrogenative-type reactions other reactions that have been

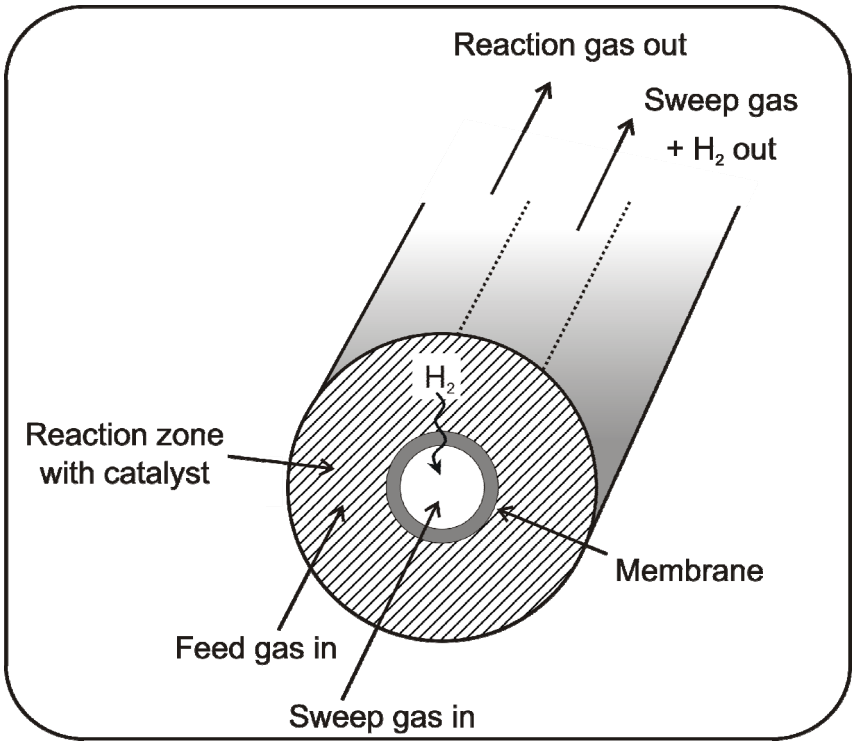


Fig. 2.6: Schematic representation of a membrane reactor setup. The catalyst is packed on one side of the membrane, with permselective species (e.g. $H_2$) being capable of permeating from the reaction zone to the sweep zone. The flow of the feed and sweep gases may be co- or countercurrent.

investigated in $H_2$-selective membrane reactors include methane steam reforming [46-48], methanol steam reforming [49-51], methane dry reforming [52-54], methane aromatization [55-57] and the water gas shift reaction [58-61].

### 2.3.2 Membrane reactor configurations

Figure 2.7 shows four possible configurations for application of inorganic membrane reactors. Configuration 2.7a) represents the most applied setup of membrane reactors in open literature: conversion or yield enhancement by removal of a product, typically applied to dehydrogenation reactions. As product C is removed the equilibrium shifts forwards, the overall effect being increased formation of D. Relevant examples will be discussed in detail in later sections. Configuration 2.7b) may be beneficial when more than one reaction is possible. A permselective membrane can enhance product selectivity by allowing permeation of an intermediate product C while rejecting undesired side products. Also, extraction of product C shifts the equilibrium to the left for the first reaction and to the right for the second reaction.

A more recent configuration is the controlled addition of reactant along the reactor by dosing

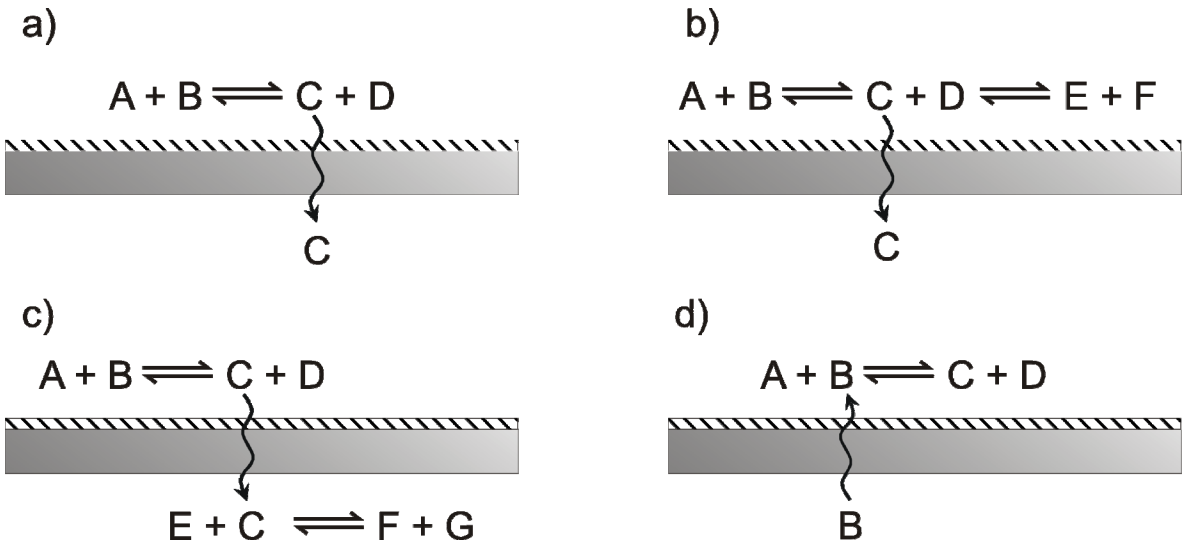


Fig. 2.7: Possible reaction schemes for application of inorganic membrane reactors. Conversion enhancement with catalytic membrane reactors: (a) yield enhancement by permeation of a reaction product of equilibrium-limited reactions; (b) selectivity enhancement by selective permeation of an intermediate, desired product, for reactions in series; (c) coupling of reactions; and (d) dosing a reactant through the membrane [42].

permeable species (cf. Figure 2.7d)). This is especially important since big improvements in selectivity can be achieved for partial hydrogenation (or oxidation) reactions if the concentration of hydrogen (or oxygen) is low throughout the reactor. In the case of oxidation-type reactions, an additional advantage is that the explosion limit may be entirely avoided. An interesting application of reactant dosing is the direct partial oxidation of benzene to phenol [62-64]. Phenol is typically produced from cumene via several reaction/separation steps. However, Niwa *et al*. [62] reported that, by dosing hydrogen in a Pd membrane reactor, benzene conversions of up to 16 % can be achieved with a selectivity to phenol of up to 97 % at 250 °C. They suggest that the reaction is possible since dissociated hydrogen on the Pd membrane surface of the reaction side reacts with oxygen, fed with benzene, forming an activated oxygen species which can then attack benzene. It is also suggested that dissociated hydrogen on the Pd membrane surface is more active [62].

Even more intriguing is a reaction scheme where two reactions are coupled on the two sides of the membrane (cf. Figure 2.7c)). On one side of the membrane the dehydrogenation-type (endothermic) reactions takes place, and on the other side hydrogenation-type (exothermic) reactions. Hydrogen formed during the dehydrogenation reactions permeates through the

membrane and takes part in the hydrogenation reaction. An added advantage to such a scheme is that the exothermic reaction can provide the heat for the endothermic reaction. However, the number of degrees of freedom for process control is decreased in such cases. Despite the potential advantages and benefits, little experimental work has been done on reaction coupling in membrane reactors. Efforts have revolved around changing of the sweep gas from an inert species (e.g., $N_2$) to air (or other such oxidants) during dehydrogenation reactions [65, 66]. Gobina *et al*. [65] observed an improvement of 20 % in conversion (almost doubling conversion) during ethane dehydrogenation as a result of using air rather than nitrogen in a membrane reactor. Itoh and Wu [66] observed conversions of about 90 % with air as the sweep gas compared to about 40 % with an inert sweep gas during dehydrogenation of cyclohexane. However, it must be pointed out that simply burning the hydrogen seems to be wasteful.

### 2.3.3 Choice of membrane type

Table 2.5 shows properties of selected $H_2$-selective membranes. There are two broad categories of hydrogen-selective membrane types, namely porous and dense. For $H_2$-selective membranes, selectivity is defined as the ratio of permeability of hydrogen to nitrogen. Selectivity for porous membranes is poor, reaching about 20 and 100 for carbon and zeolite membranes, respectively. Therefore, they are unattractive as materials for membrane reactors since in such cases high selectivity is of paramount importance. In contrast, dense membranes show a much higher selectivity, with almost 100 % selectivity to $H_2$. Ceramic membranes have a rather low flux of hydrogen, and very high temperatures are required before they

Table 2.5: Properties and operating range for selected $H_2$-selective membranes [43].

| Membrane Type | Dense | | Porous | |
|---|---|---|---|---|
| | Metallic | Ceramic | Zeolites | Carbon |
| $H_2$ selectivity[‡] | > 1000 | > 1000 | 5 - 139 | 4 - 20 |
| $H_2$ flux[†] | 60 - 300 | 6 - 80 | 60 - 300 | 10 - 200 |
| Temperature / °C | 300 - 600 | 600 - 900 | 200 - 600 | 500 - 900 |
| Materials | Palladium and Pd alloys | Proton conductors | Zeolites | Carbon |
| Transport mechanism | Solution-diffusion | Solution-diffusion | Molecular sieving | Surface diffusion |

[‡]ratio of permeability of hydrogen to nitrogen

[†]$10^{-3}$ mol·m$^{-2}$·s$^{-1}$ at pressure difference of 1 bar

become permeable. However, metal membranes have much higher flux and may be operated under somewhat milder conditions, making these particularly interesting for use in membrane reactors.

In porous membranes various mechanisms of transport may prevail, e.g., molecular sieving, surface diffusion, Knudsen diffusion, etc. [45] or a combination of these. In dense membranes solution-diffusion is the only mechanism for transport (with the precondition of high-quality membranes), hence the higher selectivity. There are five critical steps for transport of hydrogen by the solution-diffusion mechanism:

- Dissociative adsorption
- Surface to bulk transport
- Atomic diffusion
- Bulk to surface transport, and
- Recombinative desorption.

In most cases, the rate of hydrogen transfer is limited by atomic diffusion. Solubility of atomic hydrogen in the Pd lattice is described by Sieverts' constant assuming a dilute solution and minimal interaction between hydrogen atoms. The power dependency of 0.5 is due to hydrogen diffusion through the metal in the atomic form [45]. Deviations from Sieverts' law may result at low temperatures (<150 °C) or when the films are very thin and dissociation or bulk transport processes become rate limiting. Therefore the power dependency may vary between 0.5 and 1 for composite membranes. Equation (2.1) may be used to define permeance of hydrogen, $J_{H_2}$, in Pd membranes, as a function of membrane thickness, $\delta$, hydrogen partial pressure, $p_{H_2}$, and Sieverts' law rate constant, $k_{perm}$, which follows an Arrhenius-type dependency on temperature.

$$J_{H_2} = \frac{k_{perm}}{\delta}\left(p_{H_2,reaction}^{0.5} - p_{H_2,sweep}^{0.5}\right) \tag{2.1}$$

Figure 2.8 shows the hydrogen permeabilities for selected metals. Pd has a reasonably high hydrogen permeability, at least 2 orders of magnitude higher than Fe, although there are several other metals (including Ta, Zr, and Nb [45, 67], not shown in Figure 2.8) with higher permeability for hydrogen. Furthermore, the hydrogen permeability decreases for Pd with decreasing temperature (since hydrogen solubility decreases with increasing temperature)

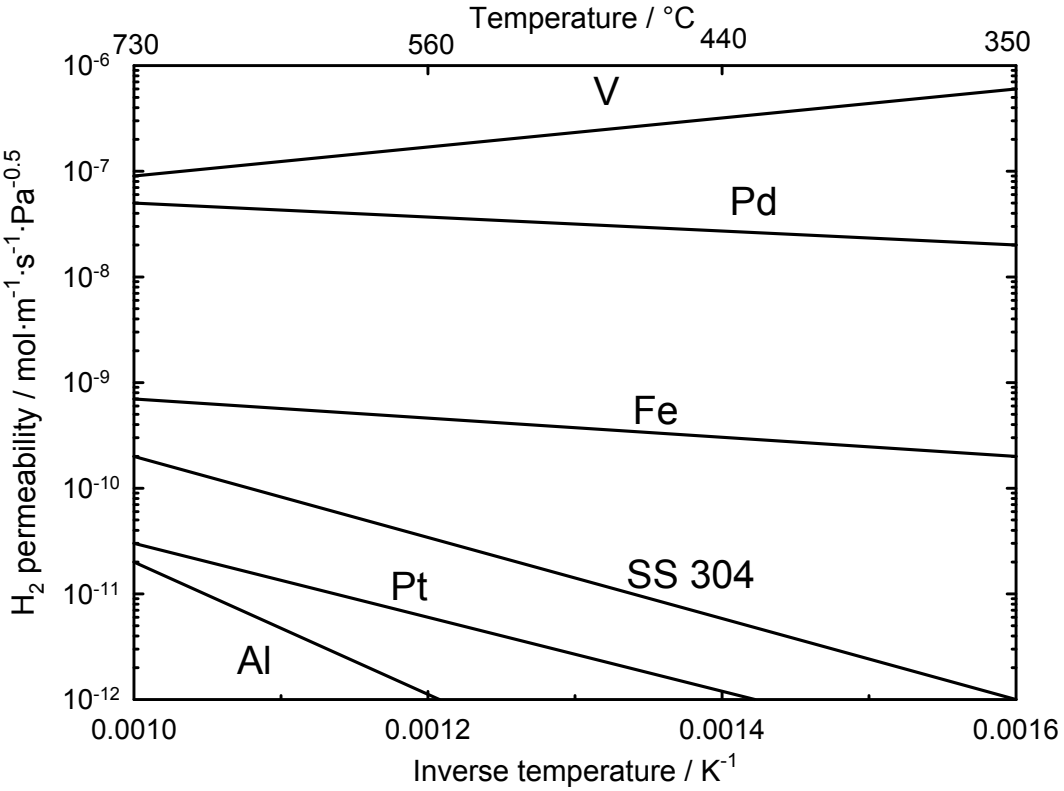


Fig. 2.8: Hydrogen permeability for selected metals (SS: stainless steel) as a function of temperature, adapted from [67]. Note, top temperature scale in not linear.

whereas for some metals, e.g., V and Nb, permeability actually increases with decreasing temperatures, making these metals very interesting for use especially since operation at lower temperatures is even encouraged. However, Pd is the best choice as a membrane material since the dissociative adsorption of hydrogen is much faster on Pd than on any other metal [67].

### 2.3.4 Benefits and limitations of Pd-based membrane reactors

Table 2.7 represents benefits versus limitations of Pd membrane reactors. Important advantages of Pd membrane reactors include an almost infinite selectivity to hydrogen at typical temperatures of common chemical processes and resistance under harsh chemical and thermal conditions. Since reaction and separation take place in one unit a smaller downstream separations train is required, resulting in process intensification. Additionally, by shifting equilibrium, higher conversions per pass are also expected for reactions where thermodynamics is limiting, reducing reactor size. Finally, high-purity hydrogen, with impurity concentrations in the ppb (parts per billion) range, can be obtained due to the high selectivity to hydrogen. However, typically a sweep gas is required in order to remove the

Table 2.7: Benefits versus limitations of Pd membrane reactors, adapted from [45].

| Benefits | Limitations |
|---|---|
| High selectivity to hydrogen | Scale up very difficult |
| Good chemical and thermal stability | High costs |
| Process intensification | Defect formation |
| High mechanical stability | Low surface area to catalyst mass |
| Higher conversion per pass | Low-pressure $H_2$ produced |
| High-purity hydrogen | Pd phase transition |

permeated hydrogen which results in an undesired dilution of hydrogen. Additionally, permeated hydrogen is typically at a low pressure so that expensive compression is required. A low membrane surface area to catalyst mass also causes additional issues for membrane synthesis, and scale up also becomes rather difficult and complicated. Pd membranes are also sensitive to $H_2S$, in the presence of which catastrophic defects may form.

Moreover, Pd is a very expensive metal, therefore, material and manufacturing costs can quickly make Pd membrane reactors economically unattractive. Pure Pd has two hydride phases, above 293 °C only the $\alpha$-phase can exist, while both the $\alpha$- and $\beta$-phases may coexist below this temperature. The single innovative solution to these problems has been alloying. Uemiya *et al.* [68] reported that alloying Pd with Ag, with an optimum composition of $Pd_{0.77}Ag_{0.23}$, can improve permeation and stability of palladium by elimination of the $\beta$-phase, simultaneously resulting in reduced Pd consumption. Even more intriguing is Pd alloyed with Cu. $Pd_{0.6}Cu_{0.4}$ membranes have shown improved permeability, while showing good stability against $H_2S$ [69-71]. Other alloying elements include: Ni, Y, and Ru [45].

### 2.3.5 Application of membrane reactors for dehydrogenation reactions

Besides the various reforming reactions of methane and methanol previously mentioned, dehydrogenation of light alkanes, alkyl aromatics and alcohols has been the main focus of experimental studies using Pd-based membrane reactors in literature. Table 2.8 gives selected examples of the aforementioned reactions. If one considers alkane dehydrogenation, a correlation can be made between the shift in conversion and the size of the reacting alkane. This may be due to an increase in equilibrium conversion with increasing alkane size. With

Table 2.8: Selected examples of dehydrogenation reactions in Pd-based membrane reactors described in the open literature.

| Dehydrogenation | Shift in $X_{reactant}$ / % | Notes | References |
|---|---|---|---|
| Ethane | ca. 20 | Reactive sweep gas; methane formation suppressed | [65, 72, 73] |
| Propane | ca. 35 | Reactive sweep gas; positive effect of pressure | [74-77] |
| *i*-/*n*-butane | ca. 15 | hydrogenolysis suppression | [78-81] |
| Cyclohexane | ca. 45 | Reactive sweep gas | [66, 82, 83] |
| Methylcyclohexane | ca. 50 | Mild conditions: 175 °C | [84] |
| Methanol/ethanol | ca. 35 | Negative effect of pressure; co-feed of oxygen required | [85, 86] |
| Ethylbenzene | ca. 15 | Severe dilution with water/ steam; temperature > 580 °C | [76, 87] |

increasing conversion, more hydrogen is produced, hence more hydrogen can permeate through the membrane reactor resulting in improved conversion.

The use of a reactive sweep gas has been popular and typically results in a significant increase in the shift of conversion regardless of the reaction. Typically, conversions are doubled in the presence of a reactive sweep gas. Using nitrogen as sweep gas Yildirim *et al.* [74] achieved 15 % conversion during propane dehydrogenation, with progressive increase in conversion with the introduction of CO or $O_2$ as sweep gas. However, it should be mentioned again that it seems wasteful to burn valuable hydrogen. The application of membrane reactors also seems to improve selectivity by suppressing side reactions which consume hydrogen [73, 81], such as methane formation by hydrogenolysis or hydrocracking of higher alkanes. It has also been reported that in a membrane reactor the hydrogen permeability of the membrane is much larger than the rate of hydrogen transfer to the membrane, so that the reaction rate was the determining factor for hydrogen recovery [80]. During ethanol/methanol dehydrogenation [85], high conversions were achieved, however, mainly side reactions of the reactant dominated. $O_2$ had to be co-fed with the alcohol in order to avoid contamination of the membrane surface by product decomposition. Finally, dehydrogenation of ethylbenzene to styrene which is an important industrial process has been studied but with little success compared to dehydrogenation of light alkanes. Typically, only a small increase in conversion

has been achieved, possibly due to dilution of ethylbenzene with water in a large excess (up to 6 times) which drastically reduces the partial pressure of hydrogen within the membrane reactor and hence the permeation rate.

Although the reaction pressure is a key parameter for industrial processes it has not gained much attention, possibly due to the fact that most dehydrogenation reactions result in an increase in the total number of moles. Hence, increasing pressure would have a negative effect on thermodynamics. Recently, Lin and Chang [86] investigated the effect of pressure up to 10 bar during ethanol dehydrogenation. They observed that with increasing pressure ethanol yield decreased from about 40 % at 1 bar to 30 % at 10 bar. Lee *et al.* [88] studied the effect of pressure, from 1 to 20 bar, applying a $H_2$-selective silica-based membrane for dry reforming of methane, observing severe losses in conversion with increasing pressure. However, hydrogen permeability through the membrane increased, consequently the yield of hydrogen first increased, and then decreased due to the unfavorable equilibrium at high pressure. During methane steam reforming, Mori *et al.* [48] observed a 25 % loss in methane conversion with increasing pressure up to 10 bar, even though hydrogen recovery improved. Interestingly, during propane dehydrogenation in a membrane reactor, Hou and Hughes [77] achieved a propane conversion of 30 % at 1 bar and 35 % at 3 bar. The authors attributed the higher conversion to an increased rate in hydrogen permeation which compensated for lowering of the equilibrium conversion.

### 2.3.6 Modeling of membrane processes

Various aspects of membrane processes have been modeled with most studies focusing on macro-scale models for tubular membrane reactors. Kinetic models for prediction of concentration profiles typically involve derivation of mole balances, applying a differential volume, on the reaction and sweep sides. The reaction side is linked to the sweep side by applying Sieverts' law for hydrogen permeation, with hydrogen formation modeled as generation and hydrogen permeation modeled as a sink. Most models assume 100 % selectivity of the membrane to hydrogen. Typically, the molar flow of a species on the reaction side, assuming that only axial concentration profiles are significant, may be represented according to equation (2.2) [26, 77, 83, 89-91]. Inclusion of radial concentration profiles has also been studied [65, 79, 92-96], however, from experimental laboratory scale results radial concentration profiles seem to be negligible due to the "small scale" units that have been used in studies [65].

$$\frac{d\dot{n}_i}{dz} = \sum_{j=1}^{n} \left( \rho_{bed} \cdot A_{reactor} \cdot \nu_{i,j} \cdot r_{i,j} \right) - J_i \cdot r_R \tag{2.2}$$

The hydrogen mass balance on the sweep side may be represented according to equation (2.3), with $J_i$ in equations (2.2 and 2.3) defined according to equation (2.1) for hydrogen and as zero for other species if one assumes 100 % selectivity to hydrogen. $r_R$ represents the ratio of reactor volume to membrane area, $A_{reactor}$ represents the cross-sectional area of the reactor, $\nu_{i,j}$ is the stoichiometric coefficient of species i in reaction j, $\rho_{bed}$ is the catalyst bed density and $r_{i,j}$ is the rate of reaction of species i in reaction j.

$$\frac{d\dot{n}_i}{dz} = J_i \cdot r_R \tag{2.3}$$

Since dehydrogenation reactions are typically endothermic by nature, energy balances have been derived to study the energy requirements of the reaction/separation system [90, 95]. However, most laboratory-scale setups are run as close to isothermal conditions as possible. Equations (2.4 and 2.5) depict the general form of the energy balances on the reaction and sweep sides, assuming inert sweep gas and that only the axial temperature profile is significant, $Cp_i$ the heat capacity of species i, $\Delta H_j^{rxn}$ change in enthalpy of reaction j, $\Delta T$ the temperature difference between the reaction and sweep side, with $J_i$ and $\dot{n}_i$ according to equation (2.1 to 2.3):

$$\sum_{i=1}^{n} \dot{n}_i \cdot Cp_i \cdot \frac{dT}{dz} = \sum_{j=1}^{n} \left( \rho_{bed} \cdot A_{reactor} \cdot -\Delta H_j^{rxn} \cdot \nu_{i,j} \cdot r_{i,j} \right) - \sum_{i=1}^{n} J_i Cp_i \cdot \Delta T \cdot r_R \tag{2.4}$$

$$\sum_{i=1}^{n} \dot{n}_i \cdot Cp_i \cdot \frac{dT}{dz} = \sum_{i=1}^{n} J_i Cp_i \cdot \Delta T \cdot r_R \tag{2.5}$$

Currently, simple models seem to be very adequate in the simulation of laboratory-scale processes. Typically, consideration of only axial profiles gives good estimates of a wide variety of systems. However, once membrane processes undergo scale-up, simple models may no longer be sufficient to accurately describe systems, therefore, it is appropriate that some work has also been done on modeling more complex systems, where especially heat transfer plays a more significant role. Resulting boundary-value problems are solved, with the appropriate boundary conditions, typically using various Runge-Kutta methods, in the case of ordinary differential equations. Partial differential equations are solved using collocation techniques. In cases where experimental data are used to fit models, a sum of squares residual

is set up, e.g., equation (2.6), and minimized [97] typically using the well known Levenberg-Marquardt algorithm (LMA) [98].

$$\mathrm{SSR} = \sum_{\mathrm{i=1}}^{\mathrm{n}} \left( \frac{x_{\mathrm{i}}^{\mathrm{exp.}} - x_{\mathrm{i}}^{\mathrm{model}}}{x_{\mathrm{i}}^{\mathrm{exp.}}} \right)^2 \tag{2.6}$$

Besides kinetic models, some work has been done in order to evaluate the maximum shift in equilibrium in a membrane reactor. Several approaches have been taken; however, the same criterion must always be met, namely, the shift in equilibrium reaches a maximum when the radial driving force for hydrogen across the membrane is zero as shown in equation (2.7):

$$\left( \frac{dp_{\mathrm{H_2}}}{dr} \right)_{T,P} = 0 \tag{2.7}$$

One approach [96] has been applying kinetic models as described in equations (2.1 to 2.3) and solving the differential equations until the hydrogen pressure is equal on the reaction and sweep sides. In an attempt to take a simple approach, a tanks-in-series model has been proposed [90, 99] where hydrogen is removed in steps until the hydrogen pressures on both sides of the membrane are equal. An alternative approach has originally been taken by Itoh [100, 101] who proposed a thermodynamic model for both the reaction and the separation. Various flow models have also been applied for the reaction/sweep sides [72, 101, 102], the best being a countercurrent model, although experimentally, on laboratory-scale, there is little difference between these setups as there is significant back-mixing/dispersion.

# 3 Experimental and modeling sections

The first part of the following chapter will outline the experimental approach including details on synthesis and characterization of zeolites and the membrane. Furthermore, the experimental setup for catalytic experiments, product analysis, and evaluation of results will be described. In the second part of this chapter, the various tools and techniques used for modeling of relevant equilibria, and kinetics of the title and side reactions will be shown.

## *3.1 Experimental section*

### 3.1.1 Catalyst synthesis

Two types of zeolite ZSM-5 were synthesized during this work, namely template-containing and template-free ZSM-5, with different $n_{Si} / n_{Al}$ ratios. Template-free zeolite ZSM-5 was synthesized from Kieselsol, sodium aluminate, sodium hydroxide (cf. Table 3.1), and demineralized water, producing a synthesis gel with the molar composition 60 $SiO_2$ : $Al_2O_3$ : 9 $Na_2O$ : 2400 $H_2O$. Crystallization occurred within 5 days in a stainless-steel autoclave ($V$ = 1000 $cm^3$) at 160 °C under stirring at 400 $min^{-1}$ [103]. Template-assisted synthesis of ZSM-5 was carried out as follows: 4.6 g tetrapropylammonium bromide and 2.00 g $Al(NO_3)_3 \cdot 9H_2O$ were dissolved in 32 $cm^3$ demineralized water. Then, 32.0 g Ludox AS 40 were added. To the well dispersed mixture, 43.6 $cm^3$ ammonia solution (25 wt.-%) were added. Crystallization occurred under rotation in stainless-steel autoclaves ($V$ = 300 $cm^3$) at 160 °C within 5 days [39]. The template was removed by calcining in air at 550 °C for 24 h.

### 3.1.2 Post-synthesis procedure

The resulting zeolite was subjected to two consecutive ion exchange steps with an aqueous solution (1 $mol \cdot dm^{-3}$) of $NH_4NO_3$ at 80 °C, each step lasting for 4 h. Pd, Ru, or Pt ion exchange was carried out by adding an aqueous solution of a noble metal salt (cf. Table 3.1) dropwise to a suspension of the ammonium ion-exchanged zeolite, under vigorous stirring, at room temperature. The zeolite powder was pressed without a binder, crushed and sieved to a particle size between 0.2 and 0.3 mm.

The catalyst was activated *in situ*, prior to starting the experiment. Typically, to achieve a high dispersion of the noble metal, the catalyst was first heated in flowing synthetic air

(50 $cm^3 \cdot min^{-1}$) at a rate of 2 °C·$min^{-1}$ to a final temperature of 300 °C, and held for 22 h at this

Table 3.1: Source and purity of chemicals for catalyst synthesis, modification and catalytic experiments.

| Chemicals | Source, purity |
|---|---|
| Zeolite synthesis and modification | |
| Ammonia solution | Merck, 25 wt.-% |
| Ammonium nitrate | Merck, >98.5 wt.-% |
| Hexaamminruthenium (III) chloride | Degussa, 32.32 % Ru |
| Kieselsol VP-AC 4038 | Bayer AG , 30 wt.-% $SiO_2$, 70 wt.-% $H_2O$ |
| Ludox AS-40 | Sigma-Aldrich, 40 wt.-% $SiO_2$ in water |
| Methanol | Riedel-de Haën, >99.8 % |
| Sodium aluminate | Riedel-de Haën , 54 wt.-% $Al_2O_3$, 41 wt.-% $Na_2O$ |
| Sodium hydroxide | Merck, >99 % |
| Tetraamminpalladium (II) chloride | ChemPur, 42.64 % Pd |
| Tetraamminplatinum (II) chloride | ChemPur, 55.63 % Pt |
| Tetrapropylammonium bromide | Fluka, >97 % |
| Catalytic experiments | |
| Chromosorb | Macherey-Nagel, P-NAW |
| Ethane | Westfalen AG, 99.95 % |
| Hydrogen | Westfalen AG, 99.999 % |
| Nitrogen | Westfalen AG, 99.999 % |
| *p*-Ethyltoluene | Merck, >97 % |
| *p*-Xylene | Fluka, >99 % |
| Synthetic air | Westfalen AG, 20.5 % $O_2$, 79.5 % $N_2$ |
| Toluene | Merck, >99.9 % |

temperature. Next, the catalyst was purged with nitrogen for 1 h to ensure that no oxygen remained before the introduction of hydrogen during the next step. During the subsequent reduction phase, the catalyst was heated in flowing hydrogen (50 $cm^3 \cdot min^{-1}$) at 2 °C·$min^{-1}$ to 350 °C, and held at this temperature for 22 h. Catalysts prepared for the investigation of the effect of noble metal type were activated with a heating rate of 0.25 °C·$min^{-1}$ during activation with synthetic air, with no holding time once 300 °C were reached, and activation with hydrogen was carried out for only 4 h. Furthermore, since Ru forms volatile, toxic oxides

in the presence of oxygen, in the first step of the activation inert nitrogen was used in place of synthetic air in order to avoid formation of ruthenium oxides.

In the case of the catalyst for application in the membrane reactor, the catalyst was activated externally first, then pre-coked, in order to avoid damage to the sensitive membrane, according to Ref. [104], since uncontrolled coking during the reaction may result in defect formation of the membrane. Pre-coking was accomplished by first activating the catalyst as described above at 2 °C·min$^{-1}$ in a quartz reactor. After the activation was complete, the reactor was cooled to room temperature and methanol was fed at room temperature through a methanol saturator containing Chromosorb for 24 h. This was followed by heating the reactor, under static condition, i.e., no gas flowing into the reactor, at 2 °C·min$^{-1}$ to 500 °C and holding for 2 h. Subsequently, the pre-coked samples were subjected to an additional coke modification treatment under hydrogen (50 cm$^3$·min$^{-1}$) at 500 °C for 24 h. Bauer *et al.* [104] showed that by pre-coking with the above procedure using methanol, only soft coke (high $n_H$ / $n_C$) is formed inside the pores of ZSM-5, whereas hard coke (low $n_H$ / $n_C$) forms on the outer surface. During the final hydrogen treatment step, the coke inside the pores can be removed more easily than the coke on the outer surface. Therefore, the loss of activity should result from deactivation of unselective catalytic sites on the outer surface of zeolite crystals.

### 3.1.3 Catalyst characterization

The crystal size and morphology of the zeolites were determined by SEM (scanning electron microscopy, CAM SCAN 44). Figure 3.1 clearly demonstrates that the template-assisted synthesis produces clean crystals with the well known coffin shape typically associated with ZSM-5 crystals. There seems to be a lot of amorphous material on the template-free synthesized ZSM-5. The two types of zeolite ZSM-5 synthesized have a similar average crystal size of about 3 to 5 μm in length (cf. Table 3.2).

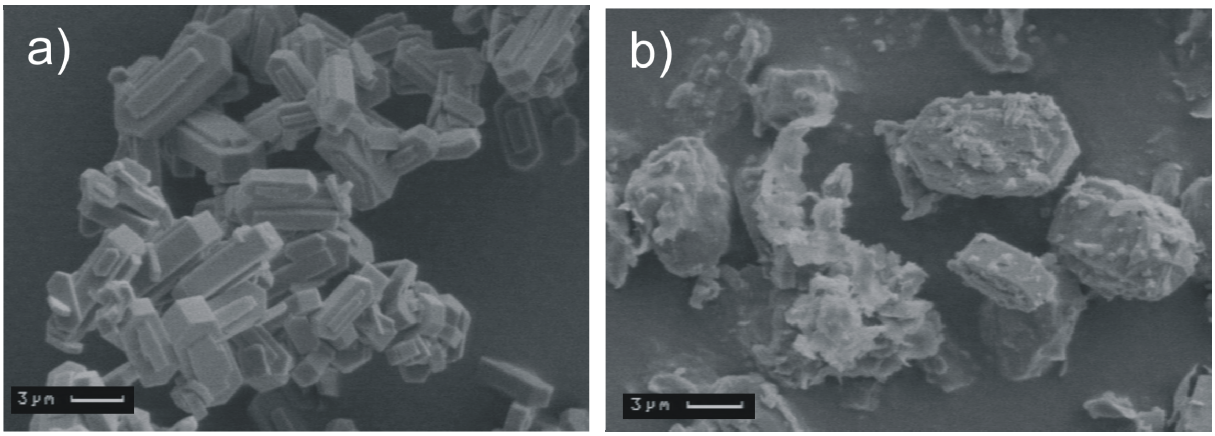

Fig. 3.1: Scanning electron micrographs of template-assisted (a) and template-free (b) as-synthesized zeolites ZSM-5.

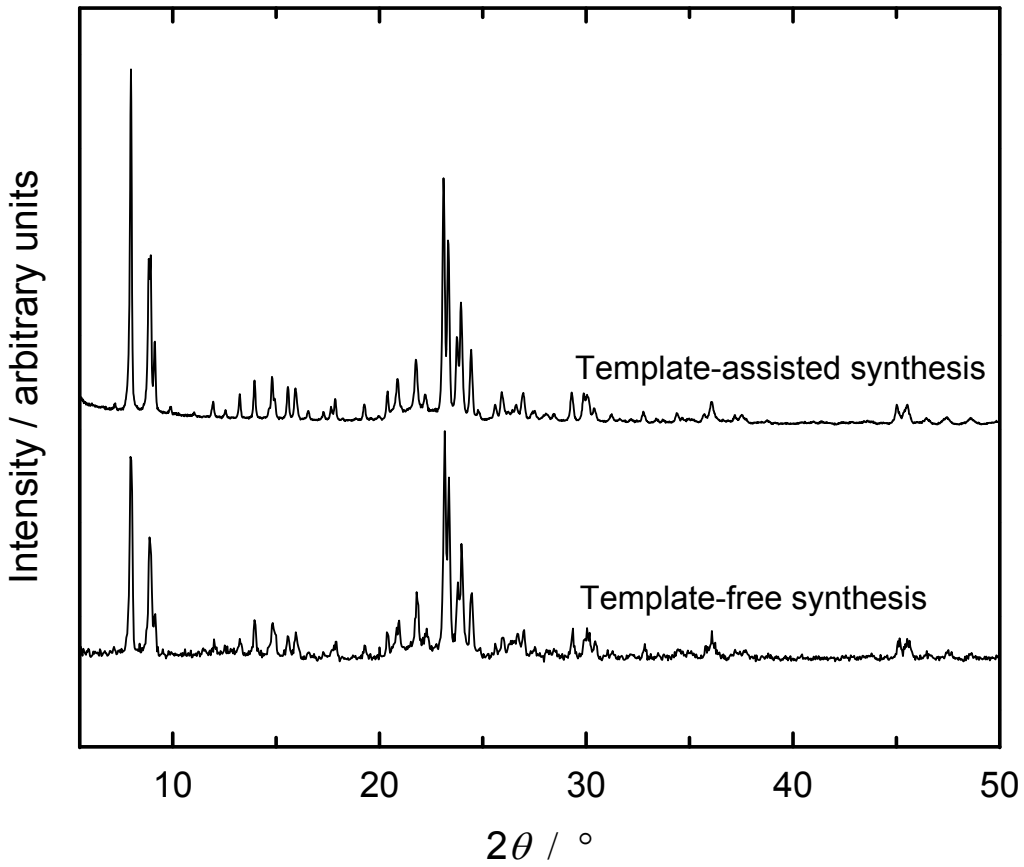


Fig. 3.2: XRD patterns for H-ZSM-5 synthesized with and without template.

The elemental composition of the catalysts was determined by ICP/OES (inductively coupled plasma optical emission spectroscopy, Varian VISTA-MPX). From the elemental analysis, the $n_{Si} / n_{Al}$ ratio was determined to be approximately 41 and 28 for the template-assisted and template-free as-synthesized zeolites, respectively. The noble metal content was also determined by elemental analysis (cf. Table 3.2). The results revealed a higher than usual amount of $Na^+$ ions after the completion of ammonium ion exchange for template-free synthesized ZSM-5, with an $n_{Na} / n_{Al}$ ratio of approximately 0.07, whereas no sodium was used during the template-assisted synthesis (cf. Table 3.2).

The zeolite phase was characterized by XRD (X-ray diffraction, Bruker Diffractometer D8Advance with a $CuK_\alpha$-source). The diffractometer was operated at 40 kV, between $5° < 2\theta < 50°$ with scans taken at 0.02° at 2 s intervals. The diffractograms showed that the

desired MFI-type zeolites were successfully synthesized (cf. Figure 3.2), with the template-assisted synthesis showing better crystallinity, in accordance with SEM micrographs.

Table 3.2: Physical properties of the as-synthesized zeolites.

| Property | Template-assisted | Template-free |
|---|---|---|
| Crystal size / µm | 3 to 5 | 3 to 5 |
| $n_{Si} / n_{Al}$ | 41 | 28 |
| $n_{Na} / n_{Al}$ | d.l.[1] | 0.07 |
| $m_{Ru} / (m_{dry\ catalyst} + m_{Ru})$ / wt.-% | 0.9 | - |
| $m_{Pd} / (m_{dry\ catalyst} + m_{Pd})$ / wt.-% | 1.0 | - |
| $m_{Pt} / (m_{dry\ catalyst} + m_{Pt})$ / wt.-% | 1.8 | 0.4 |
| Water content / wt.-% | 7.0 | 5.0 |
| BET surface area / $m^2 \cdot g^{-1}$ | 310 | - |
| Pore volume / $10^{-6}$ $m^3 \cdot g^{-1}$ | 0.02 | - |

[1] below detection limit

In order to ensure constant catalyst mass, prior to the catalytic experiments, the catalyst was placed in a desiccator with a saturated calcium nitrate solution for a minimum of 2 days at room temperature. Thereafter, the water content of the zeolite was determined by thermogravimetric analysis using a Thermowaage Setsys TG 16/18. The typical water contents were 7.0 and 5.0 for the template-assisted and template-free synthesized zeolites, respectively. The BET surface area and pore volume of the template-assisted synthesized zeolite was measured by $N_2$ adsorption at 77 K using an ASAP 2000 instrument (Micromeritics) to be approximately 310 $m^2 \cdot g^{-1}$ and $2 \cdot 10^{-8}$ $m^3 \cdot g^{-1}$, respectively. After the catalytic experiments, a CHN analysis of the coked catalysts was accomplished using a Vario EL analyzer (Elementar Analysensysteme).

### 3.1.4 Membrane characterization

Extensive characterization of the membrane was beyond the scope of this work, in contractual agreement with the provider of the membranes (REB Research & Consulting, Ferndale, MI, USA). However, permeation experiments were carried out on the membrane in order to gauge the permeation properties of the membrane. The membrane showed 100 % selectivity to hydrogen, i.e., only hydrogen was detected on the sweep side. From permeation experiments at various temperatures, the pre-exponential factor and activation energy of Sieverts' rate law constant for hydrogen permeation were determined to be $1.15 \cdot 10^{-5}$ $mol \cdot s^{-1} \cdot m^{-1} \cdot Pa^{-0.5}$ and 16.9 $kJ \cdot mol^{-1}$, respectively (cf. Figure 3.3).

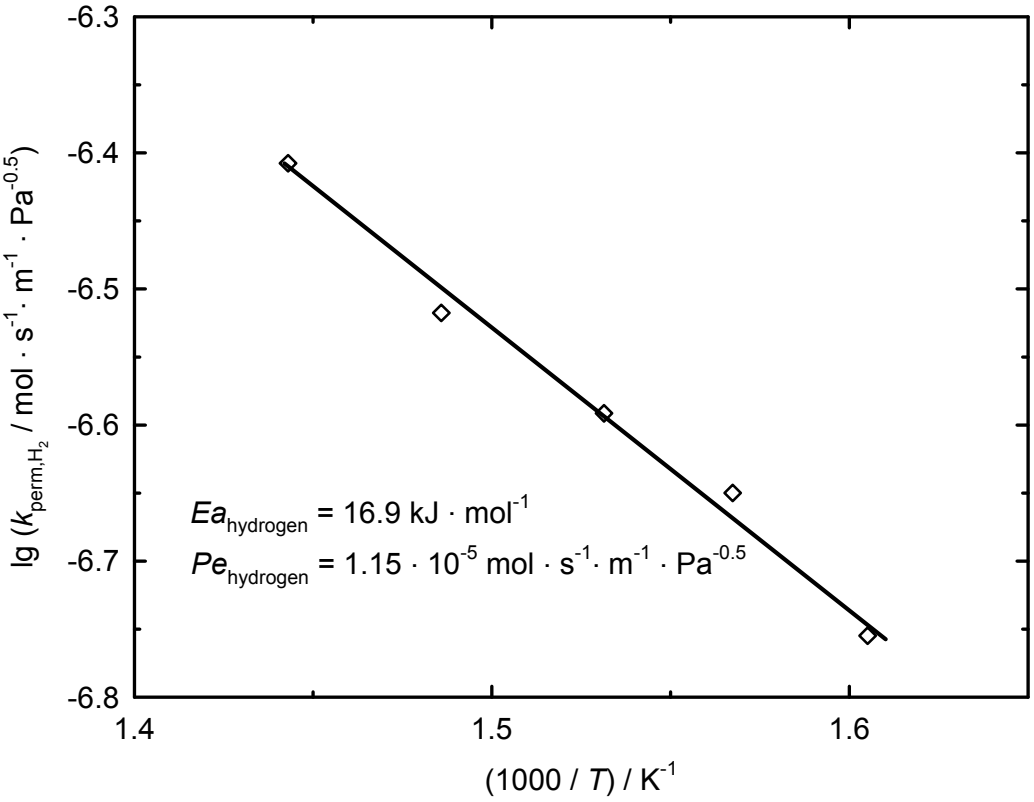


Fig. 3.3: Hydrogen permeation as a function of temperature in the membrane reactor.

### 3.1.5 Catalytic experiments

Figure 3.4 shows a schematic of the setup for catalytic testing in a packed-bed membrane reactor. Measurements for the feed composition can be taken independent of the reactor, if valve BV2 (cf. Figure 3.4) is closed. In the case of the traditional packed bed setup (cf. Figure 3.5) where the catalyst is activated *in situ*, hydrogen, nitrogen or synthetic air can be fed to the system via valve V10 during feed measurements. Once the reaction is to be started valve V10 and BV1 are closed and valve BV2 is opened so that ethane/nitrogen passes through the saturator first before entering the reactor. The ethane and nitrogen fluxes were controlled by mass flow controllers (Brooks 5800S). The mass flow controllers showed good short-term stability (cf. Figure 7.1). The $\dot{n}_{\text{aromatic}}$ feed rate was adjusted by varying the saturator temperature ($T_{\text{sat}}$) using a programmable temperature controller (Omega CN 3000). The desired saturator temperature was estimated using equation (3.1) with constants according to Ref. [105] (also cf. Table 7.1). The long-term stability of the saturator was also good, and the saturator typically ran dry after approximately 24 h (cf. Figure 7.2).

$$\ln\left(p_{\text{i}}^{vap} / p_{\text{atm}}\right) = B_{\text{i}} + \frac{C_{\text{i}}}{T_{\text{sat}}} + D_{\text{i}} \cdot \ln\left(T_{\text{sat}} / T_{\text{ref}}\right) + E_{\text{i}} \cdot \left(T_{\text{sat}} / T_{\text{ref}}\right)^{F_{\text{i}}} \qquad (3.1)$$

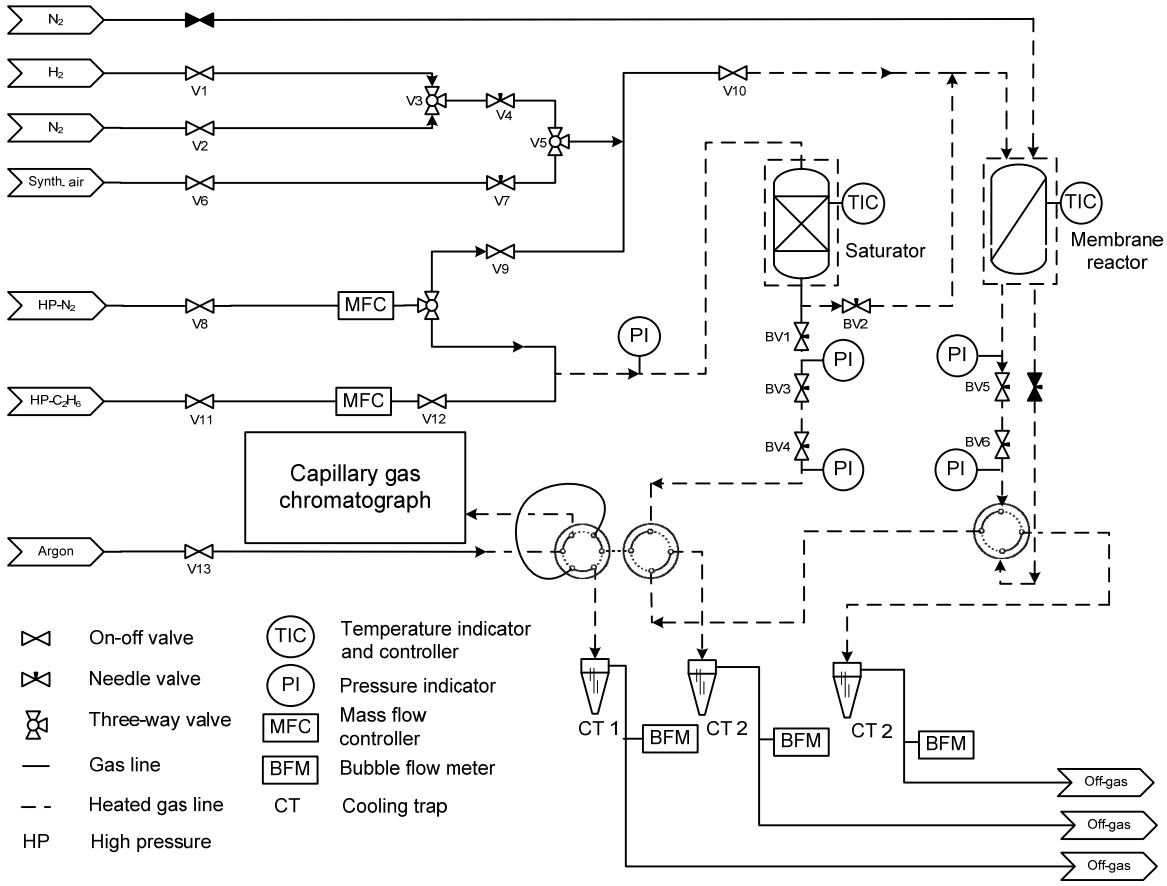


Fig. 3.4: Schematic representation of the high-pressure membrane reactor set up, with a Pd-based, packed-bed membrane reactor (cf. Figure 7.3 for schematic). Reaction-side tube inner diameter: $6.0 \cdot 10^{-3}$ m, sweep-side tube outer diameter: $2.0 \cdot 10^{-3}$ m [106].

In the case of hydrocracking experiments, a 2 % $H_2$ in $N_2$ gas mixture was prepared by mixing gases. Mass-transfer correlations were used to calculate mass-transfer coefficients in order to ensure that external mass transfer was not limiting. Calculated mass-transfer coefficients were much higher than the estimated rate constant of reaction, since activation of ethane is a slow reaction (cf. Figure 7.4), therefore, external mass transfer may be neglected. Typically, a cooling trap was used to separate aromatic products from other gases after which the flow rate of gases could be measured by a bubble flow meter. In cases where gas samples were of interest for further analysis, a train of cooling traps was applied (not shown). The first cooling trap was immersed in an acetone/solid $CO_2$ bath (-78 °C) in order to trap all aromatics. This was followed by two other cooling traps immersed in liquid nitrogen baths (-196 °C) in order to trap light alkanes including methane.

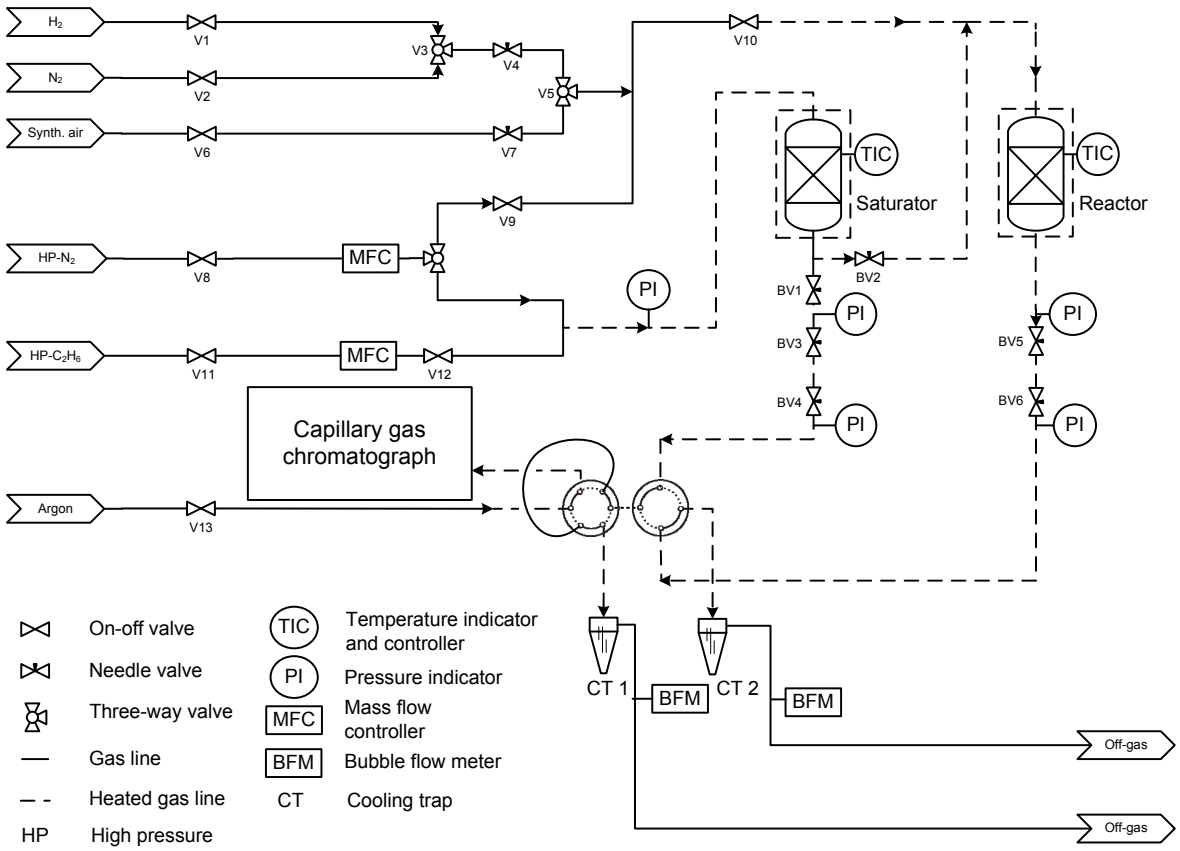


Fig. 3.5: Schematic representation of the high-pressure packed-bed reactor set up with a stainless-steel packed-bed reactor, $8.0 \cdot 10^{-3}$ m inner diameter, according to Ref. [107].

The flow rate of species i into the reactor was calculated according to equation (3.2) with $\dot{V}_{\mathrm{BFM}}$ representing the total flow rate of gases measured at the bubble flow meter (BFM) under atmospheric temperature and pressure.

$$\dot{n}_{\mathrm{i,in}} = \frac{p_{\mathrm{i,in}}}{\sum_{\mathrm{k}\neq\mathrm{i}}^{\mathrm{n}} p_{\mathrm{k,in}} - p_{\mathrm{i,in}}} \cdot \frac{p_{\mathrm{BFM}} \cdot \dot{V}_{\mathrm{BFM}}}{R \cdot T_{\mathrm{BFM}}} \tag{3.2}$$

The weight hourly space velocity (*WHSV*) can then be calculated according to equation (3.3). *WHSV* was changed by varying the mass of catalyst to ensure minimum change in the hydrodynamics of the system. Pressure drop as a result of the different catalyst masses was negligible. Each experiment was repeated with a fresh sample from the same catalyst batch. Experiments were repeated up to three times in order to ensure reproducibility of the results.

$$WHSV = \frac{\sum_{\mathrm{i=1}}^{\mathrm{n}} \dot{m}_{\mathrm{i,in}}}{m_{\mathrm{catalyst}}} \tag{3.3}$$

Table 3.3: Analytical method used for product analysis.

| | |
|---|---|
| Gas chromatograph | Agilent Technologies 6890N |
| Column type | PoraPlot Q |
| Length, inner diameter, film thickness | 30 m, 320 µm, 20 µm |
| Carrier gas | Argon |
| Carrier gas flow rate / $cm^3 \cdot min^{-1}$ | 2.5 |
| Column pressure / kPa | 120 |
| Split ratio | 1:20 |
| TCD reference gas flow rate / $cm^3 \cdot min^{-1}$ | 20 |
| FID $H_2$ flow rate / $cm^3 \cdot min^{-1}$ | 35 |
| FID synthetic air flow rate / $cm^3 \cdot min^{-1}$ | 450 |
| Injector and detector temperature / °C | 250 and 250 |
| GC temperature program | Hold at 30 °C for 5 min,<br>heat to 250 °C at 15 °·$min^{-1}$,<br>hold at 250 °C for 25 min. |

Gas samples were taken by an automated system, operating a six-way valve and a sample loop (cf. Figures 3.4 and 3.5), typically at 60 min intervals. In order to switch from feed to reaction product samples a manual four-way valve was used. Another manual four-way valve was used in order to switch between reaction and sweep sides of the membrane reactor (cf. Figure 3.4). Gas samples were analyzed using gas chromatography (GC) with thermal conductivity (TCD) and flame ionization (FID) detectors in series. Table 3.3 gives detailed specifications of the GC setup and the analytic method used.

### 3.1.6 Evaluation of results

Once gas chromatograms were collected they were evaluated in order to translate individual peak areas into selectivity, conversion, and yield. Once peak areas were assigned to specific species, according to retention times in the column (cf. Table 7.2), the peak area of each species was corrected using response factors from Ref. [108] (cf. Table 7.2) for the FID and experimentally evaluated values for the TCD. Peak areas were corrected according to equation (3.4) with $f_{i,j}$ representing the response factor for species i, and detector j.

$$A_{i,corrected} = A_i \cdot f_{i,j} \tag{3.4}$$

Using an inert as an internal standard, in this case nitrogen, the mass flow rate of any species can be calculated using ethane as the tie substance applying equation (3.5). Since nitrogen can only be detected by the TCD, first the flow rates of species that are detected from the TCD were calculated. Thereafter, flow rates of species detectable only by the FID were calculated.

$$\dot{m}_{\mathrm{k}} = \frac{A_{\mathrm{k}} \cdot f_{\mathrm{k,j}}}{A_{\mathrm{i}} \cdot f_{\mathrm{i,j}}} \cdot \dot{m}_{\mathrm{i}} \tag{3.5}$$

Molar flow rates of the species can be calculated by dividing by the molecular mass of the given species as in equation (3.6).

$$\dot{n}_{\mathrm{i}} = \frac{\dot{m}_{\mathrm{i}}}{M_{\mathrm{i}}} \tag{3.6}$$

Thereafter, conversion of the reactants can be calculated according to equation (3.7). Conversion of a reactant is calculated as the ratio of the difference in molar flux of reactant i into and out of the reactor and the molar flow rate of reactant i into the reactor.

$$X_{\mathrm{i}} = \frac{\dot{n}_{\mathrm{i,in}} - \dot{n}_{\mathrm{i,out}}}{\dot{n}_{\mathrm{i,in}}} \tag{3.7}$$

Selectivity is calculated as the ratio of the difference in molar flow of species j into and out of the reactor and the difference in molar flow of specie i into and out of reactor, equation (3.8).

$$S_{\mathrm{j}} = \frac{\dot{n}_{\mathrm{j,out}} - \dot{n}_{\mathrm{j,in}}}{\dot{n}_{\mathrm{i,in}} - \dot{n}_{\mathrm{i,out}}} \tag{3.8}$$

Product yields are calculated from equation (3.9). It must be noted that since there are two reactants in the feed, in this case two independent yields can be calculated depending on which conversion, from equation (3.7), is used. Yields are reported based on toluene conversion.

$$Y_{\mathrm{j}} = S_{\mathrm{j}} \cdot X_{\mathrm{i}} \tag{3.9}$$

## *3.2 Modeling section*

### 3.2.1 High-pressure equilibrium model

Thermodynamic equilibrium was calculated for gas phase total pressures of 1 to 100 bar, reaction temperatures of 300 and 350 °C and an $\dot{n}_{\mathrm{ethane}} / \dot{n}_{\mathrm{toluene}}$ ratio of 6. Calculations were performed separately for the alkylation reaction of toluene with ethane yielding *m*-ethyltoluene and hydrogen and for the disproportionation reaction of toluene yielding

*m*-xylene and benzene. In this work, these will be referred to as “single” reaction calculations. In addition, calculations were also carried out for a reaction network accounting for the main products observed experimentally: ethyltoluene isomers and hydrogen from toluene alkylation with ethane, xylene isomers and benzene from toluene disproportionation, and ethylbenzene and hydrogen from benzene alkylation with ethane (cf. Figure 3.6). Reactions within this network will be named as “network” in order to differentiate them from the “single” reaction calculations. Chemical equilibrium equations were set up using equation (3.10), with $a_i$ and $x_i$ representing the activity and molar fraction of species i, respectively, and $K_{\lambda,j}$ representing the product of fugacity coefficients for reaction j.

$$K_j = \prod_{i=1}^{n} a_i^{\nu_{ij}} = K_{\lambda,j} \cdot \prod_{i=1}^{n} x_i^{\nu_{ij}} \tag{3.10}$$

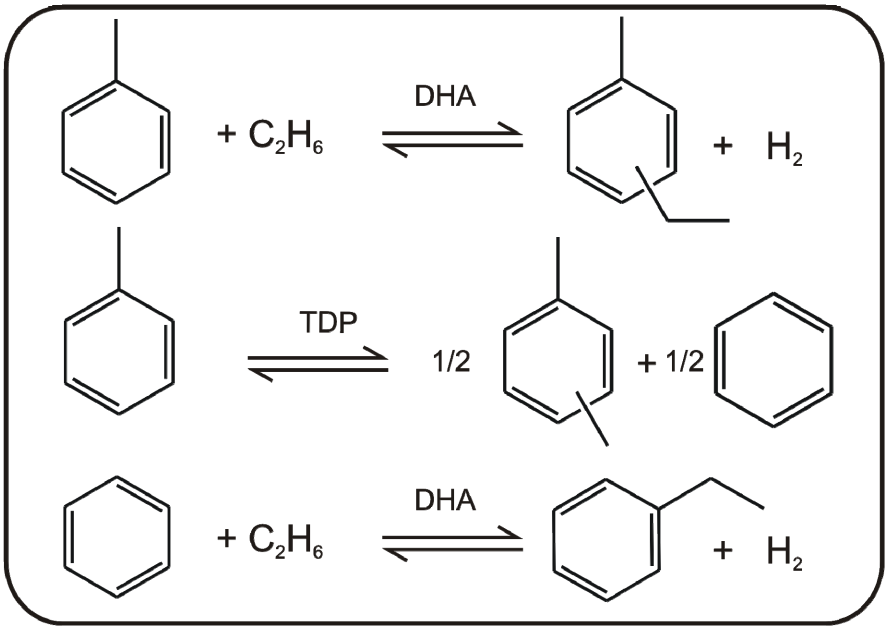


Figure 3.6: Reactions included in the network equilibrium model, including toluene dehydroalkylation (DHA) to ethyltoluenes, toluene disproportionation (TDP) to xylenes and benzene and benzene dehydroalkylation to ethylbenzene.

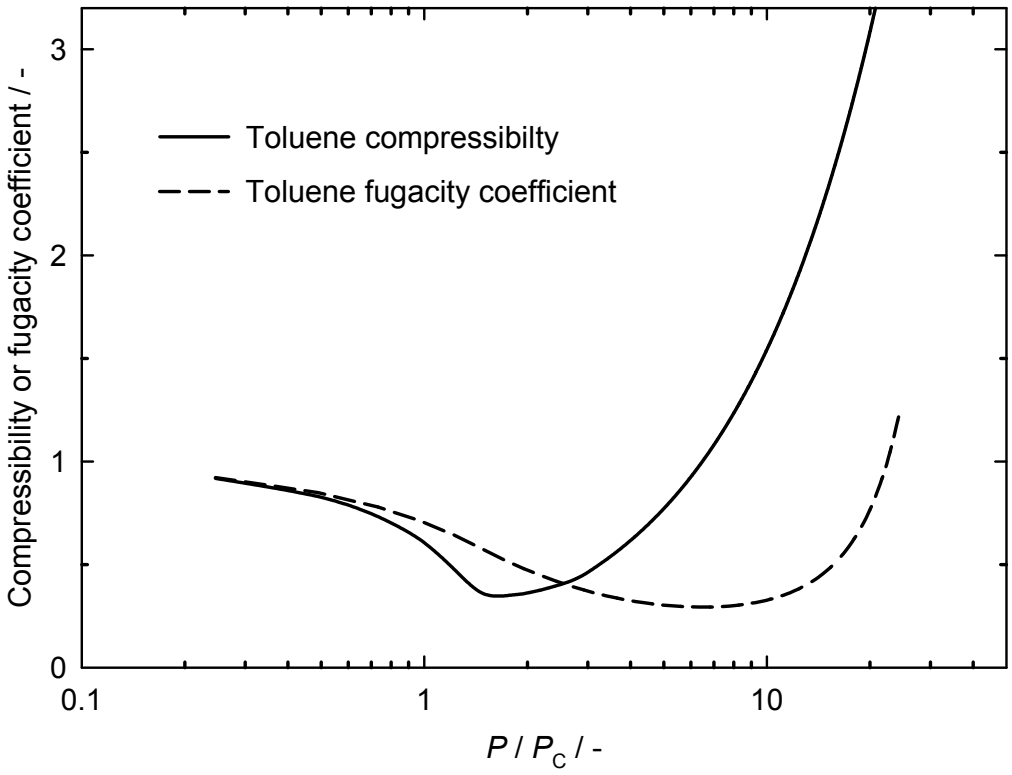


Fig. 3.7: Toluene compressibility and fugacity coefficients as a function of reduced pressure ($P / P_C$) at 350 °C.

Equilibrium constants were calculated, using equation (3.11), from standard Gibbs free energies of formation at different temperatures [13], with $\Delta G_j^{rxn}$ representing the standard Gibbs free energy of reaction at temperature $T$.

$$K_j = \exp\left(-\frac{\Delta G_j^{rxn}}{R \cdot T}\right) \tag{3.11}$$

$K_{\lambda,j}$ in equation (3.10) requires the solution of mixture fugacity coefficients. However, applying the Lewis-Randall rule, equation (3.12), mixture fugacity coefficients, $\bar{f}_i$, can be related to the molar fraction, $x_i$, of the species and the pure component fugacity coefficient, $f_i$.

$$\bar{f}_i = x_i \cdot f_i \tag{3.12}$$

In order to solve for the fugacity coefficients an equation of state route was chosen. Given that the system is made up of a predominantly organic mixture, the Peng-Robinson equation of state, equation (3.13) [109], is an appropriate choice and was applied to determine fugacity coefficients of species, first by solving equation (3.13) from which compressibility factors, $Z$, can be calculated according to equation (3.14).

$$P = \frac{R \cdot T}{\overline{V} - b} - \frac{a(T)}{\overline{V} \cdot (\overline{V} + b) + b \cdot (\overline{V} - b)} \tag{3.13}$$

$$Z = \frac{P \cdot \overline{V}}{R \cdot T} \tag{3.14}$$

Thereafter, fugacity coefficients were calculated according to equation (3.15) from which $K_{\lambda,\mathrm{j}}$ was evaluated from equation (3.16) and substituted into equation (3.10) to take into account gas non-ideality at high pressure (cf. section 7.5 for further details of each term).

$$\ln\left(\frac{f}{P}\right) = (Z-1) - \ln(Z-B) - \frac{A}{2 \cdot \sqrt{2} \cdot B} \cdot \ln\left[\frac{Z + (1+\sqrt{2}) \cdot B}{Z + (1-\sqrt{2}) \cdot B}\right] \tag{3.15}$$

$$K_{\lambda,\mathrm{j}} = \prod_{i=1}^{\mathrm{n}} \left(\frac{f_{\mathrm{i}}}{P}\right)^{\nu_{\mathrm{ij}}} \tag{3.16}$$

The set of nonlinear equations was solved using a Powell hybrid method [110]. Mole balance constraints were set in order to find the correct equilibrium concentrations of all species. In the case that more than one solution of compressibility factor was a feasible solution the largest root was taken as the gas phase compressibility factor. Figure 3.7 shows an example of the calculated compressibility and fugacity coefficients for toluene as a function of reduced pressure at 350 °C.

### 3.2.2 Membrane reactor equilibrium model

To evaluate the extent of equilibrium shift in membrane reactors, four reactions have been chosen as industrially relevant model reactions. These include the non-oxidative dehydrogenation of propane or ethane to propylene or ethylene, respectively, as well as the dehydroalkylation of benzene or toluene with propane or ethane forming cumene or *m*-ethyltoluene, respectively.

According to the second law of thermodynamics, the equilibrium of any closed system can not be changed. Therefore, in the formulation of membrane reactor equilibrium shift the closed system taken into consideration is of utmost importance. The black-box mole balance approach undertaken considers two mole balances, one for the reaction side, the other for the sweep side (cf. Table 3.4). On the reaction side, the Gibbs free energy is minimized. This mole balance is coupled with the sweep side via the hydrogen pressure equilibrium across the

Table 3.4: Mole balances for the example of alkane dehydroalkylation with an aromatic to an alkyl aromatic and hydrogen in a membrane reactor. $F$ represents the $\dot{n}_{\text{aromatic,0}} / \dot{n}_{\text{alkane,0}}$ feed ratio and $S$ represents the $\dot{n}_{\text{sweep gas}} / \dot{n}_{\text{alkane,0}}$ ratio. $\dot{n}_{\text{alkane,0}}$ is the molar flow of alkane entering the reactor.

| Side | Species | In | Out | Molar fraction out |
|---|---|---|---|---|
| Reaction | Alkane | $\dot{n}_{\text{alkane,0}}$ | $\dot{n}_{\text{alkane,0}} \cdot (1-X_1)$ | $(1-X_1) / (1+F-X_2)$ |
| | Aromatic | $F \cdot \dot{n}_{\text{alkane,0}}$ | $\dot{n}_{\text{alkane,0}} \cdot (F-X_1)$ | $(F-X_1) / (1+F-X_2)$ |
| | Alkyl aromatic | 0 | $\dot{n}_{\text{alkane,0}} \cdot X_1$ | $X_1 / (1+F-X_2)$ |
| | Hydrogen | 0 | $\dot{n}_{\text{alkane,0}} \cdot (X_1-X_2)$ | $(X_1-X_2) / (1+F-X_2)$ |
| | Total reaction | $\dot{n}_{\text{alkane,0}} \cdot (F+1)$ | $\dot{n}_{\text{alkane,0}} \cdot (1+F-X_2)$ | 1 |
| Sweep | Sweep gas | $SR \cdot \dot{n}_{\text{alkane,0}}$ | $SR \cdot \dot{n}_{\text{alkane,0}}$ | $SR / (SR+X_2)$ |
| | Hydrogen | 0 | $\dot{n}_{\text{alkane,0}} \cdot X_2$ | $X_2 / (SR+X_2)$ |
| | Total sweep | $SR \cdot \dot{n}_{\text{alkane,0}}$ | $\dot{n}_{\text{alkane,0}} \cdot (SR+X_2)$ | 1 |
| | Overall balance | $\dot{n}_{\text{alkane,0}} \cdot (1+F+SR)$ | $\dot{n}_{\text{alkane,0}} \cdot (1+F+SR)$ | - |

membrane. This effectively means that the closed system has been extended only for hydrogen to consider the sweep side and hence the removal of hydrogen by a sweep gas. In order to reach total equilibrium in a membrane reactor, both the chemical equilibrium as well as the hydrogen equilibrium across the membrane must be satisfied. Significant assumptions include:

- perfect mixing on both permeate and reaction sides, i.e., no concentration profiles,
- steady state and isothermal operation,
- application of the ideal gas law, since pressures under 10 bar will be considered,
- the activity of the catalyst and the permeation properties of the membrane are adequate to reach equilibrium, and
- the membrane shows 100 % selectivity to hydrogen (e.g., a Pd-based membrane).

Equilibrium constants of reactions are calculated using equation (3.11) with data from Ref. [13]. The pressure at the sweep side is 1 bar, the pressure at the reaction side is varied. From the thermodynamic and hydrogen pressure equilibrium constraints, equations (3.17) and equation (3.11) can be formulated and are evaluated using the molar fractions (cf. Table 3.4).

$$p_{\text{H}_2,\,\text{reaction side}} = p_{\text{H}_2,\,\text{sweep side}} \tag{3.17}$$

With regard to Table 3.4, $X_1$ is defined as the amount of alkane converted in the dehydroalkylation reaction relative to the amount of alkane fed, $X_2$ is defined as the amount of hydrogen permeated through the membrane relative to the amount of hydrogen formed. In the case of reaction network, $X_j$ (j is the number of reactions) is defined for every independent reaction in the reaction network and $X_{j+1}$ is defined as the amount of hydrogen permeated through the membrane relative to the amount of hydrogen formed in all reactions. The subsequent set of nonlinear equations is solved using a modified Powell hybrid method [110]. As the given equations are non-linear and hence there is more than one solution to the set of equations, the only acceptable solution is the one that obeys the reaction and sweep side mole balances. The hydrogen recovery is defined according to equation (3.18) and has been used as a criterion to gauge the efficiency of the membrane reactor. The selectivity at thermodynamic equilibrium was calculated from the model results defined previously, equation (3.8).

$$\mathrm{H_2\ recovery} = \frac{\dot{n}_{\mathrm{H_2,\ sweep\ side}}}{\dot{n}_{\mathrm{H_2,\ sweep\ side}} + \dot{n}_{\mathrm{H_2,\ reaction\ side}}} \tag{3.18}$$

### 3.2.3 Kinetic rate law model

A Hougen-Watson approach was taken in order to derive a rate law for toluene alkylation with ethane to ethyltoluenes and hydrogen based on Eley-Rideal adsorption kinetics. The reaction on a bifunctional catalyst (Pd/H-ZSM-5) has been shown to take place in two steps (cf. Figure 3.8). First, ethane is dehydrogenated to ethene, an intermediate, followed by alkylation of toluene with the intermediate ethene [7, 32]. Elementary reaction steps have been proposed based on a dual-site mechanism. The six elementary reactions can be grouped into two parts, the first three steps account for the dehydrogenation of ethane, and the latter three for the alkylation of toluene. Noble metals are in general well known as dehydrogenation catalysts. The resulting ethene intermediate can interact with the acid catalyst to form an activated electrophile which in turn adds to the aromatic ring. In the derivation of the rate law, several assumptions have to be made including:

- The dehydrogenation of ethane (equation (3.20)) is rate-limiting,
- Pseudo-steady-state hypothesis can be assumed, i.e., the net rates of formation of intermediates are zero,
- The concentration of adsorbed hydrogen is close to zero on the metal surface, and
- Adsorption sites are energetically uniform, i.e., species occupy one active site.

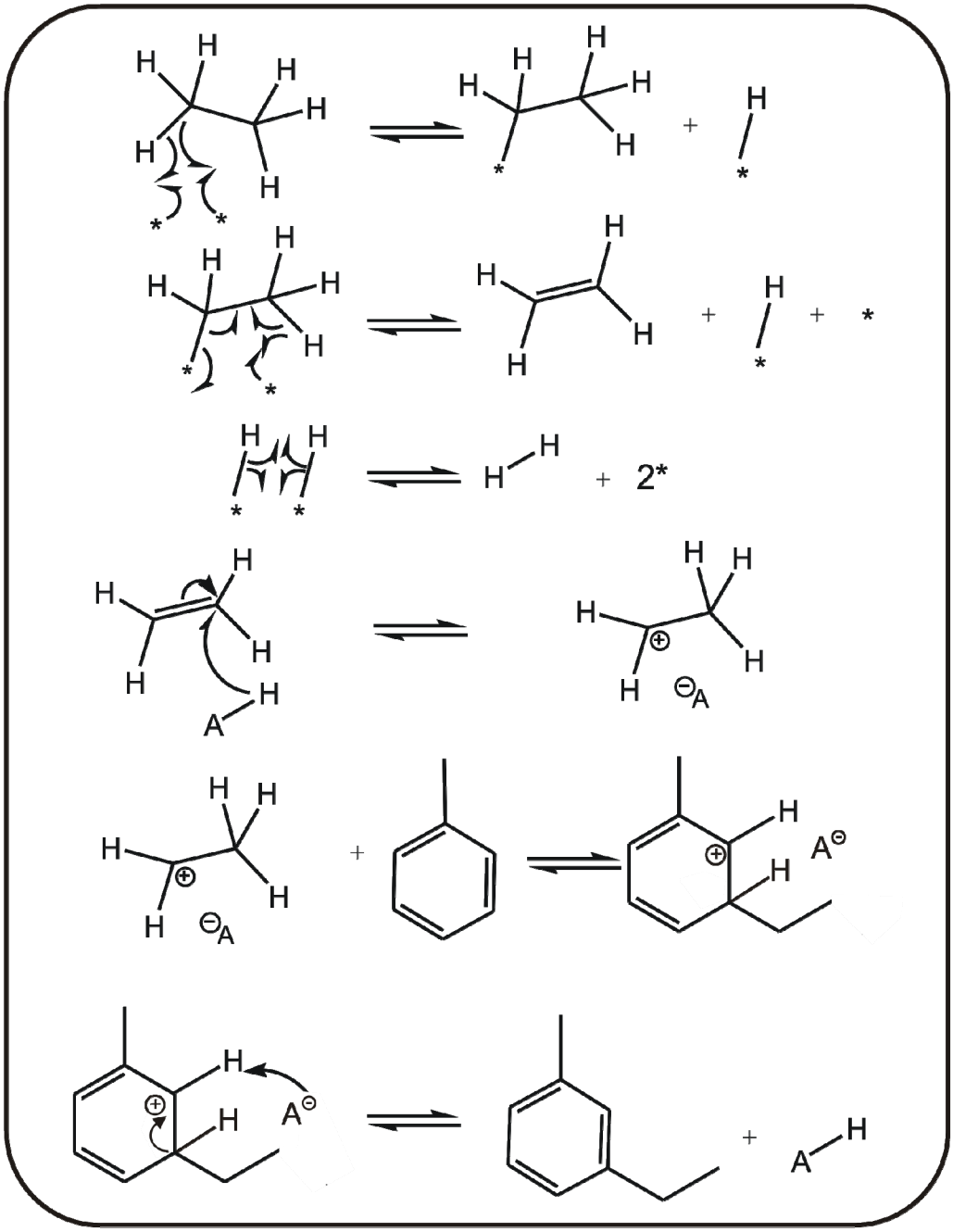

Fig. 3.8: Elementary reaction steps for the conversion of ethane and toluene to ethyltoluene and hydrogen on a noble metal-loaded zeolite catalyst. First the alkane is dehydrogenated on the noble metal (represented by *), forming ethene, an intermediate, and hydrogen. Then ethene is protonated on the zeolite (A represents an anion) and attaches toluene [7].

If these assumptions hold then equilibrium expressions can be written for each of the non-rate limiting steps, i.e., equations (3.19 and 3.21 to 3.24) [97], with $^*$ and $H^{\oplus}$ representing metal and acid sites, respectively, and $\theta_i$ describing the surface concentration of species i.

$$K_1 = \frac{\theta_{C_2H_5^*}\theta_{H^*}}{p_{C_2H_6}\theta_*^2} \tag{3.19}$$

$$r_{\text{reaction}} = k_i\theta_{C_2H_5^*} - k_j p_{C_2H_4}\theta_{H^*} \tag{3.20}$$

$$K_3 = \frac{p_{H_2}\theta_*^2}{\theta_{H^*}^2} \tag{3.21}$$

$$K_4 = \frac{\theta_{C_2H_5^\oplus}}{p_{C_2H_4}\theta_{H^\oplus}} \tag{3.22}$$

$$K_5 = \frac{\theta_{E\text{-}ToH^\oplus}}{p_{To}\theta_{C_2H_5^\oplus}} \tag{3.23}$$

$$K_6 = \frac{p_{E\text{-}To}\theta_{H^\oplus}}{\theta_{E\text{-}ToH^\oplus}} \tag{3.24}$$

Substitution of intermediate species, total site balances and simplification of the resulting equations gives rise to equation (3.25), a rate law for the toluene dehydroalkylation with ethane (cf. section 7.6 for full derivation). The rate law is consistent with typical Hougen-Watson rate law kinetics, i.e., it consists of the product of rate factor and driving force, with an inhibition term. The fraction inside the parentheses in equation (3.25) gives the driving force for the reaction, i.e., the rate of toluene consumption in reaction 1 (according to Figure 3.9), $r_{To,\,1}$, tends to zero close to equilibrium, as would be expected. If the partial pressure, $p$, of ethane is assumed to be constant, e.g., when ethane is in large excess, then the rate of reaction is inversely proportional to the hydrogen partial pressure with a power dependency of 0.5.

$$-r_{To,1} = \frac{k_a p_{C_2H_6}}{p_{H_2}^{0.5} + k_b p_{C_2H_6}}\left(1 - \frac{p_{E\text{-}To}\,p_{H_2}}{K_{DHA}\,p_{To}\,p_{C_2H_6}}\right) \tag{3.25}$$

$$k_a = k_{f,2}K_1K_3^{0.5} \tag{3.26}$$

$$k_b = K_1K_3^{0.5} \tag{3.27}$$

$$K_{DHA} = K_1K_2K_3K_4K_5K_6 \tag{3.28}$$

The derived rate law may be used to model the kinetics of the toluene dehydroalkylation reaction with ethane.

### 3.2.4 Parameter estimation by nonlinear regression

From the experimental results a simplified kinetic model was proposed based on the derivation of the rate law for ethane dehydroalkylation with toluene and other required rate laws found in the literature. Formulation of the model can give insight into favorable reaction conditions for operation of the membrane reactor. In order to adequately describe the product distribution, four chemical reactions were considered, namely dehydroalkylation of toluene with ethane giving ethyltoluenes, toluene disproportionation forming xylenes and benzene, ethyltoluene hydrodealkylation forming ethylbenzene and methane, and toluene hydrodealkylation forming benzene and methane (cf. Figure 3.9). Equation (3.25) was used for the rate law for toluene dehydroalkylation, equation (3.29) for toluene disproportionation [111], and equations (3.30 and 3.31) for the rate law for ethyltoluene or toluene hydrodealkylation [112]. Hydrogen permeation was modeled according to Sieverts' law, equation (2.1).

$$-r_{\mathrm{To},2} = \frac{k_c p_{\mathrm{To}}^2}{1 + k_{\mathrm{d}} \cdot (p_{\mathrm{To}} + p_{\mathrm{Xy}})} \left(1 - \frac{p_{\mathrm{Bz}} p_{\mathrm{Xy}}}{K_{\mathrm{TDP}} p_{\mathrm{To}}^2}\right) \tag{3.29}$$

$$-r_{\mathrm{E\text{-}To},3} = k_e p_{\mathrm{E-To}} p_{\mathrm{H_2}}^{0.5} \tag{3.30}$$

$$-r_{\mathrm{To},4} = k_f p_{\mathrm{To}} p_{\mathrm{H_2}}^{0.5} \tag{3.31}$$

Resulting mole balances, on the reaction side, for all species are given in equations (3.32 to 3.39) with equation (3.40) representing the molar flow of hydrogen on the sweep side. $\dot{n}_{\mathrm{i}}$ represents the molar flow of species i, $\rho_{\mathrm{bed}}$ the catalyst bed density, $z$ the reactor length, $A_{\mathrm{reactor}}$ the reactor cross-sectional area, $J_{\mathrm{H_2}}$ the permeance of hydrogen through the membrane and $r_{\mathrm{R}}$ the ratio of membrane surface area to reactor volume.

$$\frac{d\dot{n}_{\mathrm{To}}}{dz} = \rho_{\mathrm{bed}} \cdot A_{\mathrm{reactor}} \left(-r_{\mathrm{To},1} - 2 \cdot r_{\mathrm{To},2} - r_{\mathrm{To},4}\right) \tag{3.32}$$

$$\frac{d\dot{n}_{\mathrm{C_2H_6}}}{dz} = \rho_{\mathrm{bed}} \cdot A_{\mathrm{reactor}} \cdot -r_{\mathrm{To},1} \tag{3.33}$$

$$\frac{d\dot{n}_{\mathrm{E\text{-}To}}}{dz} = \rho_{\mathrm{bed}} \cdot A_{\mathrm{reactor}} \left(r_{\mathrm{To},1} - r_{\mathrm{E\text{-}To},3}\right) \tag{3.34}$$

$$\frac{d\dot{n}_{\mathrm{H_2,reaction}}}{dz} = \rho_{\mathrm{bed}} \cdot A_{\mathrm{reactor}} \left(r_{\mathrm{To},1} - r_{\mathrm{E\text{-}To},3} - r_{\mathrm{To},4}\right) - J_{\mathrm{H_2}} \cdot r_{\mathrm{R}} \tag{3.35}$$

$$\frac{d\dot{n}_{\mathrm{Xy}}}{dz} = \rho_{\mathrm{bed}} \cdot A_{\mathrm{reactor}} \cdot r_{\mathrm{To},2} \tag{3.36}$$

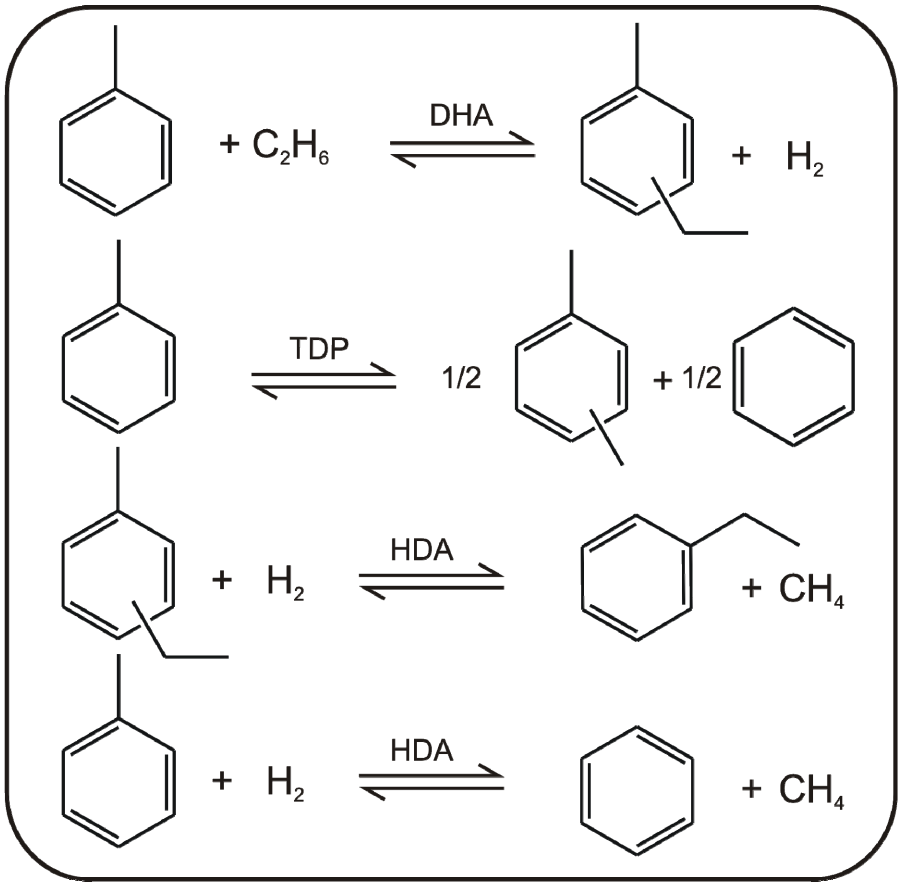


Figure 3.9: Reactions included in the kinetic network model, including toluene dehydroalkylation (DHA) to ethyltoluenes (reaction 1), toluene disproportionation to xylenes (reaction 2), ethyltoluenes hydrodealkylation (HDA) to ethylbenzene and methane (reaction 3), and toluene hydrodealkylation to benzene and methane (reaction 4).

$$\frac{d\dot{n}_{\mathrm{Bz}}}{dz} = \rho_{\mathrm{bed}} \cdot A_{\mathrm{reactor}} \left( r_{\mathrm{To},2} + r_{\mathrm{To},4} \right) \tag{3.37}$$

$$\frac{d\dot{n}_{\mathrm{CH_4}}}{dz} = \rho_{\mathrm{bed}} \cdot A_{\mathrm{reactor}} \left( r_{\mathrm{E\text{-}To},3} + r_{\mathrm{To},4} \right) \tag{3.38}$$

$$\frac{d\dot{n}_{\mathrm{E\text{-}Bz}}}{dz} = \rho_{\mathrm{bed}} \cdot A_{\mathrm{reactor}} \cdot r_{\mathrm{E\text{-}To},3} \tag{3.39}$$

$$\frac{d\dot{n}_{\mathrm{H_2,sweep}}}{dz} = J_{\mathrm{H_2}} \cdot r_{\mathrm{R}} \tag{3.40}$$

The above set of coupled ordinary differential equations was solved using the Livermore solver for ordinary differential equations (LSODE), which can handle non-stiff problems, with the Jacobian calculated internally [97]. As the experimental set up of the membrane

reactor is cocurrent (cf. Figure 7.3), this was also applied to model the membrane process. At the reactor inlet, the boundary conditions are defined by equations (3.41 to 3.43).

$$\dot{n}_{\mathrm{To}} = \dot{n}_{\mathrm{To}}^{\mathrm{exp.}} \tag{3.41}$$

$$\dot{n}_{\mathrm{C_2H_6}} = \dot{n}_{\mathrm{To}}^{\mathrm{exp.}} \cdot \dot{n}_{\mathrm{C_2H_6}} \,/\, \dot{n}_{\mathrm{To}} \tag{3.42}$$

$$\dot{n}_{\mathrm{E\text{-}To}} = \dot{n}_{\mathrm{H_2,reaction}} = \dot{n}_{\mathrm{Xy}} = \dot{n}_{\mathrm{Bz}} = \dot{n}_{\mathrm{CH_4}} = \dot{n}_{\mathrm{E\text{-}Bz}} = \dot{n}_{\mathrm{H_2,sweep}} = 0 \tag{3.43}$$

Data collected from experimental results were used to estimate parameters for the rate law using non-linear regression applying the Levenberg-Marquardt algorithm [98]. The form of the objective function, sum of squares residual (SSR), is given in equation (3.44). Since GC results give the same absolute error for all data, weighting of data by least squares is appropriate. Model parameters are varied at each data point in order to come as close to the experimental values as possible, the criterion being minimization of the sum of squares for the total number of data points (TND). To check validity of the estimated parameters, the variance of each parameter was calculated. The linear variance of each parameter was obtained from the covariance matrix.

$$\mathrm{SSR} = \sum_{\mathrm{TND}} \sum_{\mathrm{i=1}}^{\mathrm{n}} \left( x_{\mathrm{i}}^{\mathrm{exp.}} - x_{\mathrm{i}}^{\mathrm{model}} \right)^2 \tag{3.44}$$

# 4 Results and discussion

During the course of this work efforts were divided into experimental and modeling parts. In the following chapter, first the effect of pressure by a non-ideal gas law model will be presented, complemented by experimental results. The effect of changing the weight hourly space velocity (*WHSV*) on product yield and selectivity will be discussed. Results on catalyst activity for hydrogenolysis/hydrocracking will be presented.

In the second part of this chapter, experimental and modeling results will be presented for a Pd-based membrane reactor which was applied in order to improve the equilibrium. A thermodynamic model will be proposed in order to quantify the maximum attainable shift in equilibrium and compared to experimental results. Finally, modeling results from estimation of kinetic parameters using the proposed kinetic model are presented.

## *4.1 Influence of pressure on equilibrium conversion*

Since the equilibrium conversion during the dehydroalkylation of toluene with ethane is severely limited, several attempts have been made in order to improve the yields of the desired products. In the direct alkylation of toluene with ethane, Sealy *et al.* [7] achieved an order of magnitude increase in conversion and 30 % increase in selectivity to ethyltoluenes with the addition of 0.9 wt.-% Pd to an H-ZSM-5 catalyst. Doubling of this Pd content further increased conversion, however, the selectivity to ethyltoluenes was reduced with a simultaneous formation of methane and propane, possibly as a result of secondary reactions. In order to address the low conversion, due to equilibrium limitations, Smirnov *et al.* [4] introduced intermetallic $Zr_2Fe$, a hydrogen scavenger, to shift equilibrium. Thus, a 2- to 8-fold increase in conversion could be achieved, however, the high conversions could not be maintained, either due to saturation of the hydrogen scavenger or as a result of fast catalyst deactivation at high conversions [4]. During previous experiments, it was observed that at high pressure there is a large increase in conversion, even though from stoichiometry, no influence of pressure is expected for ideal gases. Therefore, thermodynamic calculations taking into consideration non-ideal gas behavior at high pressure, assuming that the Peng-Robinson equation of state adequately describes the system, were carried out.

### 4.1.1 Single reaction model

Figure 4.1 presents the results of thermodynamic equilibrium calculations as a function of pressure at 300 and 350 °C for the independently calculated, single dehydroalkylation or disproportionation reaction of toluene with ethane to *m*-ethyltoluene and hydrogen or to *m*-xylene and benzene [3]. Thermodynamically, the disproportionation reaction is very much favored under the pressure range of interest. At 1 bar and 300 °C, the equilibrium conversion of the dehydroalkylation and disproportionation reactions are 4 and 45 %, respectively. An initial increase in conversion is predicted for both reactions; however, the disproportionation reaction shows a maximum at 30 bar and 48 % conversion. The maximum equilibrium conversion for the disproportionation reaction shifts from 30 bar at 300 °C to 50 bar at 350 °C. The maximum equilibrium conversion for the disproportionation reaction is due to a minimum in the product of fugacity coefficients (cf. Figure 4.2). For the dehydroalkylation reaction, a plateau of 5 % equilibrium conversion above 30 bar is calculated at 300 °C (cf. Figure 4.1). The plateau shifts to 50 bar and 7 % at 350 °C. At 300 and 350 °C, the increase in conversion for the alkylation reaction is 30 and 25 %, respectively. These effects are due to real gases resembling ideal gases more closely at the higher temperature.

### 4.1.2 Reaction network model

Results of equilibrium calculations carried out for the network (cf. Figure 3.6) are illustrated in Figure 4.3. Comparison of Figures 4.1 and 4.3 shows that there is no significant difference in equilibrium conversion trends for the single reactions versus the network. At 1 bar, equilibrium conversion for the disproportionation reactions in the network has increased to 53 % from 45 % for the single reaction yielding *m*-xylene and benzene. In contrast, the equilibrium conversion for the alkylation reactions in the network decreases to 3 % at 1 bar and 300 °C, compared to 4 % equilibrium conversion for the independently calculated, single alkylation reaction forming *m*-ethylbenzene. This is as a result of competition in the network with the thermodynamically more favored disproportionation reaction. In the reaction network, the disproportionation of toluene producing benzene, needed for ethylbenzene formation, has a positive effect on the alkylation of benzene with ethane since there is more benzene being formed.

Figure 4.4 shows the experimental conversion of toluene at 300 and 350 °C as well as the toluene conversion from a model using the equilibrium calculations for the reaction network. Pore restrictions within zeolite ZSM-5 channels and the high $\dot{n}_{\text{ethane}} / \dot{n}_{\text{toluene}}$ ratio suppress the

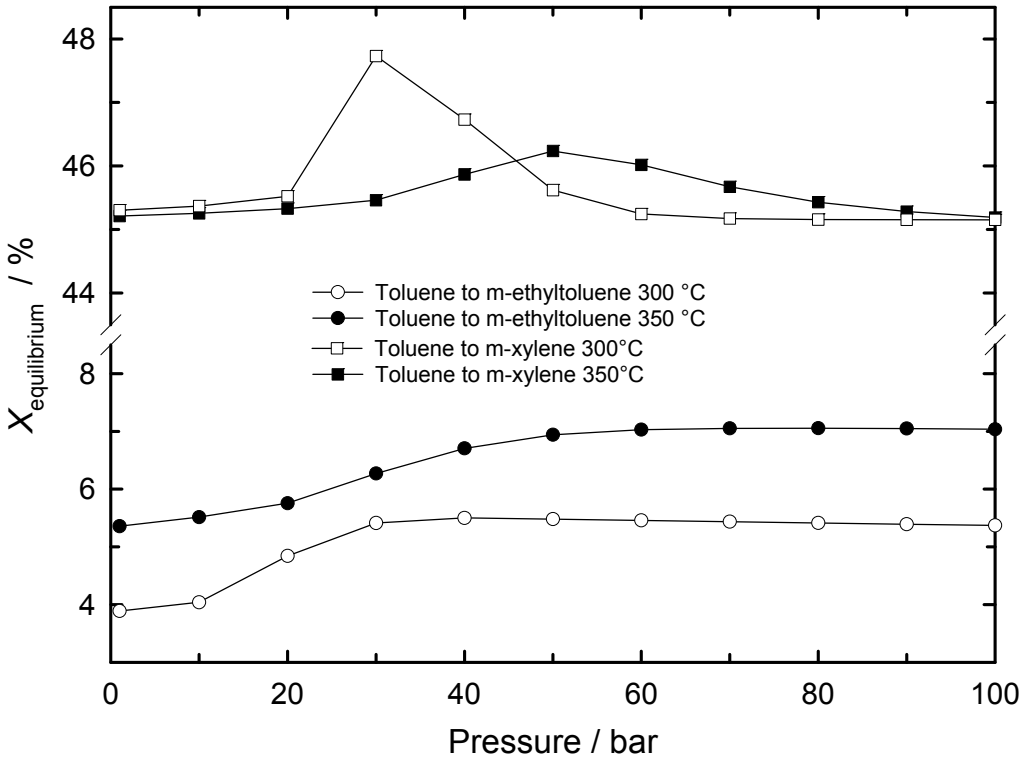


Fig. 4.1: Equilibrium conversion of toluene for independent single dehydroalkylation and disproportionation reactions as a function of pressure ( $\dot{n}_{ethane} / \dot{n}_{toluene} = 6$) [3, 13].

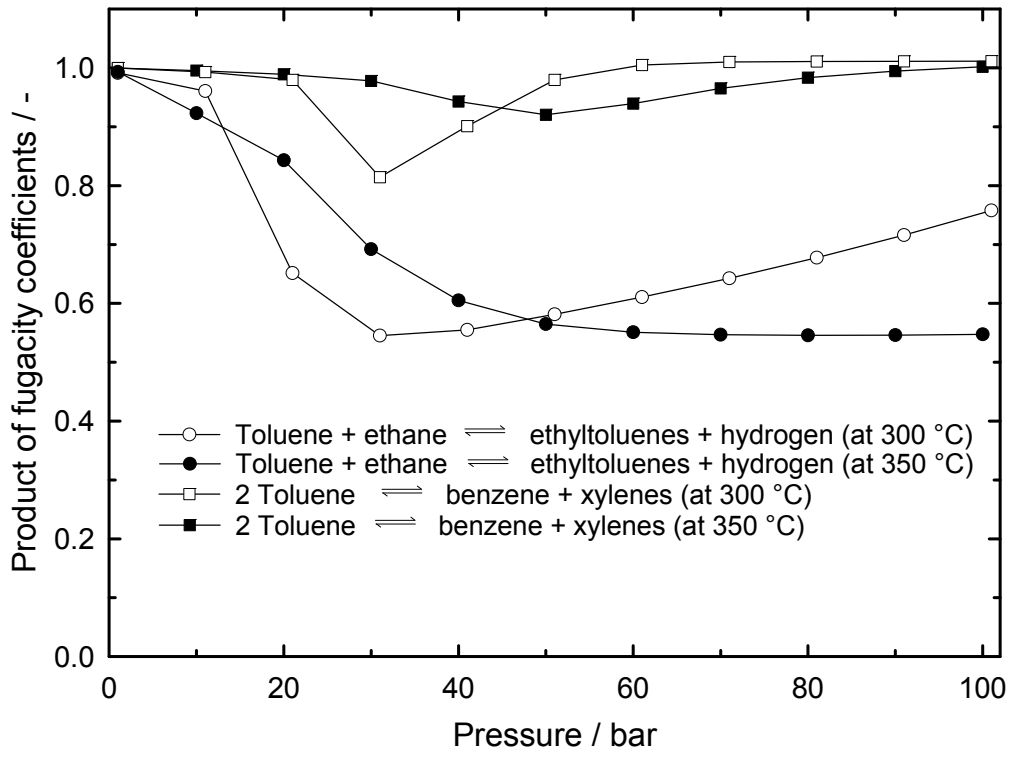


Fig. 4.2: Product of reaction fugacity coefficients for the dehydroalkylation and disproportionation reactions at 300 and 350 °C as a function of pressure [3, 13].

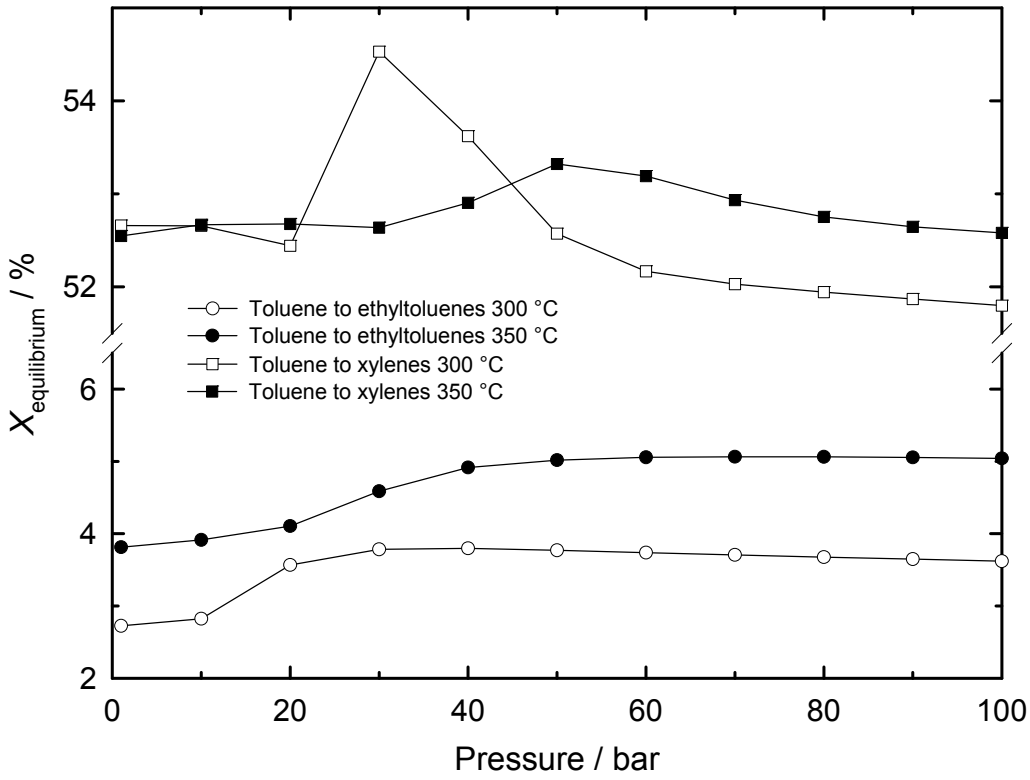


Fig. 4.3: Equilibrium conversion of toluene for a reaction network including dehydroalkylation and disproportionation of toluene and dehydroalkylation of benzene as a function of pressure ( $\dot{n}_{ethane} / \dot{n}_{toluene} = 6$) [3].

toluene disproportionation reaction requiring two toluene molecules as opposed to the dehydroalkylation reaction requiring only one. Therefore, the model combines thermodynamic data with the kinetic assumption that only 1 and 5 %, respectively, of the disproportionation reaction can take place at 300 and 350 °C. At 300 °C the experimental results are in line with the model calculations, however, at 350 °C there is no correlation between experimental results and the calculated model. In order to explain the large deviations at 350 °C, the experimentally observed selectivity to light products is given as a function of pressure in Figure 4.5. Hydrogen selectivities are much lower than expected in comparison to ethyltoluene isomer selectivities. Furthermore, at 1 bar hydrogen and methane selectivity are about 40 and less than 5 %, respectively. However, at 50 bar hydrogen selectivity has decreased to approximately 10 %, whereas methane selectivity has increased to 25 %. In fact, the decrease in hydrogen selectivity is mirrored perfectly by an increase in methane selectivity indicating strongly a direct relationship between methane formation and hydrogen consumption. Smaller amounts of propane are also present at higher pressures;

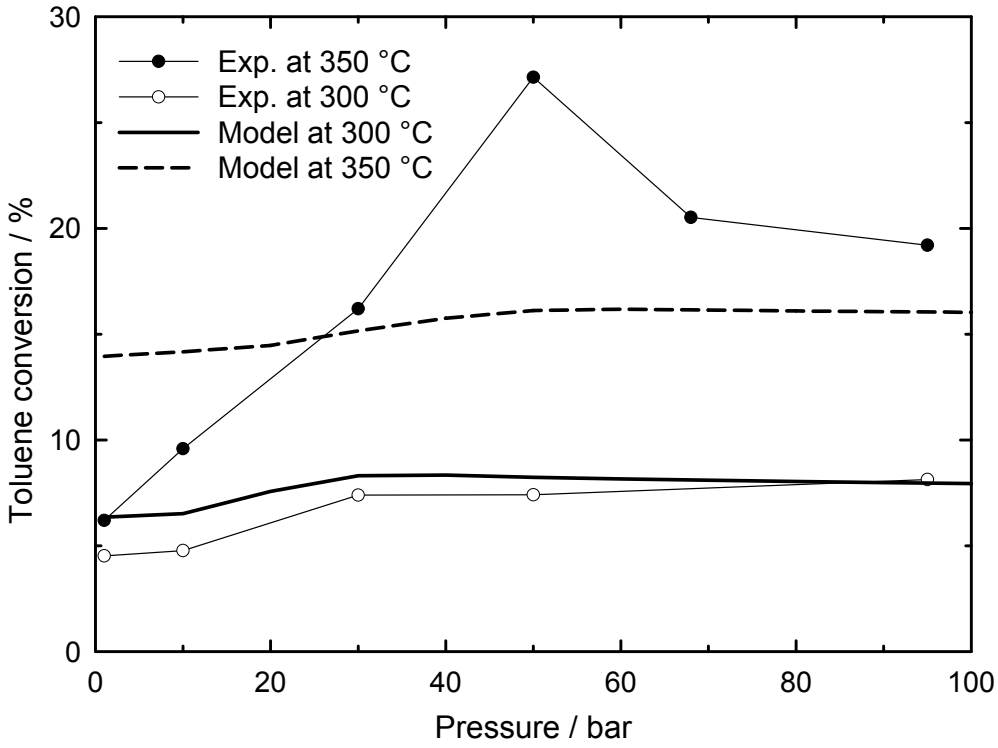


Fig. 4.4: Experimental conversion of toluene on 1.0Pd/H-ZSM-5 ($n_{Si}$ / $n_{Al}$ = 20, $\dot{n}_{ethane} / \dot{n}_{toluene}$ = 6) in comparison to the toluene conversion from the model using the equilibrium calculations for the reaction network (experimental work carried out by D. Singer [3]).

however, the propane selectivity is constant at about 5 %. Light alkanes may form more readily at high pressure via hydrocracking and hydrogenolysis. The formation of methane may act as a *hydrogen sink* and, since hydrogen is a product of the desired toluene alkylation reaction, the conversion towards ethyltoluenes increases to values above equilibrium for this reaction. It must be noted that inclusion of a reaction path in the reaction network to take into account the formation of methane, for example toluene hydrodealkylation, forming benzene and methane, results in complete equilibrium conversions to benzene and methane as the formation of methane is highly thermodynamically favored. Therefore, a reaction forming methane was not considered in the reaction network.

### 4.1.3 Conclusions

At 300 °C, the thermodynamic model is in agreement with the experimental results. However, at 350 °C conversions are well over the expected values calculated from the same model. The "supra-equilibrium" may be due to the formation of hydrogen-rich methane, acting as a hydrogen sink, hence shifting equilibrium towards the formation of ethyltoluenes.

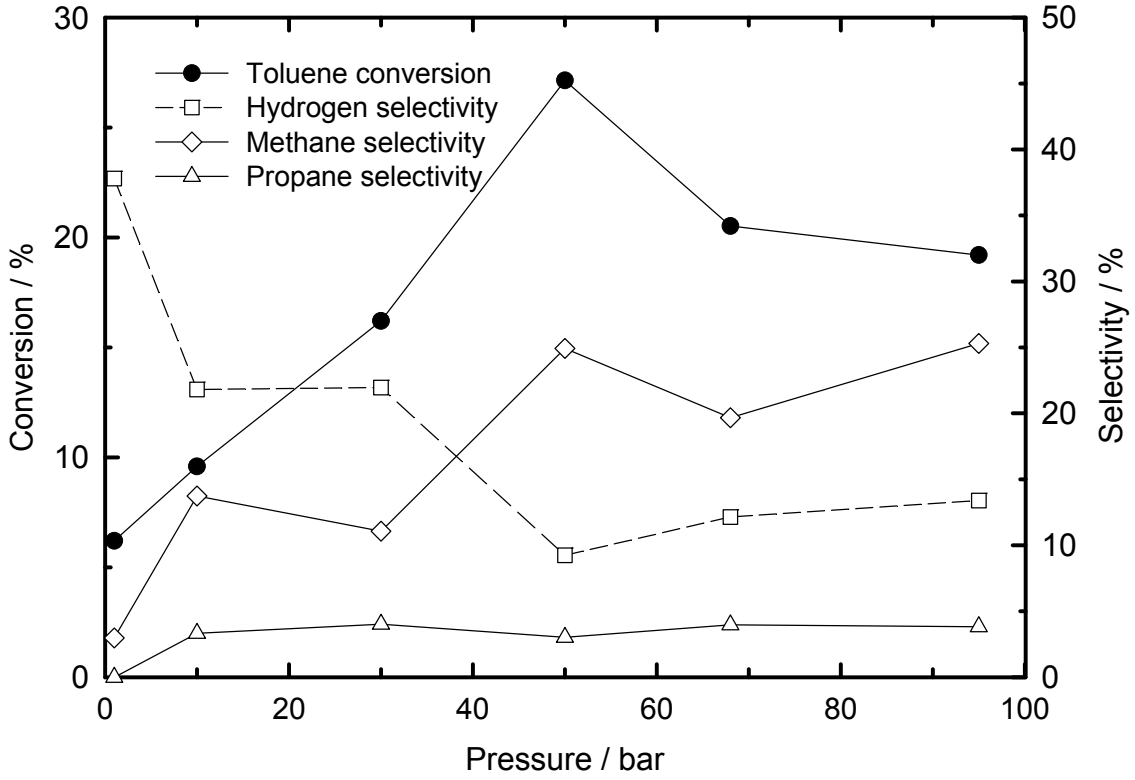


Fig. 4.5: Toluene conversion and selectivity of light products at 350 °C on 1.0Pd/H-ZSM-5 ($n_{Si}$ / $n_{Al}$ = 20) as a function of pressure (experimental work carried out by D. Singer [3]).

The use of pressure to shift equilibrium has several advantages. Typically, high reactant pressures translate to high rates of reaction, which is industrially attractive. Furthermore, the shift in equilibrium can be consistently maintained (in comparison to using a hydrogen scavenger, see Ref. [4]) over a long time on stream giving relatively high yields of the products.

## 4.2 Influence of residence time

Whereas heterogeneously catalyzed processes are preferred for the production of chemical intermediates by alkylation, higher selectivities are desired. The importance of selectivity enhancement for alkylation reactions is evident in recent research using conventional alkylating agents where new materials or catalyst modifications resulted in cumene selectivities of > 99 % during the reaction of benzene with *propene* [113] or *isopropanol* [114]. Older work on the alkylation of toluene with *ethene* has also reported [115] selectivities to ethyltoluenes and *p*-ethyltoluene (the desired isomer relative to other ethyltoluene isomers) of 95 % and 98 % (of the 95 %), respectively. Zeolites have especially gained more importance as selective catalysts for alkylation and disproportionation reactions of aromatics. Recently, *propane* [4, 33, 38, 116] and *ethane* [2, 3, 8] have been investigated as alkylating agents for benzene and toluene on metal-loaded (including Ga and platinum group metals) zeolite catalysts. The bifunctionality is required since an effective dehydroalkylation catalyst typically demands two types of active sites: a metal site for the dehydrogenation of the alkane and an acid site for the alkylation of the aromatic with the alkene intermediate [32].

Although the alkylation of aromatics with alkanes is thermodynamically impaired [2-4], high conversions, even surpassing equilibrium, have been reported [3, 4]. However, these high conversions come at the expense of severe losses in selectivity. Typically, along with the desired products, light alkanes including methane, ethane or propane as well as other alkylated or transalkylated side products are observed. This is in contrast to conventional alkylation where the loss in selectivity is usually a result of polyalkylated aromatics formation and oligomerization of the alkylating agent, because of its high reactivity [27]. Using propane for benzene alkylation on a 0.3Pt/H-ZSM-5 catalyst (0.3 wt.-% Pt referenced to the mass of the dry catalyst, $n_{Si} / n_{Al}$ = 25), Smirnov *et al.* [4] achieved a propane conversion of 45 %; however, the combined selectivity toward *n*-propylbenzene and cumene was only 5 %, with selectivities of 30 % to light alkanes and 20 % to toluene and ethylbenzene. At a lower conversion of 0.5 % on 0.02Pt/H-ZSM-5 ($n_{Si} / n_{Al}$ = 150), the combined selectivity to the desired *n*-propylbenzene and cumene was 85 % (excluding hydrogen) with no light alkanes being detectable. Therefore, the authors concluded that losses in selectivity are a simultaneous result of propane cracking and alkyl aromatic dealkylation [4]. Using a similar catalyst, viz. 1.0Pd/H-ZSM-5, the more inert ethane as alkylating agent and toluene as substrate, Singer *et al.* [3] observed similar trends. At a toluene conversion of 27 %, the selectivity to

ethyltoluenes was only 29 %. Cracking and hydrodealkylation may be due to the nature of the catalyst, i.e., bifunctional catalysts of this type are well known to be also active for hydrocracking and hydrogenolysis of aromatics and alkanes [117-120]. However, the catalyst may only become active for such reactions with the formation of hydrogen, resulting in secondary reactions of hydrogen with the products or reactants. During the Friedel-Crafts-type alkylation of toluene with *alkyl bromides*, using nearly stoichiometric quantities of aluminum bromide, Brown and Jungk [121] succeeded in the elimination of the undesired toluene disproportionation reaction by reducing the contact time of the reactants with the catalyst by two orders of magnitude. It appears that the toluene disproportionation reaction, although a primary reaction, is kinetically less favored than the alkylation reaction, therefore disappearing at low contact times. Hence, the residence time was varied with the aim of suppressing side reactions.

### 4.2.1 Time-on-stream behavior

Figure 4.6 shows the time-on-stream behavior of the conversions of toluene and ethane over a 0.4Pt/H-ZSM-5 catalyst at varying contact times, defined here as the reciprocal of *WHSV* [122]. At a contact time of 0.12 h, the toluene conversion at 2 h on stream is about 11 %. Toluene conversion increases with increasing contact times. The conversions after 2 h on stream at contact times of 0.25 and 0.33 h are 15 % and 20 %, respectively. However, beyond this point large increases in contact times result in insignificant improvements in conversions. At and above a contact time of 0.59 h, the toluene conversion at about 2 h on stream is about 25 %. Ethane conversions are much lower than toluene conversions, since ethane is available in large excess. Still, a small increase in the ethane conversion can be observed with increasing contact time. Ethane conversion is about 1 % at a contact time of 0.12 h, and is doubled at a contact time of 1.0 h. Ethane conversions stay almost constant during the entire run, whereas toluene conversions decrease strongly with increasing time on stream. However, after approximately 60 h on stream the toluene conversions level off and are thereafter relatively constant. The drop in toluene conversion varies according to the contact times. At a contact time of 1.0 h, the conversion at the end of run is about 0.7 times lower than the conversion after 2 h (cf. Table 4.1). The loss of conversion is higher as contact time decreases, and at a contact time of 0.12 h, the same conversion ratio is about 0.4. This variation appears not to be a result of different coking characteristics as contact time changes,

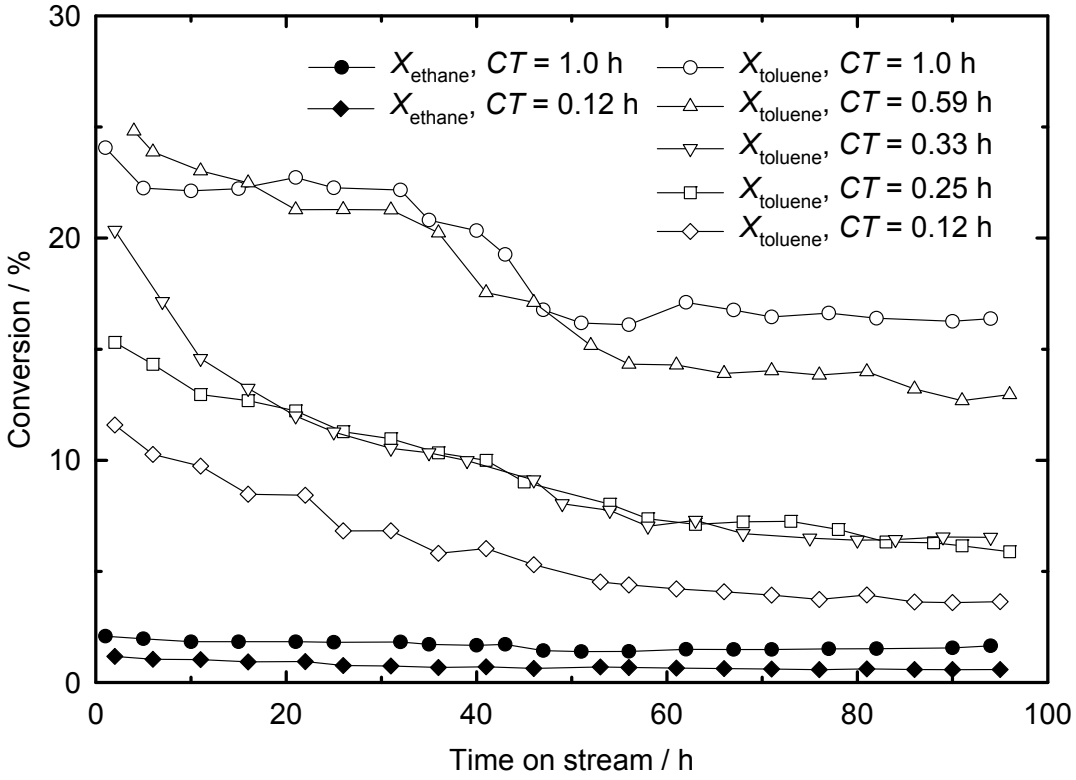


Fig. 4.6: Conversions of toluene and ethane on 0.4Pt/H-ZSM-5 ($n_{Si} / n_{Al} = 28$) at 350 °C and 30 bar with varying contact times ($CT$) as a function of time on stream ($\dot{n}_{ethane} / \dot{n}_{toluene} = 7$, $\dot{n}_{nitrogen} / \dot{n}_{ethane} = 5$) [122].

since the carbon contents of all catalysts are around 6 wt.-% independent of the contact time. The stronger deactivation tendency as compared to previous results (cf. Ref. [3]) can be explained by the nearly fivefold increase in time on stream and the considerably lower metal content of the catalyst which makes hydrogenation of coke precursors more difficult.

The time-on-stream behavior for product selectivities at the lowest contact time (0.12 h) is shown in Figure 4.7. The selectivities of the desired ethyltoluene isomers and hydrogen are approximately 20 % and 18 %, respectively, after 2 h on stream. Methane selectivity is 36 %, methane being the most abundant product at this short time on stream. Selectivities to other side products including propane, benzene, xylenes, and ethylbenzene are low, between 3 and 10 %. With increasing time on stream, the methane selectivity decreases sharply, and is below detection limit after approximately 60 h on stream. The selectivities of the other side products also decrease with time on stream, however, less rapidly. Benzene and xylenes are below detection limit after about 85 h on stream. As a result, the selectivity to the desired products

Table 4.1: Ethane and toluene conversions ($X$), product selectivities ($S$), and ratios of aromatic by-products during the dehydroalkylation of toluene with ethane on 0.4Pt/H-ZSM-5 ($n_{Si} / n_{Al}$ = 28) with varying contact times ($CT$ = 1/$WHSV$) at 350 °C, 30 bar and approximately 90 h on stream ($\dot{n}_{ethane} / \dot{n}_{toluene}$ = 7, $\dot{n}_{nitrogen} / \dot{n}_{ethane}$ = 5). In addition, ratios of conversions and selectivities at 2 and 90 h on stream ($TOS$ = time on stream) are given to indicate approximate changes between the beginning and end of each experiment [122].

| $CT$ / h | 1.0 | 0.59 | 0.33 | 0.25 | 0.12 |
|---|---|---|---|---|---|
| $WHSV$ / $h^{-1}$ | 1.0 | 1.7 | 3.3 | 4.0 | 8.2 |
| $m_{dry\ catalyst}$ / g | 0.85 | 0.50 | 0.26 | 0.21 | 0.10 |
| $X_{ethane}$ / % | 1.6 | 1.2 | 0.9 | 1.0 | 0.6 |
| $X_{toluene}$ / % | 16.3 | 13.0 | 6.5 | 6.3 | 3.6 |
| $S_{ethyltoluenes}$ / % | 27.4 | 35.8 | 58.8 | 52.9 | 60.5 |
| $S_{hydrogen}$ / % | 11.7 | 19.6 | 22.6 | 30.8 | 39.5 |
| $S_{methane}$ / % | 19.9 | 23.4 | 11.3 | 10.5 | d.l. [a] |
| $S_{propane}$ / % | 4.8 | 3.8 | d.l. [a] | d.l. [a] | d.l. [a] |
| $S_{benzene}$ / % | 15.9 | 8.0 | 5.0 | 4.1 | d.l. [a] |
| $S_{xylenes}$ / % | 17.2 | 6.5 | d.l. [a] | d.l. [a] | d.l. [a] |
| $S_{ethylbenzene}$ / % | 3.1 | 2.9 | 2.1 | 1.7 | d.l. [a] |
| $\frac{S_{benzene}}{S_{xylenes}}$ | 0.9 | 1.2 | > 9 [b] | > 9 [b] | - |
| $\frac{S_{benzene}}{S_{ethylbenzene}}$ | 5.1 | 2.8 | 2.4 | 2.4 | - |
| $\frac{S_{xylenes}}{S_{ethylbenzene}}$ | 5.5 | 2.2 | < 0.2 [b] | < 0.2 [b] | - |
| $\frac{X_{toluene,\,TOS\approx 90h}}{X_{toluene,\,TOS\approx 2h}}$ | 0.7 | 0.5 | 0.3 | 0.4 | 0.4 |
| $\frac{S_{ethyltoluenes,\,TOS\approx 90h}}{S_{ethyltoluenes,\,TOS\approx 2h}}$ | 1.3 | 2.2 | 3.0 | 2.9 | 2.9 |

[a] below detection limit

[b] based on the detection limit

increases with time on stream, and after approximately 85 h on stream ethyltoluenes and hydrogen are the only detectable products. Thus, the selectivity to the title reaction is 100 %.

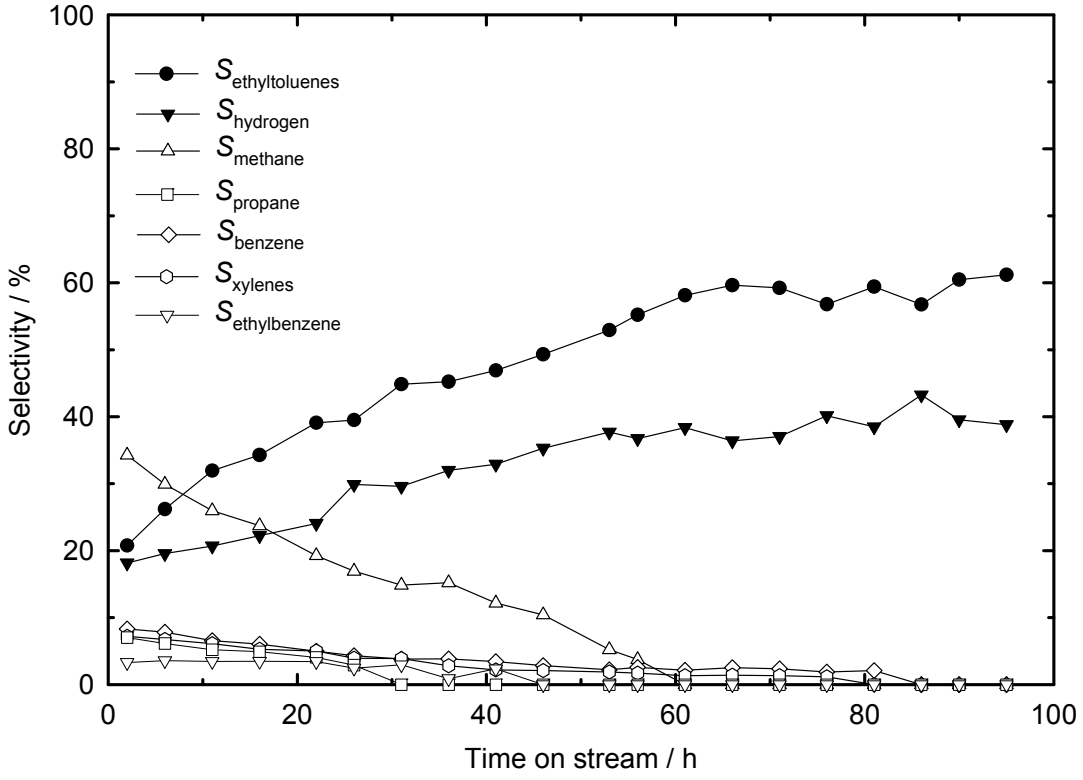


Fig. 4.7: Product selectivity on 0.4Pt/H-ZSM-5 ($n_{Si} / n_{Al}$ = 28) at a contact time of 0.12 h, 350 °C and 30 bar as a function of time on stream ($\dot{n}_{ethane} / \dot{n}_{toluene}$ = 7, $\dot{n}_{nitrogen} / \dot{n}_{ethane}$ = 5) [122].

This is due to coke selectivation and the short contact times, where the kinetically favored alkylation reaction is preferred over the disproportionation reaction.

According to the reaction stoichiometry, for the dehydroalkylation of toluene with ethane (cf. Figure 4.8) it would be expected that the molar ratio of ethyltoluenes and hydrogen be approximately one to one. However, after about 90 h on stream the selectivity of ethyltoluenes is about 60 % and that of hydrogen about 40 %. The large differences may be a result of the fact that the hydrogen yields are determined using the thermal conductivity detector, and its response factor is much smaller than response factors for hydrocarbons determined from the flame ionization detector. From the evaluation of several mixtures of hydrogen and ethane by the thermal conductivity detector, it is estimated that the error in the hydrogen correction factor may be as much as 20 %, whereas the same error is approximately 1 % for ethane. Hence, hydrogen yields are much less accurate than hydrocarbon yields.

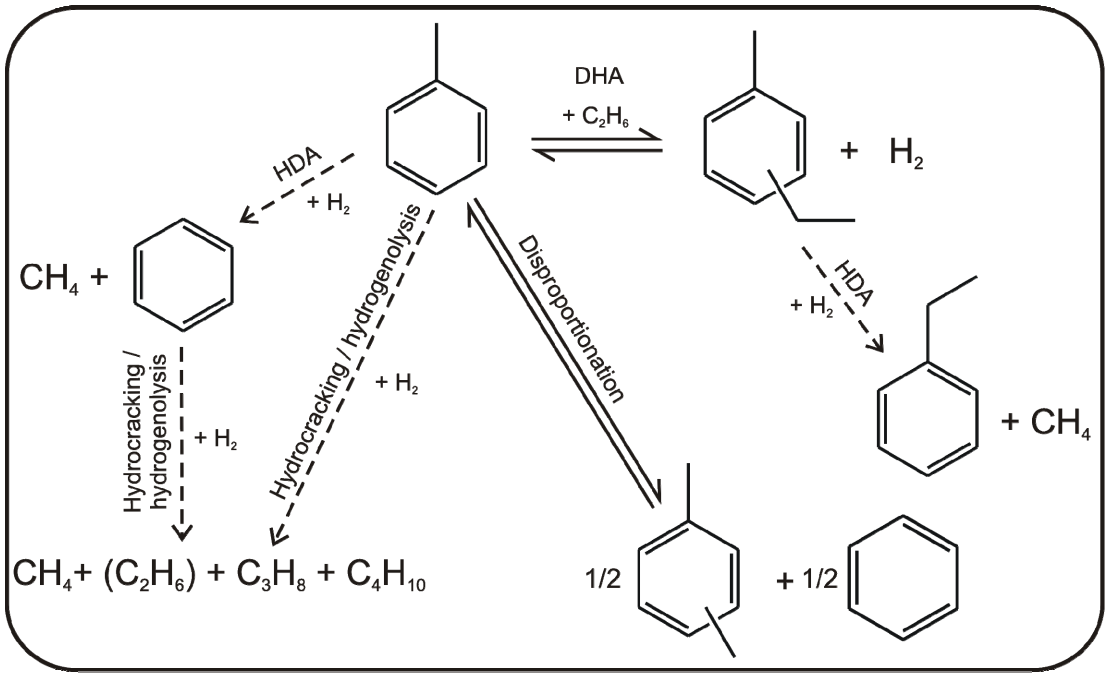


Fig. 4.8: Different reaction pathways possible during the dehydroalkylation of toluene with ethane. The solid arrows represent primary reactions, i.e., dehydroalkylation (DHA) of toluene with ethane yielding ethyltoluene isomers and hydrogen, and the disproportionation of toluene to xylenes and benzene. The dashed lines represent secondary reactions with hydrogen, including the hydrodealkylation (HDA) of toluene forming benzene and methane as well as hydrocracking/ hydrogenolysis of toluene producing $C_1$ to $C_4$ alkanes. Ethane is given in parentheses as its formation from this reaction path cannot be detected since it is a feed component [122].

### 4.2.2 Influence of contact time on selectivity

At all contact times, the initial selectivity to ethyltoluenes is approximately 20 % (not shown). The selectivity increases with increasing time on stream. The trend of increasing selectivity is similar for all contact times, but at different rates depending on the contact time. At a contact time of 0.12 h, the selectivity to ethyltoluenes increases sharply, and is about 2.9 times higher at the end of the experiment than the selectivity after 2 h on stream (cf. Table 4.1). At the higher contact times, the increase in selectivity is less pronounced. For a contact time of 1.0 h, the selectivity to ethyltoluenes during 90 h on stream is essentially constant, with the ratio of the selectivity after 90 h on stream relative to 2 h on stream being approximately 1.3. The increase in selectivity, with a simultaneous decrease in conversion, means that the yield of ethyltoluenes remains almost constant throughout the experiment. Similarly, at high contact

times the drop in selectivity to the undesired side products is less severe. The methane selectivity after 2 h on stream is approximately 35 % at all contact times on the 0.4Pt/H-ZSM-5 catalyst (not shown). At a contact time of 1.0 h, methane selectivity is high during the entire experiment, 32 % after 2 h on stream (not shown), dropping to 20 % after approximately 90 h on stream (cf. Table 4.1), whereas at a contact time of 0.12 h, methane selectivity drops to zero (see above).

On a 1.0Pd/H-ZSM-5 catalyst [3] and under similar reaction conditions, methane selectivity is about 10 %. Methane is presumably formed mainly by hydrodealkylation of toluene (cf. Figure 4.8), and Pt has been reported to be approximately five times more active than Pd at very similar selectivities for toluene hydrodealkylation at similar reaction conditions [117]. Hence, this could explain the higher methane selectivities observed with the Pt-containing catalyst. However, whereas Grenoble observed only methane and benzene as reaction products during toluene hydrodealkylation [117] the light products in our study also included propane and even trace amounts of $C_4$ hydrocarbons at high contact times. This can be explained by the higher acid strength and acid site concentration of zeolite H-ZSM-5 as compared to that of γ-alumina used as a support in the work of Grenoble [117]: Hence, light hydrocarbons may also be produced as a result of mild hydrocracking or hydrogenolysis of hydrocarbon species in our study (cf. Figure 4.8). During the hydrocracking of methylcyclohexane on a similar Pd/H-ZSM-5 catalyst at 400 °C [123], but at a much higher *hydrogen* pressure of 60 bar (resulting in complete conversion), similar products were observed, however with a lower contribution of methane and higher amounts of propane compared to the results presented here. However, due to the lower temperature, the low conversion and the lower hydrogen pressure applied here (compared to Ref. [123]) the catalyst is not active for hydrocracking at low contact times. With increasing conversion, more hydrogen is available for such secondary reactions and has a chance to undergo secondary reactions. Thus, the selectivities to light hydrocarbons increase with increasing contact time, whereas selectivity to hydrogen decreases since it is consumed (cf. Table 4.1).

Table 4.1 also shows the selectivities to the aromatic side products formed during the reaction after 90 h on stream as well as certain selectivity ratios. At a contact time of 1.0 h, benzene and xylenes selectivities are about 16 % and in the same range of the selectivity to the ethyltoluenes. However, the selectivity to these by-products decreases with decreasing contact time to values much lower than the ethyltoluenes. Whereas benzene and xylenes are formed in

very similar molar amounts at a contact time of 1.0 h, the selectivity to xylenes is significantly less than that to benzene at a contact time of 0.59 h. Furthermore, Table 4.1 shows that the selectivity to benzene is 5.0 and 4.1 % at contact times of 0.33 and 0.25 h, respectively, in the absence of xylenes, resulting in benzene to xylenes ratios > 9. At a contact time of 0.12 h, no aromatic side products can be detected any more. Although small deviations from unity of the $S_{\text{benzene}} / S_{\text{xylenes}}$ ratio may be expected and explained for example by dealkylation of xylenes [124], the total absence of xylenes at low contact times strongly suggests that other reaction mechanisms also account for benzene formation. It is therefore suggested that, under conditions of *high contact time*, benzene is formed along with xylenes mainly from the disproportionation of toluene. However, at *low contact times* the disproportionation reaction appears to be not occurring, and this has been observed earlier during alkylation of toluene with ethene and ethyl bromide [121, 125-127]. Pore restrictions within the zeolite channels and the high $\dot{n}_{\text{ethane}} / \dot{n}_{\text{toluene}}$ ratio suppress the toluene disproportionation reaction requiring two toluene molecules as opposed to the alkylation reaction requiring only one [3]. At low contact times, benzene could be formed via the hydrodealkylation of toluene with hydrogen forming methane as a side product (cf. Figure 4.8), as already discussed above. However, from the relatively low yields at low contact times it appears that this contribution is small compared to the disproportionation of toluene at high yields and high contact times. Thus, hydrodealkylation is presumably also taking place to a small extent at high contact times.

Ethylbenzene selectivities are also significant at high contact times; the ratio of benzene to ethylbenzene selectivities decreases with decreasing contact time. At a contact time of 1.0 h, the ratio is 5.1 decreasing to 2.4 at a contact time of 0.25 h, and after further reduction of contact time, both hydrocarbons are below the detection limit. The relatively low ratio of benzene to ethylbenzene selectivities suggests that the dehydroalkylation of benzene with ethane is probably not the only possibility for the formation of ethylbenzene, as has been previously suggested [3], as up to about 30 % of the benzene formed would have to be alkylated to achieve such ratios. This is unlikely since less toluene is alkylated, even though its concentrations are much higher. Another possibility is the hydroisomerization of xylenes to ethylbenzene. The thermodynamics of this reaction favor ethylbenzene formation ($X_{\text{equilibrium, 600 K}}$ ca. 90 %). However, as at low contact times ethylbenzene is formed in the absence of xylenes and as at higher contact times, which would facilitate formation of ethylbenzene by hydroisomerization, the ratio of xylenes to ethylbenzene selectivity (cf. Table 4.1) is much too high according to equilibrium, the contribution of this reaction pathway is

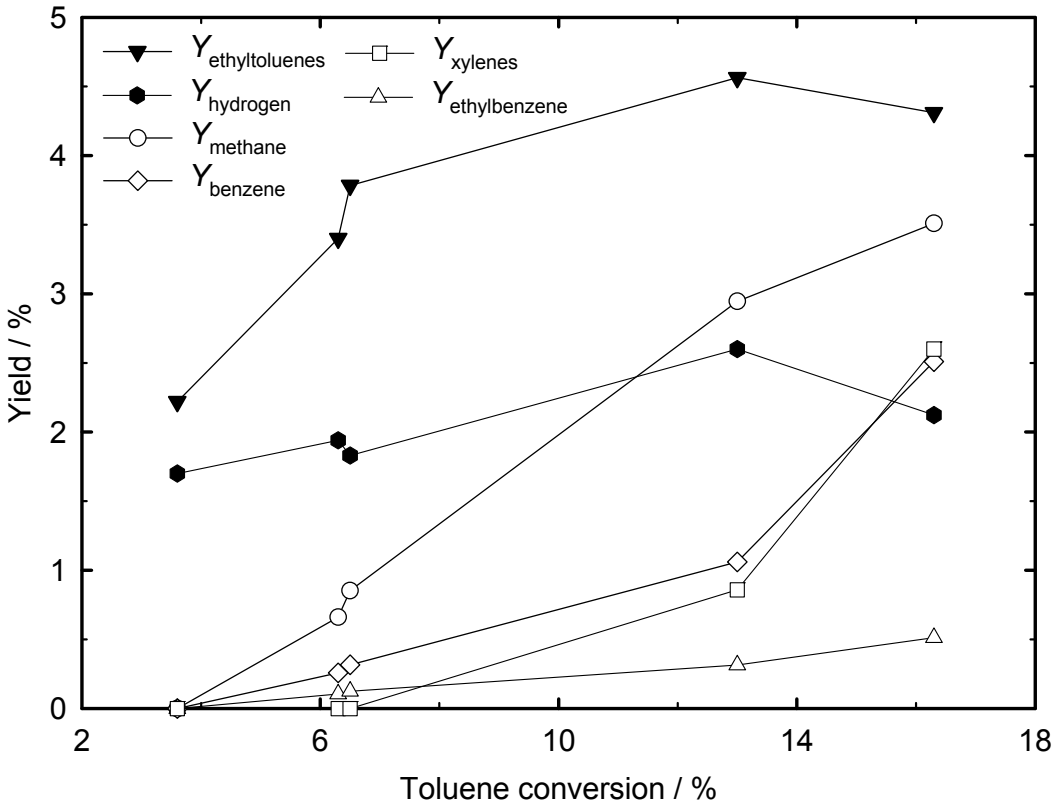


Fig. 4.9: Product yields on 0.4Pt/H-ZSM-5 ($n_{Si} / n_{Al} = 28$) at 350 °C, 30 bar and 90 h on stream as a function of toluene conversion at different contact times ($\dot{n}_{ethane} / \dot{n}_{toluene} = 7$, $\dot{n}_{nitrogen} / \dot{n}_{ethane} = 5$) [122].

probably also not too high. The third possibility for the formation of ethylbenzene is the hydrodemethylation of ethyltoluenes. Hydrodealkylation reactions could account for an excess of benzene to xylenes and ethylbenzene as well as for their selectivity ratio if one takes into account that more toluene is available than ethyltoluene. Hence, it is likely that different reactions contribute to the formation of ethylbenzene and the precise pathway could not be elucidated.

Plotting the product yields as a function of toluene conversion at 90 h on stream (cf. Figure 4.9), a maximum in ethyltoluenes yield is observed at a conversion of about 13 % (equivalent to a contact time of 0.59 h, cf. Figure 4.1). A maximum in the yield of ethyltoluenes may be a result of reactions in series, involving the primary products as reactants. The same maximum in ethyltoluene yield has also been previously observed during the alkylation of toluene with ethene [125, 126]. With ethene as alkylating agent, the maximum occurs at a lower contact time (approximately 0.3 h). Figure 4.9 also shows that the yields of xylenes and benzene

gradually increase with increasing conversion. At low conversion, the benzene yield is higher than xylenes yield but with increasing conversions, both yields become similar. This shows again that at low conversions benzene is rather formed by hydrodemethylation of toluene. In addition, there is a steep increase in both yields, showing clearly that the disproportionation reaction starts becoming more dominant at high contact times. Yields of methane increase steadily with a maximum value of about 3.5 % at high conversion. The fact that the methane selectivity is higher than the selectivity to benzene at contact times of 0.33 and 0.25 h (cf. Table 4.1) shows that methane must also be formed by total hydrogenolysis of toluene or hydrocracking (cf. Figure 4.8) or other hydrodealkylation reactions.

### 4.2.3 Influence of contact time on isomer distribution

Figure 4.10 presents the ratios of the selectivities of *m*-ethyltoluene to *p*-ethyltoluene after 2 h on stream and at the end of each experiment as a function of contact time. The bulkiest isomer, *o*-ethyltoluene, was typically observed in trace amounts only, with a maximum amount of less than 2 % of the total amount of the ethyltoluene isomers. The low yields of *o*-ethyltoluene may be ascribed to it being too bulky to form inside the channels of the zeolite, where the primary reaction takes place. Due to the extra-framework $Na^+$ ions present within the channels used here, as a result of incomplete ion-exchange after synthesis undertaken to remove $Na^+$ ions, the pore size of the channels is slightly reduced. Therefore, *o*-ethyltoluene may exclusively be formed on the external surface even at the highest contact times in this study, thus giving rise to smaller relative *o*-ethyltoluene selectivities than previously observed [2]. After 2 h on stream and at the shortest contact time of 0.12 h, the meta- to para-isomer ratio is about 1.5, increasing to 2 and staying at this value at higher contact times. After 90 h on stream at a contact time of 0.12 h, the ratio of the selectivities of *m*- to *p*-ethyltoluene is 1.1, increasing to a value of about 1.9 at higher contact times. The higher amount of *p*-ethyltoluene at low contact times has been attributed to primary formation of *p*-ethyltoluene during the alkylation of toluene with ethene on an H-ZSM-5 catalyst, with subsequent isomerization to *m*-ethyltoluene which can only take place to a small extent at low contact times [126]. The increase in para-selectivity with increasing time on stream has been explained either by enhanced diffusion rates of the slimmer para-isomer compared to the bulkier meta-isomer due to the narrowing of pores by coke deposition [115], by the deactivation of acidic sites responsible for the isomerization reaction [126], or by decreasing "effective" space time or contact time as a result of decreasing number of acid sites due to

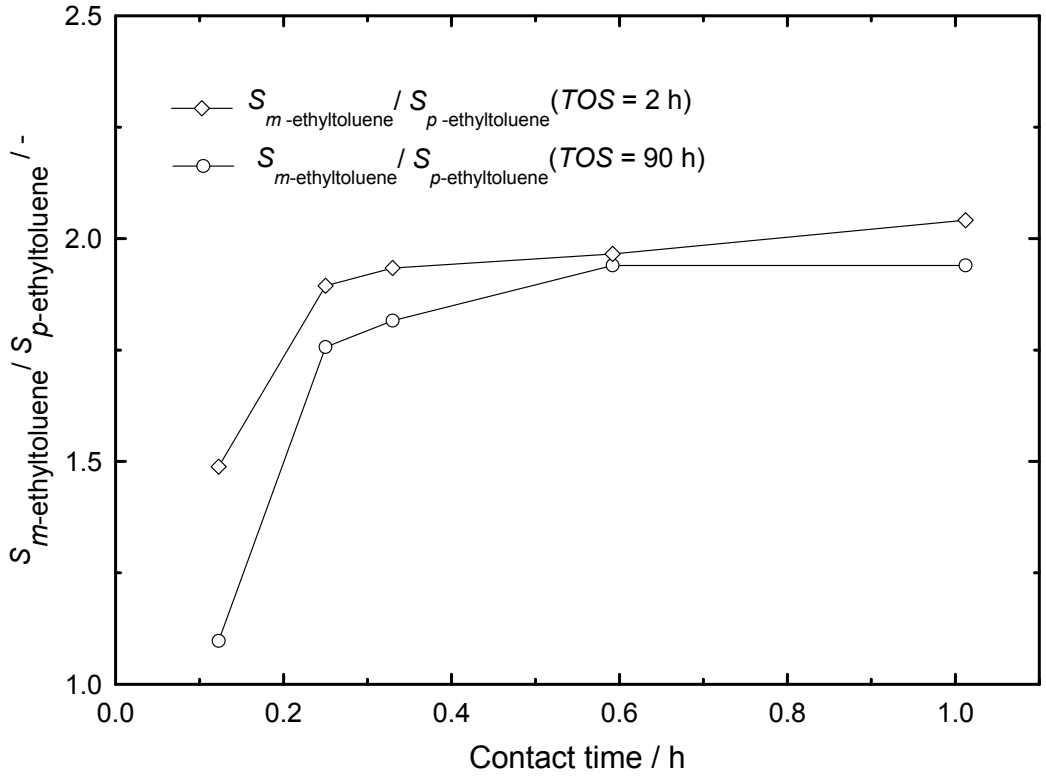


Fig. 4.10: Ratios of *m*-ethyltoluene to *p*-ethyltoluene selectivities on 0.4Pt/H-ZSM-5 ($n_{Si}$ / $n_{Al}$ = 28) at 350 °C, 30 bar and 2 or 90 h on stream (*TOS* = time on stream) as a function of contact time( $\dot{n}_{ethane} / \dot{n}_{toluene} = 7$, $\dot{n}_{nitrogen} / \dot{n}_{ethane} = 5$) [122].

deactivation during the reaction, which increases the para-selectivity since the para-isomer is a primary product [125]. During the dehydroalkylation of toluene with ethane it is conceivable that interplay of all explanations may result in improvements. The decreasing effective contact time is also the reason for the increasing selectivity to ethyltoluenes with increasing time on stream (cf. Figure 4.9), since the alkylation reaction is favored over the disproportionation reaction at low contact times.

Looking at the actual ratio of the selectivities of *m*-ethyltoluene to *p*-ethyltoluene, the values reported in this study are relatively high, being close to or higher than the value of 1.5 for thermodynamic equilibrium at 350 °C [2]. The low selectivities to the bulky ortho-isomer in zeolite ZSM-5, the formation of which is kinetically hindered, allows higher selectivities to the meta- and para- isomers, hence these isomers may exceed their respective equilibrium values. Similarly high values for the ratio of the selectivity of *m*-ethyltoluene to *p*-ethyltoluene of 1.6 [128] and even of 2.3 [115] have been reported during the alkylation of toluene with ethene also at 350 °C and *WHSV* values of 10 $h^{-1}$ [128] and 6.9 $h^{-1}$ [115], respectively, which are similar to our values. By contrast, a very low selectivity ratio of about

0.3 has also been reported at a contact time of 0.1 h during the alkylation of toluene with ethene [126]. These discrepancies may be explained if one keeps in mind that the selectivity ratio is influenced by many parameters and is a result of competition of primary alkylation and secondary isomerization reactions within the zeolite channels, subsequent diffusional transport and tertiary isomerization reactions at the external surface [126, 128]. Parameters influencing the extent to which these reactions occur are the pore size of the zeolite (which can be influenced by coking and extra-framework cations), the crystal size and chemical composition of the zeolite, the reaction temperature and many more. In addition, if one compares the alkylation of toluene with ethene and ethane, one should consider the higher reactivity of ethene as compared to ethane leading to higher net yields of ethyltoluenes. Hence, the ratio of the rate of primary alkylation to *p*-ethyltoluene to the rate of secondary isomerization of *p*-ethyltoluene to *m*-ethyltoluene should be larger for ethene than for ethane.

### 4.2.4 Conclusions

With increasing time on stream, conversions decrease but the yield of ethyltoluenes remains almost constant as a result of an increase in selectivity. The desired products, namely ethyltoluene and hydrogen, are formed exclusively at low contact times and high times on stream. The results provide significant insight into reaction pathways. At low contact times, the conversions and hence yields of the products are low. Increasing the contact time and therefore the conversions results in an initial increase in the yield of ethyltoluenes, but at higher conversions the selectivity to ethyltoluenes decreases as the dehydroalkylation has to compete with the toluene disproportionation reaction as well as with secondary reactions of the products, ethyltoluenes and hydrogen. With increasing conversion, $C_1$ to $C_4$ alkanes are also formed to a larger extent, as well as other aromatics including benzene, xylenes, and ethylbenzene. A maximum yield of ethyltoluenes is observed at a conversion of 13 % at 90 h on stream. It is suggested that this maximum is a result of secondary reactions of ethyltoluenes. The fact that, at a low contact time, a selectivity of 100 % to the title reaction can be achieved is the first step towards the industrial realization of the non-oxidative alkane activation. The second step could then be further improvement of the conversion, maintaining the high selectivity, e.g., by using a recycle or a membrane reactor.

## 4.3 Formation of light alkanes

In order to further investigate the formation of by-products, especially of light alkanes (cf. Figure 4.8), and to confirm that in fact the catalyst is active for hydrogenolysis/hydrocracking, hydrocracking experiments were carried out. Furthermore, as it is well established that different noble metals have different activities for toluene hydrodealkylation [117, 118, 120] the dehydroalkylation of toluene with ethane was also carried out on catalysts with different noble metals.

### 4.3.1 Hydrocracking of toluene, *p*-xylene and *p*-ethyltoluene

Along with the dehydroalkylation of toluene with ethane, hydrocracking experiments were carried out with the reactant toluene, the by-product *p*-xylene and the desired product *p*-ethyltoluene. Model reaction mixtures were chosen in order to approximate reaction conditions as closely as possible. Therefore, the hydrocracking experiments were carried out under mild conditions, i.e., only 2 % $H_2$ in $N_2$ was fed to the reactor along with the saturator temperature set to appropriate partial pressures to approximate typical dehydroalkylation reaction conditions (cf. Table 4.2). The time-on-stream stability of all catalysts was constant during hydrocracking experiments, although this may be due to the mild conditions applied.

Table 4.2 shows results of dehydroalkylation of toluene and hydrocracking of toluene, *p*-xylene and *p*-ethyltoluene. The conversion of toluene is 10.7 % with a selectivity of 37 % to methane. The combined benzene and xylenes (from the disproportionation reaction) selectivity is about 18 % but the benzene selectivity is slightly higher. Selectivity to the desired ethyltoluenes is about 21 % whereas the selectivity to hydrogen is approximately 14 %. During the hydrocracking of toluene, the toluene conversion is 5.3 %, about half of the conversion observed during the dehydroalkylation reaction. Benzene and methane are the most abundant products with near equimolar selectivities of 46 and 41 %, respectively. This is a clear indication of the fact that toluene dehydroalkylation is the primary reaction for the formation of methane. The selectivity to xylenes is similar to that during the dehydroalkylation reaction. However, the yield of xylenes is lower due to the lower conversion. The lower yield to xylenes may also be explained by competition of the toluene hydrodealkylation reaction (which is no longer a secondary reaction) with the toluene disproportionation reaction. Therefore, it appears as though the activity of the catalyst for the disproportionation reaction is reduced. Small amounts of ethane and propane are indicative for the catalyst being not highly active for hydrocracking under such mild conditions.

Table 4.2: Toluene dehydroalkylation with ethane and toluene, *p*-xylene, *p*-ethyltoluene hydrocracking on 0.4Pt/H-ZSM-5 ($n_{Si}/n_{Al}$ = 28) catalyst at 350 °C, 30 bar (make-up gas was nitrogen in all cases) and 90 min on stream. The dehydroalkylation reaction $\dot{n}_{ethane}/\dot{n}_{toluene}$ feed ratio is 7.

| Reaction | Toluene dehydroalkylation | Toluene hydrocracking | *p*-Xylene hydrocracking | *p*-Ethyltoluene hydrocracking |
|---|---|---|---|---|
| $p_{aromatic\ feed}$ / bar | 1.0 | 1.0 | 0.2 | 0.2 |
| $\dot{n}_{H_2}/\dot{n}_{aromatic\ feed}$ | - | 0.8 | 3.0 | 3.0 |
| $WHSV$ / $h^{-1}$ | 2.3 | 0.69 | 0.14 | 0.14 |
| $X_{aromatic\ feed}$ / % | 10.7 | 5.3 | 11.3† | 99.8 |
| $S_{hydrogen}$ / % | 13.8 | n.a.[1] | n.a.[1] | n.a.[1] |
| $S_{methane}$ / % | 37.4 | 41.0 | 16.9 | 1.1 |
| $S_{ethane}$ / % | n.a.[1] | 0.8 | 2.0 | 42.6 |
| $S_{propane}$ / % | 7.0 | 2.6 | 3.7 | d.l.[2] |
| $S_{benzene}$ / % | 9.9 | 45.9 | 2.0 | 1.9 |
| $S_{ethylbenzene}$ / % | 3.1 | d.l.[2] | d.l.[2] | d.l.[2] |
| $S_{toluene}$ / % | n.a.[1] | n.a.[1] | 51.5 | 53.2 |
| $S_{xylenes}$ / % | 8.0 | 9.7 | n.a.[1] | 1.2 |
| $S_{ethyltoluenes}$ / % | 20.8 | d.l.[2] | 2.4 | n.a.[1] |
| $S_{trimethylbenzenes}$ / % | d.l.[2] | d.l.[2] | 21.8 | d.l.[2] |

[1] not applicable as the species is the reactant

[2] below detection limit

† isomerization of *p*-xylene was not included in the conversion

During the hydrocracking of *p*-xylene, a higher conversion was observed. In Table 4.2, the conversion of *p*-xylene by isomerization is excluded, which appeared to be the dominating reaction. Besides the xylene isomerization reaction, *p*-xylene disproportionation also takes place to a large extent, forming toluene and trimethylbenzenes, with a selectivity of over 20 % to the latter product. Toluene selectivity is much higher, over 50 %. This is presumably due to the hydrodealkylation of xylenes forming toluene and methane. A small amount of benzene is also observed. This may be due to secondary reactions of toluene, either by disproportionation or hydrodealkylation. Again, the activity of the catalyst for xylenes hydrodealkylation is high, whereas hydrocracking takes place to a smaller extent only (6 % combined selectivity to ethane and propane). Interestingly, small amounts of ethyltoluenes are also formed during the

hydrocracking reaction of xylenes. During the hydrocracking of *p*-ethyltoluene, essentially complete conversion, 99.8 %, was achieved. This gives a good indication of the instability of ethyltoluenes in a hydrogen-containing atmosphere and explains the difficulties in achieving high conversion and selectivities during the dehydroalkylation of toluene with ethane. During the hydrodealkylation of *p*-ethyltoluene, it is possible that either the ethyl or the methyl group is broken off. Selectivity to ethane is about 43 % (cf. Table 4.2) and selectivity to toluene is about 53 %. This indicates that the catalyst is highly active for the hydrodealkylation of the ethyl group in *p*-ethyltoluene which would yield ethane and toluene as products. In contrast, the catalyst seems inactive for hydrodealkylation of the methyl group yielding methane and ethylbenzene (which appears to take place during the dehydroalkylation of toluene with ethane), with only 1 % selectivity to methane and no detectable ethylbenzene. However, since there is a large excess of ethane during the dehydroalkylation experiments there may be a higher kinetic preference toward dealkylation of the methyl group during these experiments. Small amounts of benzene and xylenes may result from the toluene disproportionation reaction.

From Table 4.2 it is clear that the catalyst is highly active for hydrodealkylation of the toluene, xylenes and especially ethyltoluenes. According to de Graaf *et al.* [129], after introduction of Pt by ion exchange and during activation of the catalyst, a clear particle size distribution of the metal is observed. Depending on the activation procedure (heating rate and flow rate of activating gases), a large fraction of the active metal may be on the outer surface of the catalyst rather than inside the pores. Both metal and acid sites are required in close vicinity of each other for the toluene dehydroalkylation. Since the concentration of acid sites is lower on the outer surface, it is conceivable that the toluene dehydroalkylation with ethane takes place predominantly inside the pores of ZSM-5 on small metal particles. In contrast, toluene hydrodealkylation may take place, predominantly, on large metal particles on the outer surface of zeolite crystals (cf. Figure 4.11). Also, Grenoble [118] reports that toluene hydrodealkylation resembles hydrogenation rather than hydrogenolysis reactions. On Pt-containing catalysts, the reaction order with regard to hydrogen is even slightly negative, hence increasing the rate of the reaction at lower conversions and hydrogen partial pressures [118]. This may further explain the selectivity as a function of time on stream for methane: selectivity to methane decreases rather fast, whereas the selectivities to ethyltoluenes and hydrogen increase sharply (cf. Figure 4.7). During the reaction, due to the low hydrogen

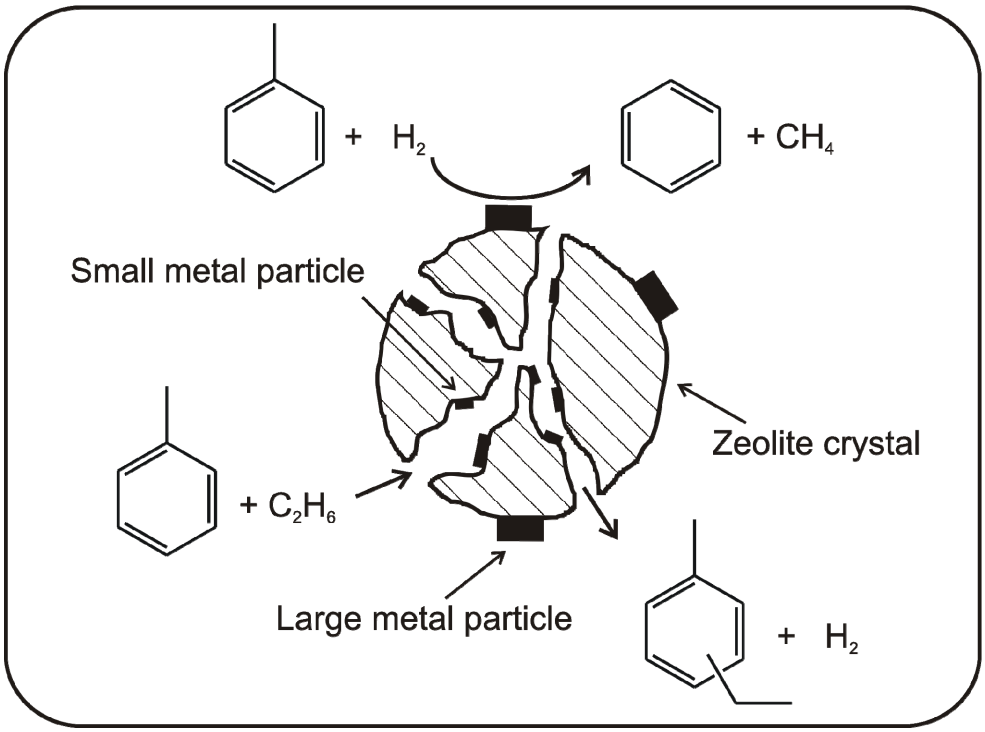


Fig. 4.11: Toluene dehydroalkylation with ethane inside the pores on small metal particles versus toluene hydrodealkylation on large metal particles on the external crystal surface.

concentration, toluene hydrodealkylation should be rather fast and probably occurs mainly on the metal clusters at the external surface of the catalyst. These metal sites are more susceptible to fast deactivation by coking, since coke precursors can form more easily on the external surface of the ZSM-5 crystals as compared to inside the pores. As the external surface is covered by coke, the metal sites active for hydrodealkylation of toluene become inactive, resulting in the decrease in methane formation.

### 4.3.2 Influence of metal type

Since the noble metal/H-ZSM-5 catalyst seems to be so active for hydrodealkylation and, according to Grenoble [117], the noble metal type can have a large influence on the activity for hydrodealkylation, Pt was compared to Pd and Ru in order to investigate the role of the noble metal for hydrodealkylation. For toluene hydrodealkylation at ca. 380 °C, Grenoble [117] reports turnover rates of 17000, 3100, and 700 molecules of benzene formed per second per metal site for Ru, Pt, and Pd, respectively.

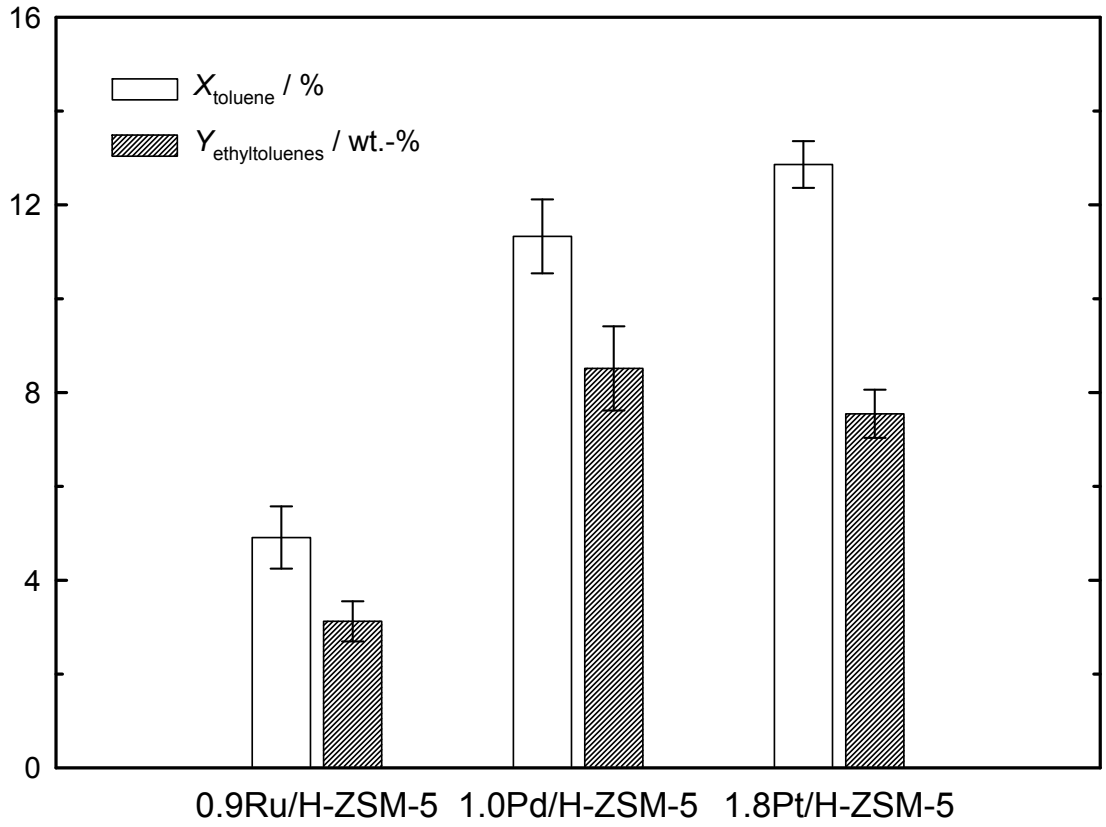


Fig. 4.12: Average (20 h time on stream) toluene conversion and yield of ethyltoluenes on H-ZSM-5 catalysts with different noble metals at 20 bar, 350 °C, $\dot{n}_{ethane} / \dot{n}_{toluene}$ = 7 and $\dot{n}_{nitrogen} / \dot{n}_{ethane}$ = 5 (molar amount of noble metal is the same).

Figure 4.12 shows the conversion of toluene in its dehydroalkylation with ethane and the yield to ethyltoluenes on various noble metals, (with a constant molar amount of the noble metal) at 350 °C and 20 bar. Toluene conversion is highest on the 1.8Pt/H-ZSM-5 catalyst at about 13 %. The 1.0Pd/H-ZSM-5 catalyst shows good activity, conversion reaching almost 12 %. The activity, and hence conversion, of the 0.9Ru/H-ZSM-5 catalyst is significantly lower than that of the Pt- or Pd-loaded catalysts. Conversion reaches approximately 5 % on the 0.9Ru/H-ZSM-5 catalyst. Consequently, the yield of ethyltoluenes for the 0.9Ru/H-ZSM-5 catalyst is also low, less than 4 wt.-%. Comparison of ethyltoluenes yield for the 1.8Pt/H-ZSM-5 and 1.0Pd/H-ZSM-5 catalyst shows that the latter catalyst has a higher activity for the toluene dehydroalkylation, with an ethyltoluenes yield of over 8 wt.-%, whereas the former catalyst gives under 8 wt.-% ethyltoluenes, although a higher conversion is attained.

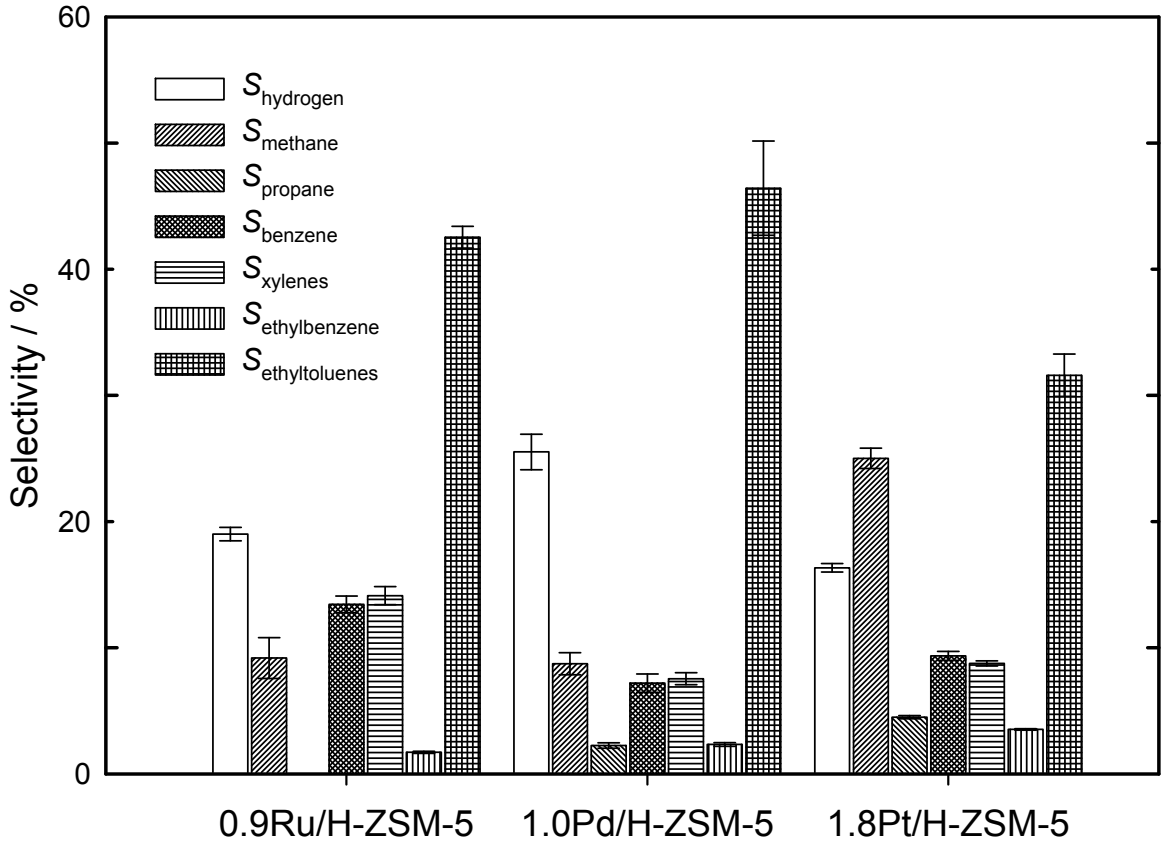


Fig. 4.13: Average (20 h time on stream) product selectivity on H-ZSM-5 catalysts with different noble metals at 20 bar, 350 °C, $\dot{n}_{ethane} / \dot{n}_{toluene} = 7$ and $\dot{n}_{nitrogen} / \dot{n}_{ethane} = 5$ (molar amount of noble metal is the same).

Comparison of the product selectivity for the three catalysts (cf. Figure 4.13) shows that the Pt-loaded catalyst has the lowest selectivity to ethyltoluenes (about 30 %) whereas the other catalysts show higher selectivity, with Pd selectivity almost reaching 50 %. Hydrogen selectivity follows the same trend as that of ethyltoluenes selectivity, i.e., the Pd-loaded catalyst has the highest hydrogen selectivity. The selectivity to methane is reversed with the Pt-loaded catalyst showing the highest selectivity, about 25 %, with a hydrogen selectivity of approximately 10 % for the Pd- and Ru-loaded catalysts. From turnover frequencies of Grenoble [117], it would be expected that Ru shows the highest selectivity to methane, however, this trend is not observed during our experiments. Since the conversion on the 0.9Ru/H-ZSM-5 catalyst is low, it is not very active for the dehydroalkylation of toluene with ethane. Hence, the production rate of hydrogen is low, and since the dehydroalkylation reaction is a secondary reaction the amount of methane formed is lower than expected.

### 4.3.3 Conclusions

Although a noble metal is required for a dehydroalkylation catalyst with good activity it can also promote undesired side reactions including hydrocracking/hydrogenolysis and, mainly, the hydrodealkylation of the reactants and products.

The 1.8Pt/H-ZSM-5 catalyst has the highest toluene conversion. However, the 1.0Pd/H-ZSM-5 catalyst has better activity for toluene dehydroalkylation and hence the highest ethyltoluenes yield. This may be as a result of Pd being less active for hydrodealkylation. Therefore, less hydrogen and ethyltoluenes are lost in secondary hydrodealkylation reactions. The lowest selectivity to hydrogen, the most abundant undesired side product, is observed on the 1.8Pt/H-ZSM-5 catalyst. The Pd-loaded catalyst is the best choice for the dehydroalkytion of toluene with ethane.

## 4.4 Equilibrium shift in membrane reactors: a thermodynamic analysis

Over the last several decades, tremendous advances have been made in understanding membrane synthesis and catalysis as well as in development of mathematical models that describe reaction/permeation processes. By contrast, little has been done with regard to predicting the extent that membrane reactors shift the equilibrium of a reaction, i.e., thermodynamic equilibrium in a membrane reactor. Often a relatively low increase in conversion with the application of a membrane reactor has been observed. This was typically explained by reasons including lack of catalyst activity in order to sustain the high conversions achievable in a membrane reactor, increased catalyst deactivation due to the removal of hydrogen or membrane degradation [40-42]. However, one possibility rarely considered is that the thermodynamic limit has been reached for extraction of a product in a membrane reactor. Since the experimental conversions during toluene dehydroalkylation with ethane are low (cf. Chapter 4.2), due to thermodynamic limitation, and as hydrogen is formed as a by-product, the application of a membrane reactor may be of interest in order to shift the equilibrium. The following chapter shows results from a simple model developed (cf. Chapter 3.2), based on thermodynamics, in order to understand the possible attainable gain in conversion for membrane reactors. Dehydroalkylation using ethane/propane as alkylating agents is compared with the extensively studied dehydrogenation of ethane/propane in membrane reactors. Although for the dehydroalkylation reaction a low $\dot{n}_{\text{aromatic},0} / \dot{n}_{\text{alkane},0}$ ratio is typically applied experimentally, an $\dot{n}_{\text{aromatic},0} / \dot{n}_{\text{alkane},0}$ of 1 is chosen for the model in this chapter to make comparison with the dehydrogenation reaction simpler. The influence of the $\dot{n}_{\text{aromatic},0} / \dot{n}_{\text{alkane},0}$ ratio is shown in the last part of this chapter, and Chapter 4.5 will give results with $\dot{n}_{\text{aromatic},0} / \dot{n}_{\text{alkane},0}$ ratios comparable to the experimental conditions.

Barbieri *et al.* [90] used a tank-in-series model for methane steam reforming, removing hydrogen at intervals until the partial pressure of hydrogen was equal on both sides of the membrane. Abashar and Al-Rabiah [96] applied equations from a mass balance on a differential volume using kinetic models, along the reactor length, equilibrium being reached when the hydrogen concentration profile was constant. Itoh [100, 101] used hydrogen balances and also the condition of equal hydrogen pressures on both sides of the membrane to calculate a maximum conversion. In all works, the sweep gas was identified as a critical

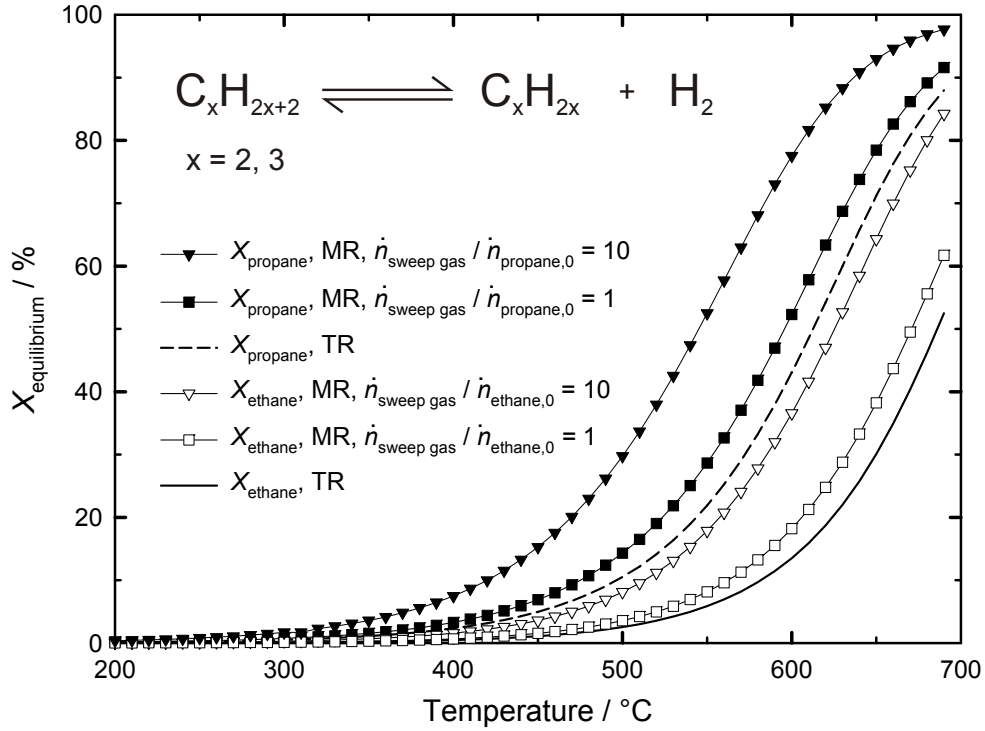


Fig. 4.14: Equilibrium conversion $X_{equilibrium}$ as a function of temperature for traditional reactors (TR) and membrane reactors (MR) for $\dot{n}_{sweep\ gas} / \dot{n}_{alkane,0}$ ratios of 1 and 10 and pressures of 1 bar at the reaction and the sweep side for ethane/propane dehydrogenation [130].

parameter for thermodynamic equilibrium in membrane reactors, directly affecting the extractive capacity of the membrane. Using the same tank-in-series model as in Ref. [90], Barbieri and coworkers [99] studied the effect of pressure during methane steam reforming in a membrane reactor. Although the number of moles increases in this reaction and, hence, increasing pressure has a negative effect on equilibrium conversion in a traditional reactor (i.e., a reactor constructed of material that does not allow permeation of any species), the equilibrium conversion increases with increasing pressure in a membrane reactor [99]. Abashar and Al-Rabiah [96] showed the benefits of higher conversion as a result of coupling a dehydrogenation reaction (ethane to ethene) with a hydrogenation reaction (benzene to cyclohexane) on the sweep side, i.e., using benzene as a reactive sweep gas. Additional increase of conversion by using a reactive sweep gas was also demonstrated by Itoh [101] for the dehydrogenation of cyclohexane to benzene, where hydrogen reacted at the sweep side with oxygen.

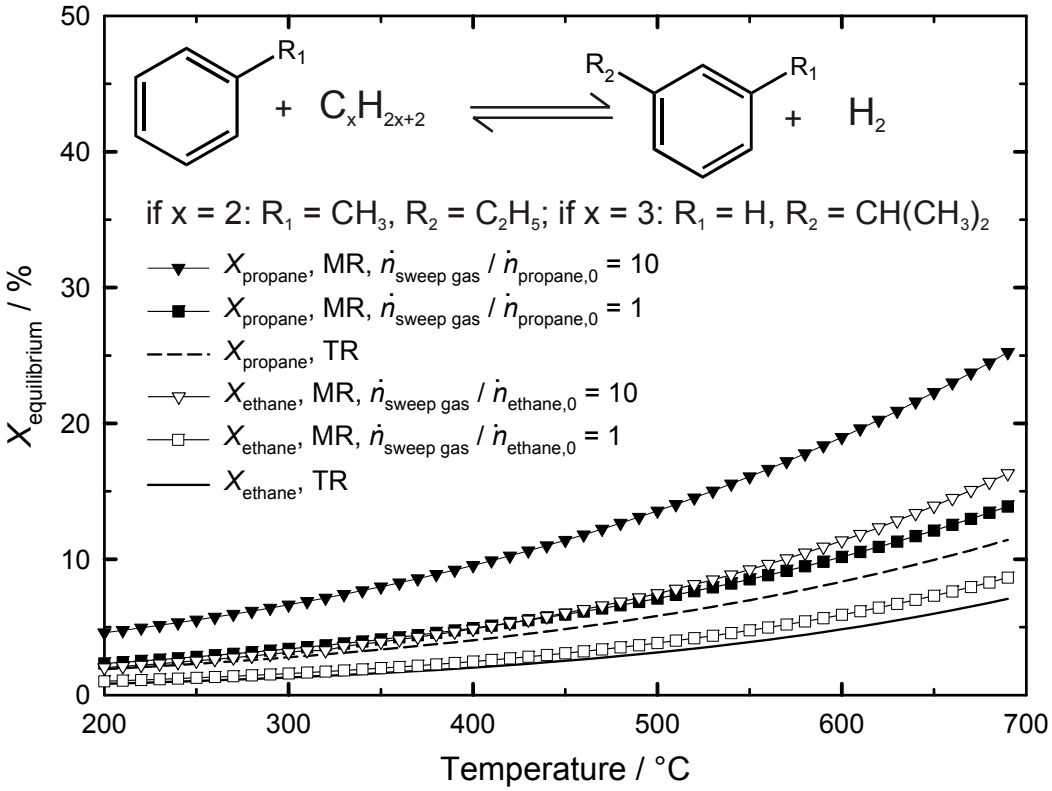


Fig. 4.15 Equilibrium conversion as a function of temperature for traditional reactors and membrane reactors for $\dot{n}_{\text{sweep gas}} / \dot{n}_{\text{alkane,0}}$ ratios of 1 and 10 and pressures of 1 bar at the reaction and the sweep side for dehydroalkylation of benzene/toluene with propane/ethane at $\dot{n}_{\text{aromatic,0}} / \dot{n}_{\text{alkane,0}} = 1$. Insert shows the chemical equations for dehydroalkylation of benzene/toluene with propane/ethane [130].

### 4.4.1 Effect of temperature

Figure 4.14 shows the equilibrium conversion, $X_{\text{equilibrium}}$, as a function of temperature for the dehydrogenation reactions of propane and ethane [130]. As dehydrogenation reactions are by nature endothermic, the equilibrium conversion increases with increasing temperature. With a traditional reactor setup (abbreviated with TR in the figure legend), the conversions for both reactions are very small below 400 °C; however, with increasing temperature up to 700 °C the conversions reach over 50 and nearly 90 % for ethane and propane dehydrogenation, respectively. In a membrane reactor (abbreviated with MR in the figure legend), the equilibrium conversion improves. At an $\dot{n}_{\text{sweep gas}} / \dot{n}_{\text{alkane,0}}$ ratio ($\dot{n}$ is the molar flow entering the reactor) of one, there is little improvement in conversion. Since at higher temperatures more hydrogen is produced, more hydrogen can also be extracted by the membrane reactor, hence higher conversions can be achieved. At an $\dot{n}_{\text{sweep gas}} / \dot{n}_{\text{alkane,0}}$ ratio of 10, the effects are exaggerated, and the equilibrium conversion starts to climb at lower temperatures. For the

dehydrogenation of propane, to achieve a conversion of 10 % in a traditional reactor a temperature of about 500 °C is required, whereas in a membrane reactor with an $\dot{n}_{\text{sweep gas}} / \dot{n}_{\text{alkane,0}}$ ratio of 10 the same conversion can be reached at about 420 °C. At 700 °C, the propane conversion reaches a value of 99 % in the membrane reactor with $\dot{n}_{\text{sweep gas}} / \dot{n}_{\text{alkane,0}} = 10$.

Figure 4.15 shows the effect of temperature on the dehydroalkylation reactions of benzene with propane to cumene as well as of toluene with ethane to *m*-ethyltoluene. A trend similar to that of the dehydrogenation reactions is observed for these reactions, since they are also endothermic. However, as the thermodynamics of the reactions are different there are significant differences in the shift of conversion in a membrane reactor. In a traditional reactor, the equilibrium conversions for the dehydroalkylation reactions (cf. Figure 4.15) are higher at lower temperatures than for the dehydrogenation reactions (cf. Figure 4.14). However, the increase in conversion with temperature is not as strong for the dehydroalkylation as for the dehydrogenation reactions. For the dehydroalkylation of benzene with propane in a traditional reactor, 650 °C are required to reach 10 % conversion, and about 400 °C in a membrane reactor with $\dot{n}_{\text{sweep gas}} / \dot{n}_{\text{alkane,0}} = 10$ (cf. Figure 4.15). Thus, the reduction in temperature to reach the same conversion in the membrane reactor as in the traditional reactor is much more pronounced for the dehydroalkylation reaction at low conversions than for the dehydrogenation reaction. However, a disadvantage of the dehydroalkylation reaction is that even at temperatures of 700 °C the highest possible conversion for dehydroalkylation of benzene with propane with an $\dot{n}_{\text{sweep gas}} / \dot{n}_{\text{alkane,0}}$ ratio of 10 is about 25 %, i.e., very severe conditions have to be applied to achieve higher conversions.

### 4.4.2 Effect of molar flow of the sweep gas

Figure 4.16 shows the equilibrium conversion for the above named reactions as a function of the $\dot{n}_{\text{sweep gas}} / \dot{n}_{\text{alkane,0}}$ ratio between the sweep and the reaction side at a moderate temperature of 400 °C and a pressure of 1 bar at the reaction and the sweep side. This represents the maximum capacity of the membrane reactor at this temperature and pressure, i.e., the most favorable possible shift in equilibrium at high molar flows of the sweep gas. At low $\dot{n}_{\text{sweep gas}} / \dot{n}_{\text{alkane,0}}$ ratios, the equilibrium conversions are generally low, all increasing with

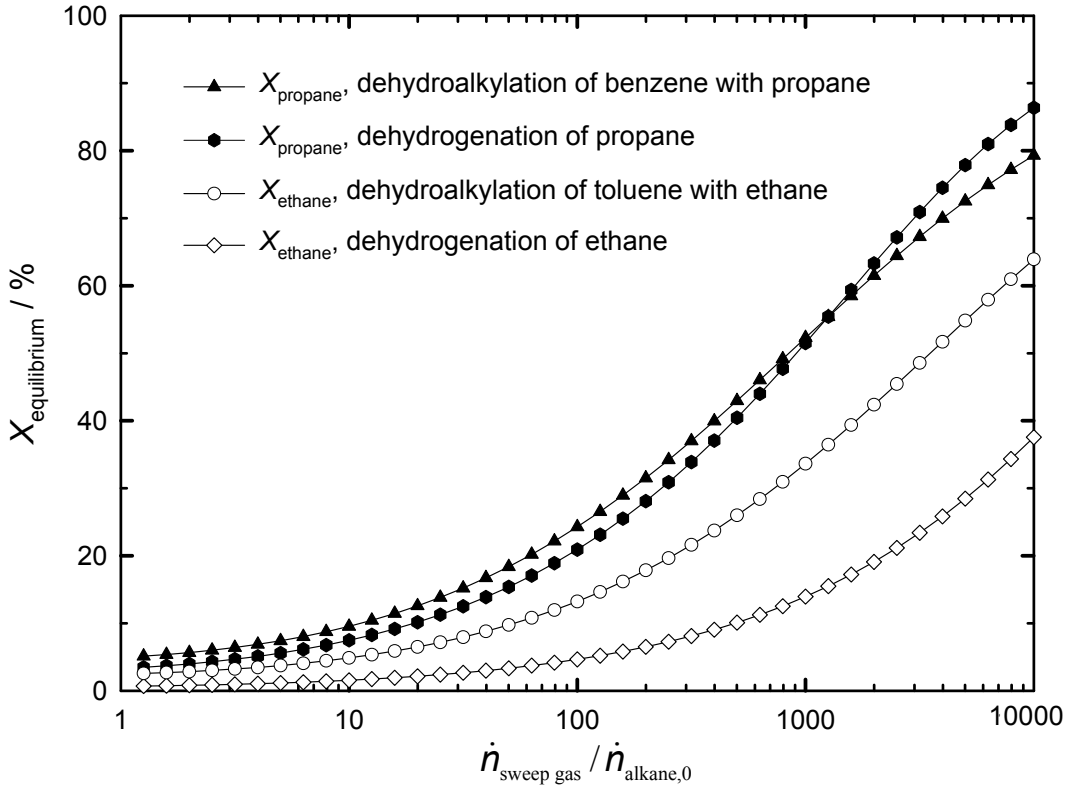


Fig. 4.16: Equilibrium conversion at 400 °C and a pressure of 1 bar at the reaction and the sweep side for all reactions as a function of the $\dot{n}_{sweep\ gas} / \dot{n}_{alkane,0}$ ratio at $\dot{n}_{aromatic,0} / \dot{n}_{alkane,0} = 1$ [130].

increasing $\dot{n}_{sweep\ gas} / \dot{n}_{alkane,0}$ ratios. Comparison between the dehydrogenation of propane and the dehydroalkylation of benzene with propane shows that, although the extents of both reactions increase with increasing $\dot{n}_{sweep\ gas} / \dot{n}_{alkane,0}$ ratio, at low $\dot{n}_{sweep\ gas} / \dot{n}_{alkane,0}$ ratio the equilibrium conversion of the dehydrogenation reaction is low; its rate of increase is higher than that of the dehydroalkylation reaction. At $\dot{n}_{sweep\ gas} / \dot{n}_{alkane,0}$ ratios around 1000, the equilibrium conversions for the two reactions are similar and are starting to flatten out. The increase in conversion is a result of a decrease in partial pressure of hydrogen on the sweep side. As the $\dot{n}_{sweep\ gas} / \dot{n}_{alkane,0}$ ratio increases hydrogen can be swept away faster, meaning that the concentration of hydrogen becomes very low, allowing a stronger shift of the equilibrium. However, it must be noted that an unnecessarily high dilution of the permeated hydrogen is undesirable. Therefore, hydrogen recovery is used as an indicator in order to find the minimum $\dot{n}_{sweep\ gas} / \dot{n}_{alkane,0}$ ratio which is still high enough to allow the membrane reactor to perform at a high efficiency.

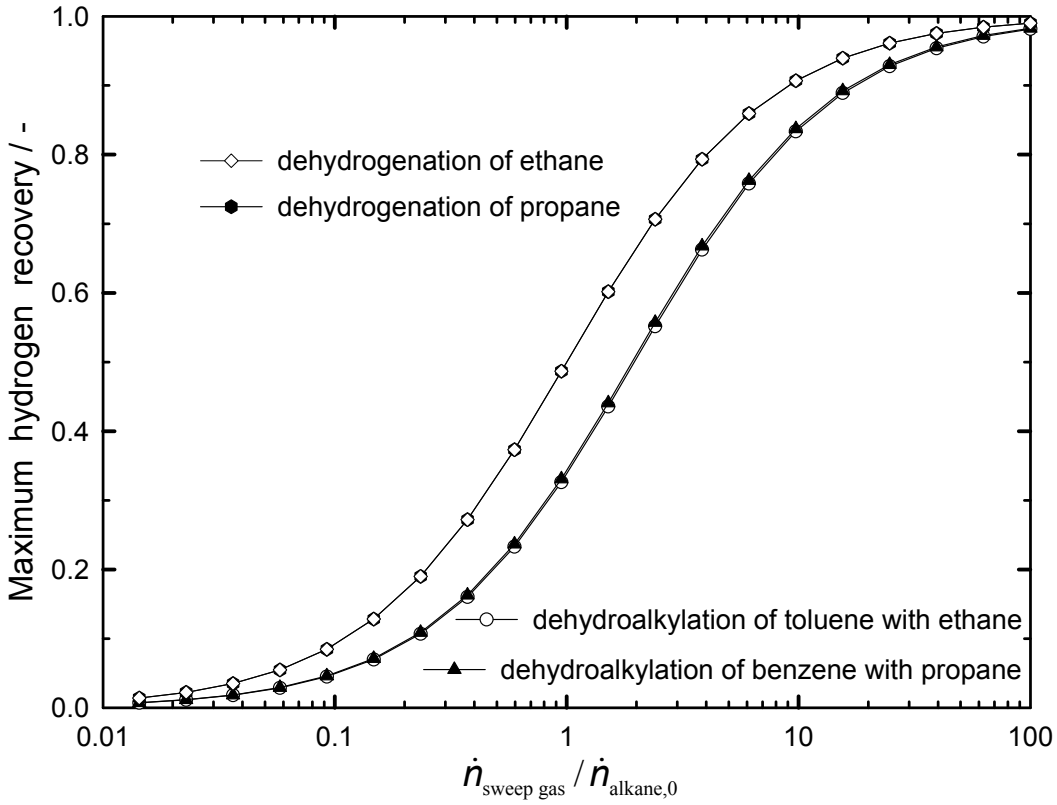


Fig. 4.17: Maximum hydrogen recovery at 400 °C and a pressure of 1 bar at the reaction and the sweep side for all reactions ($\dot{n}_{\text{aromatic,0}} / \dot{n}_{\text{alkane,0}} = 1$) as a function of the $\dot{n}_{\text{sweep gas}} / \dot{n}_{\text{alkane,0}}$ ratio [130].

Figure 4.17 shows the maximum hydrogen recovery as a function of the $\dot{n}_{\text{sweep gas}} / \dot{n}_{\text{alkane,0}}$ ratio for the dehydrogenation and dehydroalkylation reactions. At a low $\dot{n}_{\text{sweep gas}} / \dot{n}_{\text{alkane,0}}$ ratio, the maximum hydrogen recovery is close to zero, sharply increasing at a value of $\dot{n}_{\text{sweep gas}} / \dot{n}_{\text{alkane,0}}$ around one and leveling off to a value of one above an $\dot{n}_{\text{sweep gas}} / \dot{n}_{\text{alkane,0}}$ ratio of 10. At a value of 10, the maximum hydrogen recovery is 0.85 and 0.90 for the dehydroalkylation and dehydrogenation reactions, respectively. Hence, at a value of approximately 10 the membrane reactor is operating with a high efficiency, since most of the hydrogen produced in the reaction can be extracted. The curves for the two dehydrogenation reactions are nearly the same. The same holds for the curves of the two dehydroalkylation reactions. Thus, the maximum hydrogen recovery is independent of the actual thermodynamics of the reaction. However, at intermediate $\dot{n}_{\text{sweep gas}} / \dot{n}_{\text{alkane,0}}$ ratios the hydrogen recovery is higher for the dehydrogenation reactions than for the dehydroalkylation reactions. This is due to the difference in the stoichiometry between the dehydrogenation and

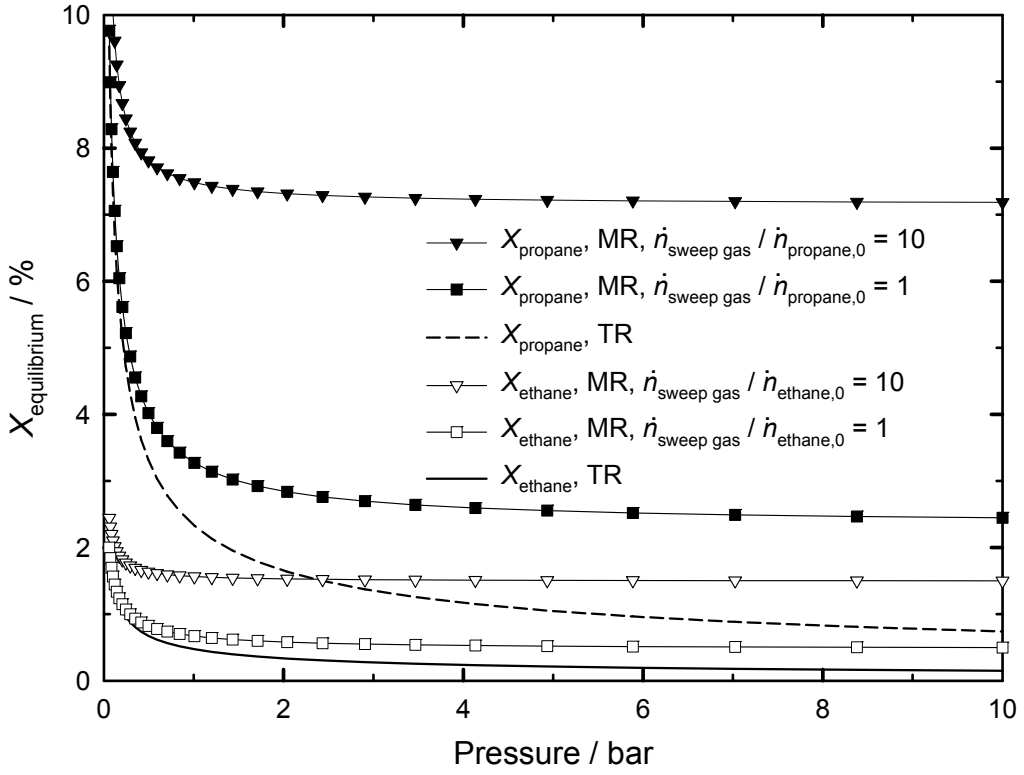


Fig. 4.18: Effect of reaction pressure on equilibrium conversion during ethane / propane dehydrogenation for traditional reactors and membrane reactors for $\dot{n}_{\text{sweep gas}} / \dot{n}_{\text{alkane},0}$ ratios of 1 and 10 at 400 °C assuming ideal gas behavior (pressure at the sweep side: 1 bar) [130].

dehydroalkylation reactions which affects the relative concentration of hydrogen at the reaction side. Below an $\dot{n}_{\text{sweep gas}} / \dot{n}_{\text{alkane},0}$ ratio of one, the molar flow of hydrogen at the reaction side is higher than that at the sweep side, leading to unfavorable conditions for the extraction of hydrogen produced, and hence the hydrogen recovery is poor. Assuming no vacuum is applied on the sweep side, with $\lim_{\dot{n}_{\text{sweep gas}} \to 0}$ hydrogen permeation decreases, and the hydrogen molar fraction on the sweep side tends to one. Therefore, as $\lim_{\dot{n}_{\text{sweep gas}} \to 0}$ and at steady state, the model predicts that the membrane reactor will have no capacity to operate by separating hydrogen and behaves as a traditional reactor.

### 4.4.3 Effect of pressure

Figure 4.18 presents the equilibrium conversion for the dehydrogenation of propane and ethane as a function of reaction pressure at 400 °C. As mentioned before, the pressure at the sweep side is 1 bar, the pressure at the reaction side is varied. In a traditional reactor, the

conversion for propane dehydrogenation is about 10 % in vacuum as the reaction is favored at low reaction pressure due to the increasing number of moles. With increasing reaction pressure, the conversion drops monotonously to below 1 % at 10 bar. The equilibrium conversion for ethane dehydrogenation is essentially zero at 400 °C and 10 bar in a traditional reactor. In a membrane reactor with an $\dot{n}_{\text{sweep gas}} / \dot{n}_{\text{alkane,0}}$ ratio of 1, both reaction equilibria improve. Furthermore, although there is a drop in the conversion with increasing reaction pressure, it is less severe in the membrane reactor as compared to the traditional reactor, e.g., propane conversion drops by more than 90 % in a traditional reactor but about 30 % in a membrane reactor at an $\dot{n}_{\text{sweep gas}} / \dot{n}_{\text{alkane,0}}$ ratio of 10. This means that although it is typically preferred to apply lower than atmospheric pressure for the dehydrogenation of propane, when using a membrane reactor higher reaction pressures can be used without sacrificing too much conversion.

Figure 4.19 shows the reaction pressure effects for the dehydroalkylation reactions of benzene and toluene with, respectively, propane and ethane at 400 °C. In this case, as the number of moles does not change, in a traditional reactor the equilibrium conversion is constant at 2 and 4 % for toluene and benzene dehydroalkylation with ethane and propane, respectively, as long as the gases can be considered to be ideal gases, which is generally the case at pressures below 10 bar. In a membrane reactor, there is an increase in conversion with increasing reaction pressure for both reactions. At an $\dot{n}_{\text{sweep gas}} / \dot{n}_{\text{alkane,0}}$ ratio of 1 and a reaction pressure of 10 bar, ethane and propane conversions are about 5 and 10 %, respectively, representing more than a twofold increase in conversion. At an $\dot{n}_{\text{sweep gas}} / \dot{n}_{\text{alkane,0}}$ ratio of 10 and a reaction pressure of 10 bar, ethane and propane conversions are about 14 % and 25 %, respectively. The increase in conversion is more pronounced in the case of the dehydroalkylation of benzene with propane as the conversion is higher and, with increasing reaction pressure, the partial pressure of hydrogen is much higher on the reaction side, hence more hydrogen can be removed. The maximum hydrogen recovery generally also improves with increasing reaction pressure. Hence, for the dehydroalkylation of benzene with propane at an $\dot{n}_{\text{sweep gas}} / \dot{n}_{\text{alkane,0}}$ ratio of 10 similar conversions can be achieved at 400 °C and 10 bar as compared to 700 °C and 1 bar (cf. Figure 4.15), making the effect of pressure very valuable for this reaction. The same effect can be observed for the dehydroalkylation of toluene with ethane.

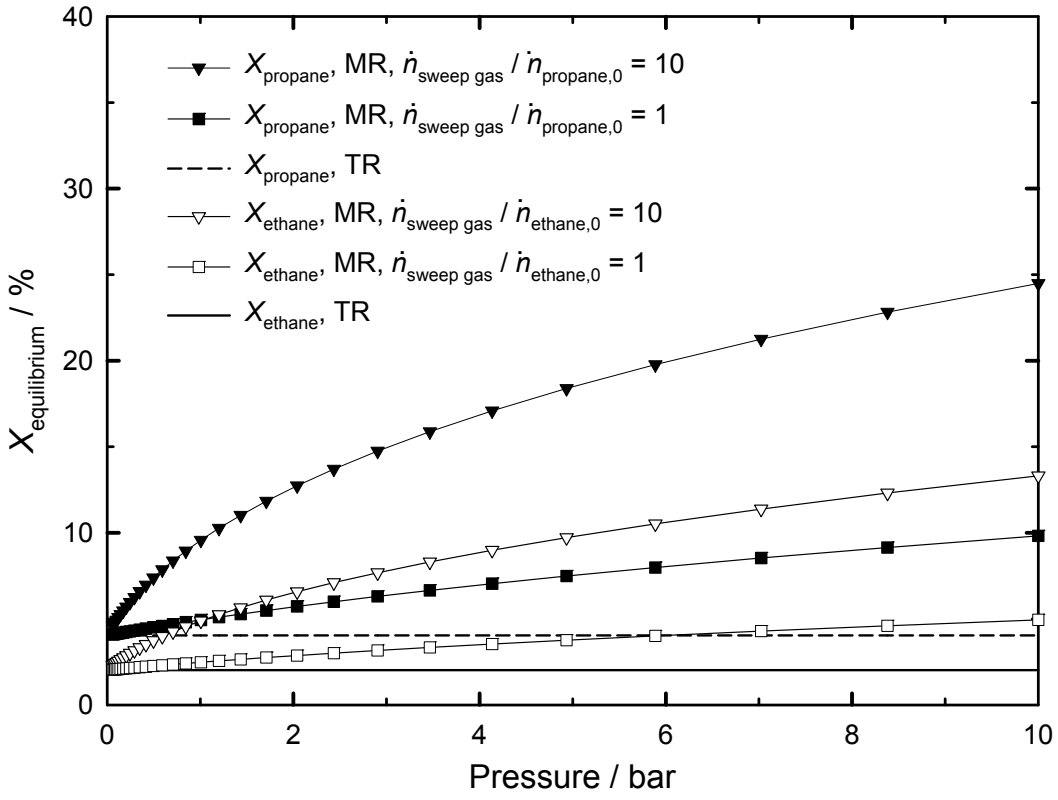


Fig. 4.19: Effect of reaction pressure on equilibrium conversion during dehydroalkylation of benzene/toluene with propane/ethane for traditional reactors and membrane reactors for $\dot{n}_{sweep\ gas} / \dot{n}_{alkane,0}$ ratios of 1 and 10 at 400 °C and $\dot{n}_{aromatic,0} / \dot{n}_{alkane,0} = 1$, assuming ideal gas behavior (pressure at the sweep side: 1 bar) [130].

## 4.4.4 Selectivity enhancement

The improvements on equilibrium conversion with regards to the $\dot{n}_{sweep\ gas} / \dot{n}_{alkane,0}$ ratio, temperature and pressure have been discussed. However, catalysts active for dehydrogenation or dehydroalkylation may also be active for other reactions. Then, membrane reactors may impact the selectivity of reactions. In order to investigate these effects, a reaction network was considered for one example reaction. Besides toluene dehydroalkylation with ethane, side reactions that were considered include: toluene disproportionation to xylenes and benzene as well as the consecutive dehydroalkylation of benzene, produced during the disproportionation of toluene, with ethane to form ethylbenzene. Figure 4.20 shows the selectivity at equilibrium $S_{equilibrium}$ for the aforementioned set of reactions. As the disproportionation reaction is thermodynamically favored, selectivity to xylenes is about 45 % at an $\dot{n}_{sweep\ gas} / \dot{n}_{alkane,0}$ ratio

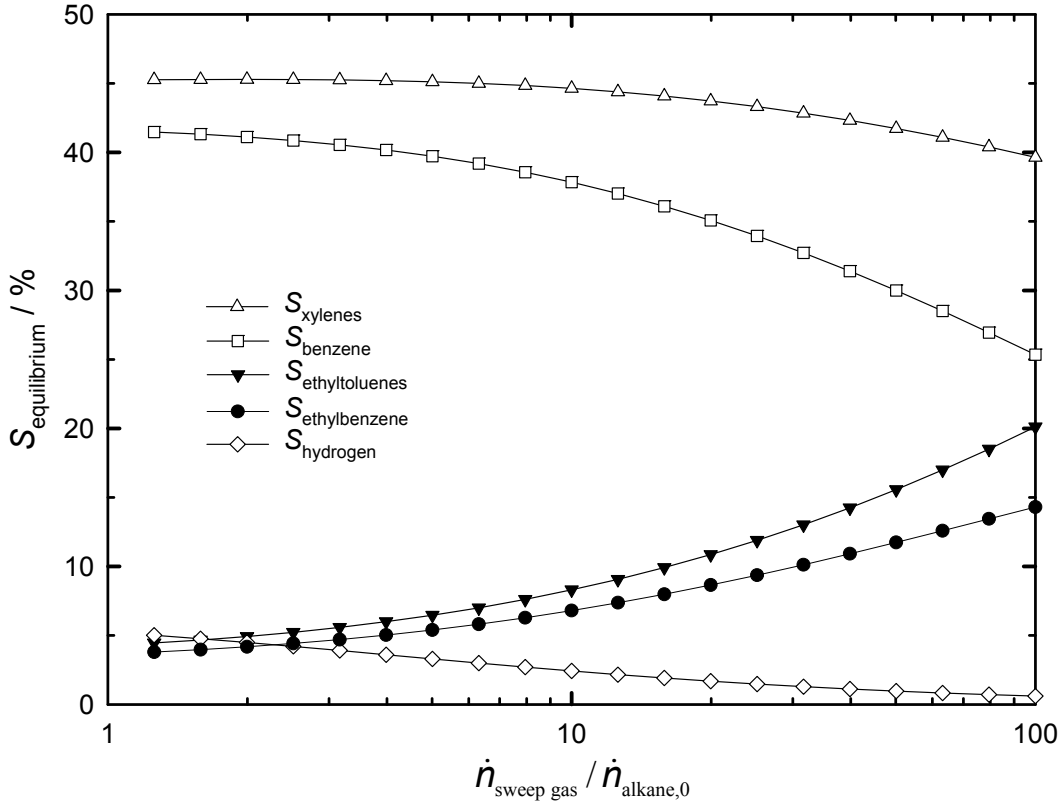


Fig. 4.20: Effect of $\dot{n}_{\text{sweep gas}} / \dot{n}_{\text{alkane,0}}$ ratio on the equilibrium selectivity $S_{\text{equilibrium}}$ during competitive reactions in a membrane reactor at 400 °C and pressures of 1 bar at the reaction and the sweep side. The desired reaction is the dehydroalkylation of toluene with ethane to the isomeric ethyltoluenes, with side reactions including the disproportionation of toluene to xylenes and benzene and consecutive dehydroalkylation of benzene with ethane to ethylbenzene with $\dot{n}_{\text{aromatic,0}} / \dot{n}_{\text{alkane,0}} = 1$ [130].

of 1. Benzene selectivity is somewhat lower since benzene is consumed forming ethylbenzene. With increasing $\dot{n}_{\text{sweep gas}} / \dot{n}_{\text{alkane,0}}$ ratio, the selectivity to xylenes decreases, however, not at a considerable rate. Benzene selectivity drops faster as a result of the improvements in the dehydroalkylation with ethane. From this result, at the optimum $\dot{n}_{\text{sweep gas}} / \dot{n}_{\text{alkane,0}}$ ratio of about 10 the gains in selectivity for the example reaction chosen are not large. However, if side reactions that consume hydrogen are also considered (dehydroalkylation catalysts will typically also catalyze the hydrodealkylation reaction of toluene to benzene and methane), then the membrane reactor could have a more pronounced effect on selectivity since it acts as a scavenger of the reactant for the side reaction besides

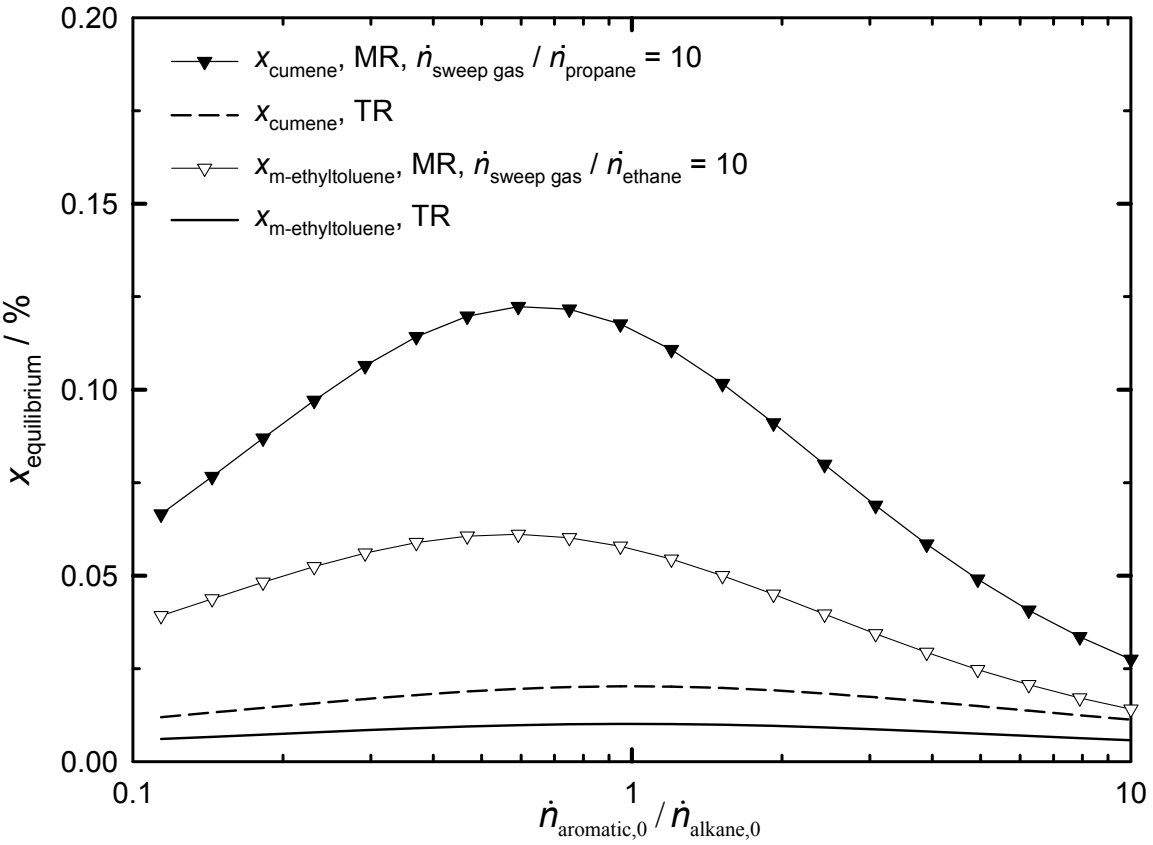


Fig. 4.21: Equilibrium molar fractions $x_{equilibrium}$ for the dehydroalkylation of benzene/toluene with propane/ethane as a function of the $\dot{n}_{aromatic,0} / \dot{n}_{alkane,0}$ ratio for traditional reactors and membrane reactors for an $\dot{n}_{sweep\ gas} / \dot{n}_{alkane,0}$ ratio of 10 at 400 °C and a pressure of 10 bar at the reaction side and 1 bar at the sweep side [130].

increasing the selectivity due to removal of hydrogen in the desired reaction. However, since in this case the thermodynamically very stable methane is formed, the current model cannot deal with these cases. Figure 4.21 shows the effect of the $\dot{n}_{aromatic,0} / \dot{n}_{alkane,0}$ feed ratio on the molar fractions at equilibrium $x_{equilibrium}$ for dehydroalkylation reactions. In a traditional reactor in the given range, the composition of the alkyl aromatics formed is essentially independent of the feed ratio. However, in a membrane reactor with increasing $\dot{n}_{aromatic,0} / \dot{n}_{alkane,0}$ ratio there is a distinct maximum for both reactions. Although an increasing $\dot{n}_{aromatic,0} / \dot{n}_{alkane,0}$ ratio has a positive effect on the conversion of the deficient reactant, it has a simultaneous effect to reduce the concentration of hydrogen which is

detrimental to the total amount of hydrogen that can be removed. Therefore, a value slightly less than one is the optimum $\dot{n}_{\text{aromatic},0} / \dot{n}_{\text{alkane},0}$ ratio.

### 4.4.5 Conclusions

The shift in equilibrium for dehydrogenation and dehydroalkylation reactions as a result of selective extraction of specific products in a membrane reactor can be evaluated by a simple model taking into account chemical reaction equilibrium and simultaneously the hydrogen equilibrium across the membrane. Based on the maximum hydrogen recovery, the molar flow of the sweep gas must be about 10 times higher than the molar flow of the alkane to ensure a high hydrogen recovery from the reactor. Under these conditions, an optimum shift in equilibrium can be achieved with a minimum dilution of the hydrogen on the sweep side. A careful choice of the sweep gas may help to overcome the negative effects of the dilution of hydrogen with sweep gas: Using steam as a sweep gas would minimize downstream separation costs for hydrogen and would have the added advantage of providing heat to the endothermic reaction. As the dehydrogenation of ethane or propane results in a net increase in the number of moles, a low pressure is favored. However, in a membrane reactor removal of hydrogen means that high conversions can still be maintained at high pressure. In the case of dehydroalkylation of benzene or toluene with propane or ethane, the number of moles is not changing. Thus, the reaction is independent of pressure within the range of ideal gas behavior in a traditional reactor. However, in a membrane reactor an increase in conversion can be achieved at higher pressures. The result of having increased conversion at higher pressures for the membrane reactor allows for applying higher pressures favorable for hydrogen permeation and affords to decrease the size of the reactor which is important for applications of membrane reactors for chemical processing.

Hence, membrane reactors may be beneficial for the removal of hydrogen during dehydrogenative-type reactions. However, there is a limit to which the equilibrium can be shifted, depending on the thermodynamics of the given reaction. The model suggested here may be applied to simply estimate optimum conditions for specific reactions in order to achieve the highest attainable conversions when applying membrane reactors. Thus, besides the lack of catalyst activity, excessive coking or membrane degradation, some reactions may not show favorable improvements in membrane reactors due to the limited shift in equilibrium that can be achieved or due to non-optimal reaction conditions.

## 4.5 Dehydroalkylation in a Pd-based membrane reactor

Hydrogen-selective, Pd-based membranes have been of great interest for a host of reactions [49, 55, 64, 131], in particular for dehydrogenation of alkanes or alkyl aromatics where thermodynamic equilibrium is severely limiting [65, 74, 80, 83, 87]. However, the success in the application of membrane reactors to dehydrogenation reactions has been limited. One issue is increased catalyst deactivation in membrane reactors. Since dehydrogenation reactions are highly endothermic it has not been possible to operate at mild conditions, and at high temperatures, removal of hydrogen favors coke formation [40-42]. Secondly, dehydrogenation reactions result in an increase in the number of moles, so that high pressures impair thermodynamics. This works against membrane reactors, as hydrogen permeation improves with increasing pressure.

As shown in Chapter 4.4 the dehydroalkylation of aromatics with alkanes in a membrane reactor has the advantage that with increasing pressure a positive effect on conversion may be observed since the net number of moles does not change during this reaction. Therefore, it is possible to operate at higher reaction pressures without sacrificing conversion (from a thermodynamic point of view). In the following chapter the experimental application of hydrogen-selective membranes for the dehydroalkylation of toluene with ethane is demonstrated. Furthermore, according to Chapter 4.4, due to the thermodynamics of the reaction, it is possible to operate under milder conditions.

### 4.5.1 Catalyst activity in the membrane reactor

Figure 4.22 shows toluene conversion and product selectivity as a function of time on stream at 2 bar and 350 °C [132]. Toluene conversion is stable throughout the entire experiment at approximately 5 %. The same trend applies to product selectivities. Therefore, further results are given after 90 min on stream, several experiments have been carried out with the same catalyst, with repetition to ensure reproducibility and on stream stability. Ethyltoluenes selectivity is about 50 % during the entire run with a lower hydrogen selectivity, about 30 %. This may be due to transport of hydrogen to the sweep side and formation of methane, about 5 %, via hydrodealkylation of toluene and hydrogenolysis or hydrocracking of higher alkanes, which consumes hydrogen [3]. Suppression of side reactions which consume hydrogen has previously been reported for ethane and *n*-butane dehydrogenation in membrane reactors where an improvement in selectivity was also observed [73, 81]. Toluene disproportionation, responsible for the formation of benzene and xylenes, is also limited with under 10 %

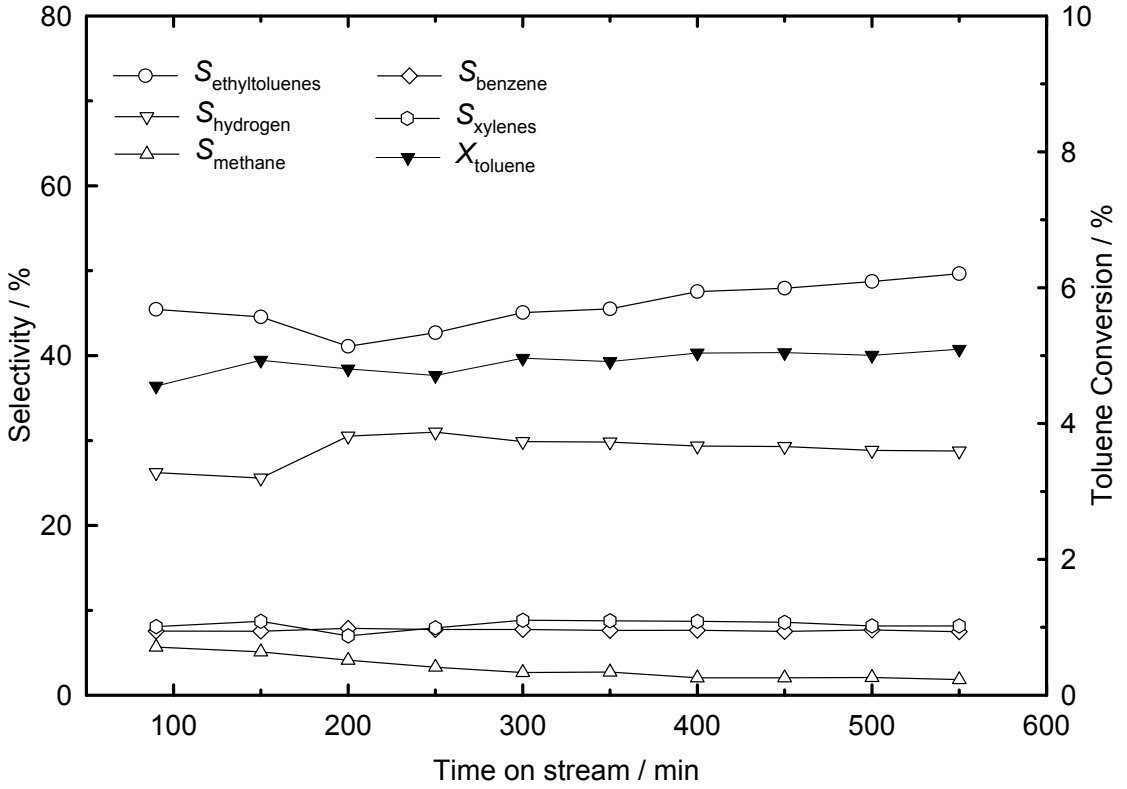


Fig. 4.22: Time-on-stream behavior for toluene conversion and product selectivity in the membrane reactor at 350 °C and 2 bar on 1.0Pd/H-ZSM-5 with $\dot{n}_{\text{sweep gas}} / \dot{n}_{\text{ethane,0}} = 1$, $\dot{n}_{\text{ethane}} / \dot{n}_{\text{toluene}} = 7$, $\dot{n}_{\text{nitrogen}} / \dot{n}_{\text{ethane}} = 5$ and $WHSV = 2.5$ h$^{-1}$ [132].

selectivity for both products. Other side products formed in minor amounts include propane, ethylbenzene, and trimethylbenzenes. Increased catalyst deactivation due to hydrogen removal is often blamed for loss in catalyst activity [40-42]. The improved catalyst stability observed here as compared to other dehydrogenation reactions carried out in membrane reactors may be explained by a combination of pre-coking of the catalyst (where only about 10 % of typical coke amount is found) as well as the milder reaction temperature, which does not encourage the formation of coke.

## 4.5.2 Influence of sweep gas flow rate

The effects of sweep gas has enjoyed much attention [65, 66] with best results coming from oxidation of the permeating hydrogen using a reactive sweep gas, e.g., air. However, since hydrogen is a valuable product, oxidation of hydrogen was avoided here. Figure 4.23 shows toluene and ethane conversions as a function of $\dot{n}_{\text{sweep gas}} / \dot{n}_{\text{ethane,0}}$. At low $\dot{n}_{\text{sweep gas}} / \dot{n}_{\text{ethane,0}}$ ratios, conversions are low, viz. 4.6 and 0.6 % for toluene and ethane, respectively. At higher

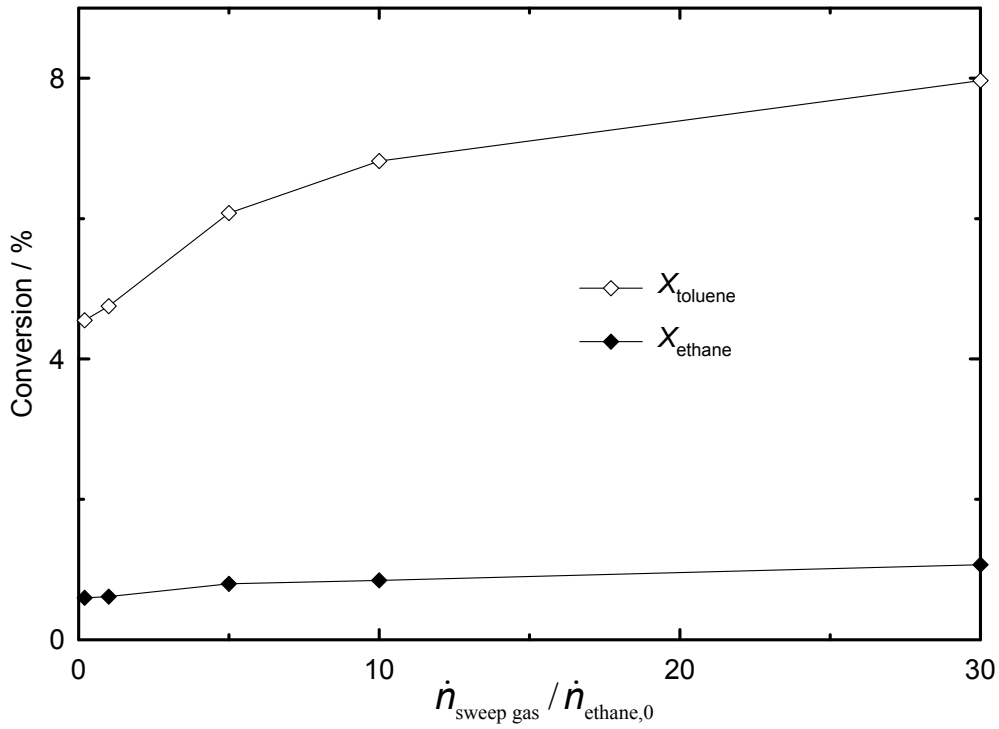


Fig. 4.23: Toluene and ethane conversion as a function of $\dot{n}_{sweep\ gas} / \dot{n}_{ethane,0}$ at 350 °C and 2 bar on 1.0Pd/H-ZSM-5 with $\dot{n}_{ethane} / \dot{n}_{toluene}$ = 7, $\dot{n}_{nitrogen} / \dot{n}_{ethane}$ = 5 and *WHSV* = 2.5 $h^{-1}$ after 90 min on steam [132].

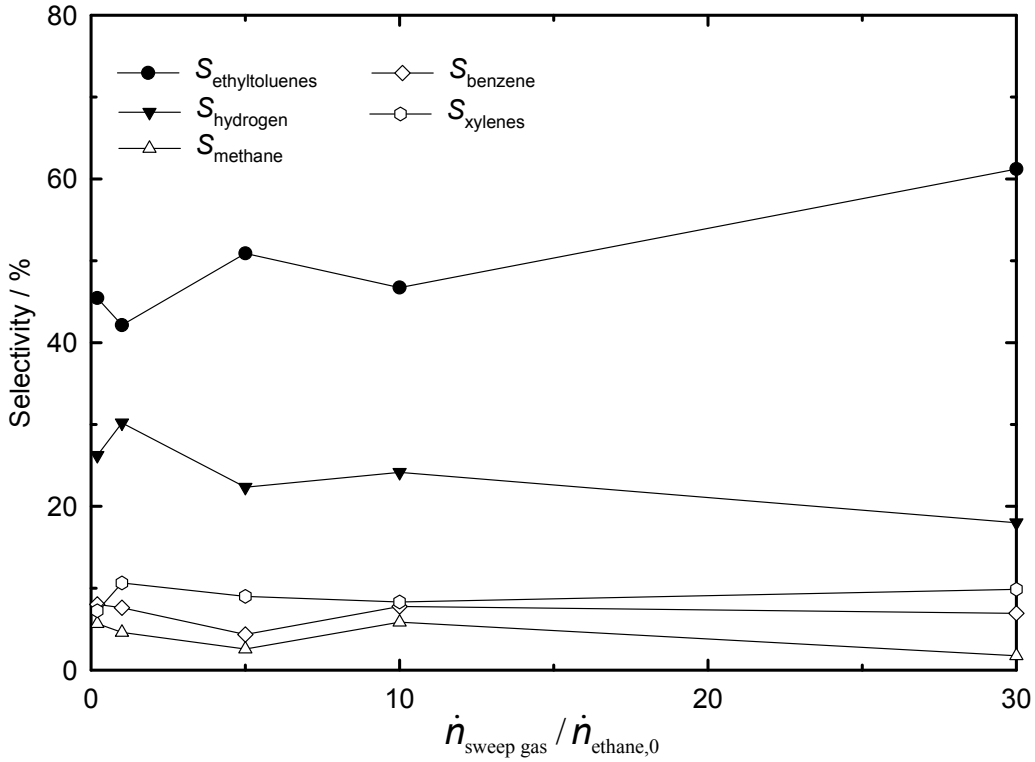


Fig. 4.24: Product selectivities as a function of $\dot{n}_{sweep\ gas} / \dot{n}_{ethane,0}$ at 2 bar and 350 °C on 1.0Pd/H-ZSM-5 with $\dot{n}_{ethane} / \dot{n}_{toluene}$ = 7, $\dot{n}_{nitrogen} / \dot{n}_{ethane}$ = 5, 90 min on stream and *WHSV* = 2.5 $h^{-1}$ [132].

Table 4.3: Toluene conversion and yields at various $\dot{n}_{\text{sweep gas}} / \dot{n}_{\text{ethane,0}}$ ratios at 2 bar and 350 °C on 1.0Pd/H-ZSM-5 with $\dot{n}_{\text{ethane}} / \dot{n}_{\text{toluene}} = 7$, $\dot{n}_{\text{nitrogen}} / \dot{n}_{\text{ethane}} = 5$, 90 min on stream and $WHSV = 2.5\ \text{h}^{-1}$ [132].

| $\dot{n}_{\text{sweep gas}} / \dot{n}_{\text{ethane,0}}$ | 0.1 | 1.0 | 5.0 | 10 | 30 |
|---|---|---|---|---|---|
| $X_{\text{toluene}}$ / % | 4.6 | 4.8 | 6.0 | 6.8 | 8.0 |
| $Y_{\text{ethyltoluenes}}$ / % | 2.0 | 2.0 | 3.1 | 3.2 | 4.9 |
| $Y_{\text{hydrogen}}$ / % | 1.2 | 1.5 | 1.4 | 1.6 | 1.4 |
| $Y_{\text{methane}}$ / % | 0.3 | 0.2 | 0.2 | 0.4 | 0.1 |
| $Y_{\text{benzene}}$ / % | 0.4 | 0.5 | 0.5 | 0.6 | 0.8 |
| $Y_{\text{xylenes}}$ / % | 0.4 | 0.4 | 0.3 | 0.6 | 0.8 |
| $Y_{\text{ethylbenzene}}$ / % | 0.3 | 0.2 | 0.1 | 0.1 | 0.1 |

$\dot{n}_{\text{sweep gas}} / \dot{n}_{\text{ethane,0}}$ ratios, both toluene and ethane conversions increase, sharply at first, almost doubling at a ratio of 30 to 8.0 and 1.1 % respectively. The increase in conversion is due to improved permeation of hydrogen as it can be removed more efficiently with increasing sweep gas flow rates. This is apparent from Figure 4.24, representing the product selectivity as a function of the $\dot{n}_{\text{sweep gas}} / \dot{n}_{\text{ethane,0}}$ ratio. The hydrogen selectivity on the reaction side decreases from 30 % to less than 20 %. This in turn shifts the reaction to form more ethyltoluenes, hence, ethyltoluenes selectivity increases from about 40 % to over 60 % at high sweep gas flow rates. Also, selectivity to the side products is generally low. Disproportionation of toluene is almost unaffected, whereas methane selectivity decreases from 5.7 % to 1.8 %; this may be explained by competition of the hydrogen permeation process with the toluene hydrodealkylation reaction for hydrogen. This is in agreement with studies on ethane and *n*-butane dehydrogenation where selectivity improvements have been observed [73, 81] in a membrane reactor. Thus, the membrane may help to avoid secondary reactions by $H_2$ removal.

Table 4.3 shows the toluene conversion and product yields at varying $\dot{n}_{\text{sweep gas}} / \dot{n}_{\text{ethane,0}}$ ratios at 2 bar. As already shown conversion improves with increasing $\dot{n}_{\text{sweep gas}} / \dot{n}_{\text{ethane,0}}$. Previously, the selectivity to ethyltoluenes has only improved in cases where conversion decreased (cf. Chapter 4.2), therefore the yield of the desired ethyltoluenes remained constant. Since here the selectivity towards the desired ethyltoluenes increases with increasing $\dot{n}_{\text{sweep gas}} / \dot{n}_{\text{ethane,0}}$ the yield of ethyltoluenes also increases, namely from 2.0 to 4.9 %, representing more than 100 % increase in the yield of the ethyltoluenes as a result of the

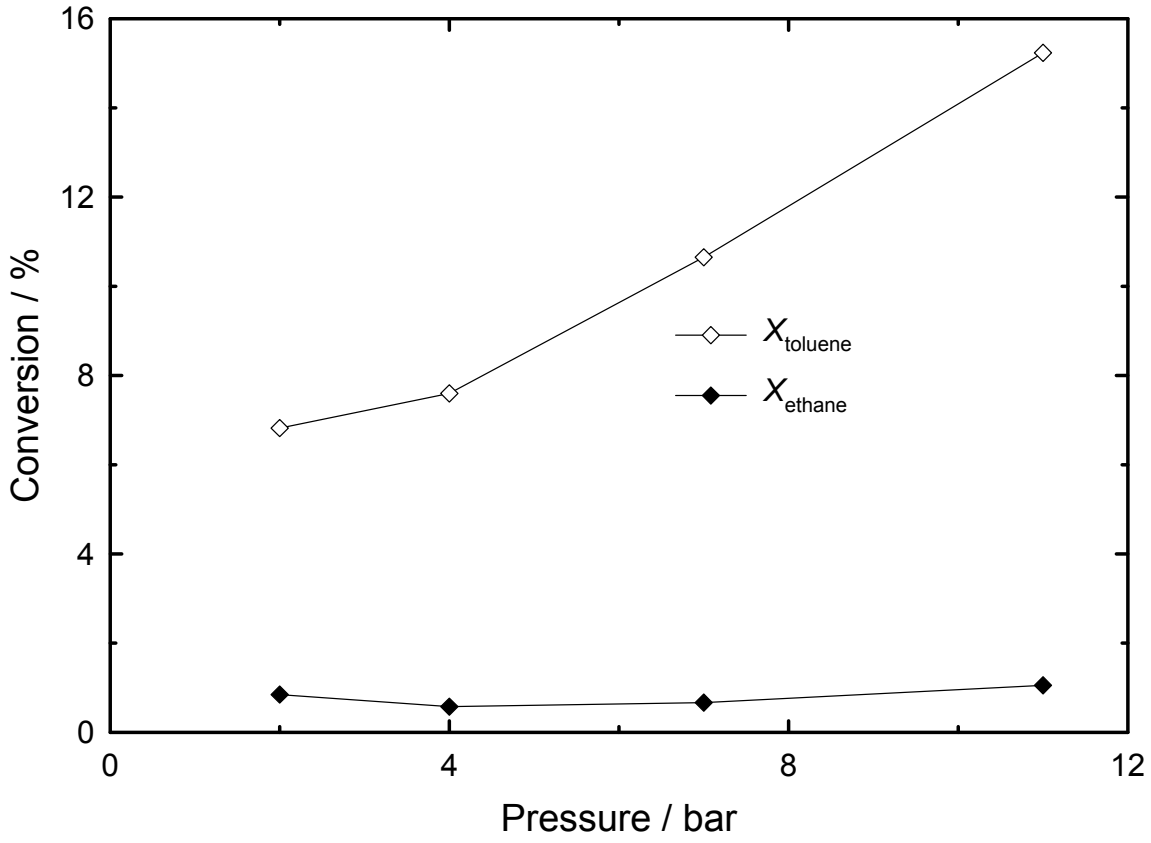


Fig. 4.25: Toluene and ethane conversion as a function of pressure on 1.0Pd/H-ZSM-5 at 350 °C with and $\dot{n}_{\text{sweep gas}} / \dot{n}_{\text{ethane,0}} = 10$, $\dot{n}_{\text{ethane}} / \dot{n}_{\text{toluene}} = 7$, $\dot{n}_{\text{nitrogen}} / \dot{n}_{\text{ethane}} = 5$ and $WHSV = 2.5\ \text{h}^{-1}$ after 90 min on steam.

higher sweep gas flow rate. The yields of methane and ethylbenzene drop, since the membrane competes for hydrogen. Yields of hydrogen stay constant at about 1.5 %, since more hydrogen is produced as a result of the equilibrium shift to replace permeated hydrogen.

### 4.5.3 Influence of pressure

The effect of pressure in membrane reactors has not enjoyed much attention mainly due to the fact that most dehydrogenation reactions result in a negative change in the total number of moles. Hence, increasing pressure would have a negative effect on dehydrogenation reactions. Figure 4.25 shows experimental toluene and ethane conversion as a function of pressure at a moderate $\dot{n}_{\text{sweep gas}} / \dot{n}_{\text{ethane,0}}$ of 10. At 2 bar, toluene conversion is 6.8 %. There is a strong increase in toluene conversion with pressure. At a pressure of 11 bar, the conversion has more than doubled to 15.2 % as compared to a pressure of 2 bar. Ethane conversion is rather low, since it is in excess, with a small increase above 4 bar.

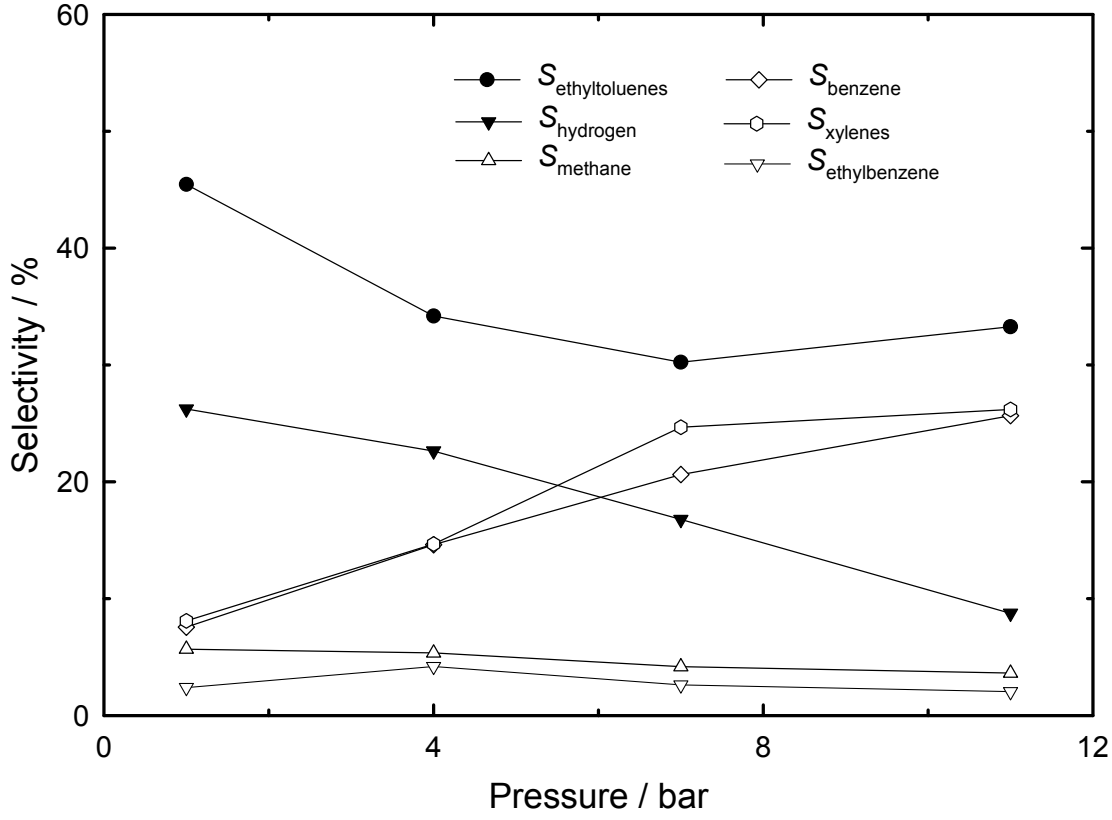


Fig. 4.26: Product selectivity as a function of pressure on 1.0Pd/H-ZSM-5 at 350 °C with $\dot{n}_{\text{sweep gas}} / \dot{n}_{\text{ethane},0} = 10$, $\dot{n}_{\text{ethane}} / \dot{n}_{\text{toluene}} = 7$, $\dot{n}_{\text{nitrogen}} / \dot{n}_{\text{ethane}} = 5$ and $WHSV = 2.5\ \text{h}^{-1}$ after 90 min on steam.

Figure 4.26 shows the effect of pressure on the product selectivities for the same reaction. Ethyltoluenes selectivity is initially high at about 45 %. With increasing pressure, the selectivity to ethyltoluenes decreases to ca. 30 % at 11 bar. Hydrogen selectivity is initially ca. 25 % dropping to under 10 % at 11 bar. The larger decrease in selectivity in hydrogen may be due to increased hydrogen permeation at higher pressure. Although a large increase in methane selectivity is observed with increasing pressure in a packed-bed reactor without a permeable membrane (cf. Figure 4.5), methane selectivity drops by 3 % with the increase in pressure in the membrane reactor. The same holds for ethylbenzene selectivity. There is a large increase in the selectivity to benzene and xylenes, products of the toluene disproportionation reaction. The combined selectivity to benzene and xylenes is 16 % at 2 bar, however at 11 bar the combined selectivity is about 50 %.

Figure 4.27 shows the product yields as a function of pressure. The yield of ethyltoluenes increases with pressure. The yield of ethyltoluene is over 5 % at a pressure of 11 bar, i.e., the

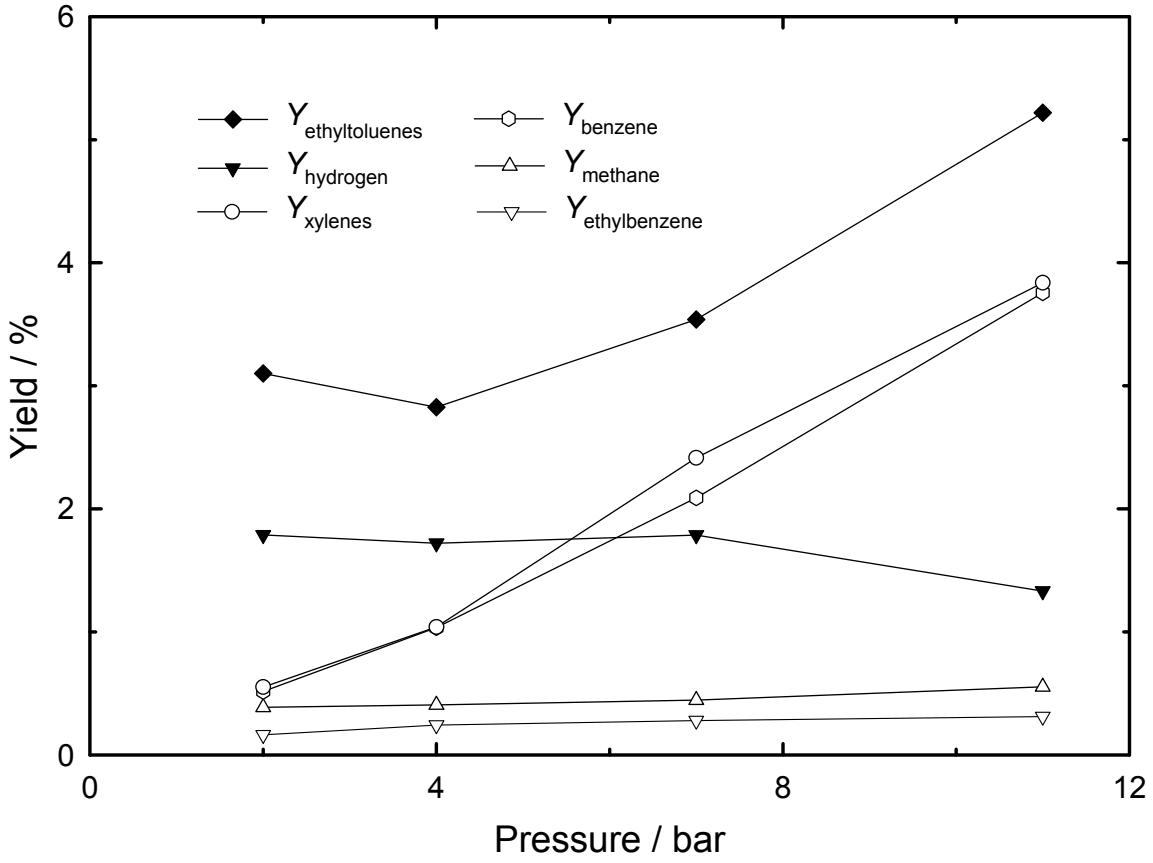


Fig. 4.27: Product yield as a function of pressure on 1.0Pd/H-ZSM-5 at 350 °C with $\dot{n}_{\text{sweep gas}} / \dot{n}_{\text{ethane,0}} = 10$, $\dot{n}_{\text{ethane}} / \dot{n}_{\text{toluene}} = 7$, $\dot{n}_{\text{nitrogen}} / \dot{n}_{\text{ethane}} = 5$ and $WHSV = 2.5\ \text{h}^{-1}$ after 90 min on steam.

yield of ethyltoluenes has doubled. Since the number of moles does not change, there is no negative effect on equilibrium when pressure is increased, so that the beneficial effects of increased hydrogen permeation at higher pressure is not countered by reduced equilibrium due to thermodynamics. The yield towards other side products that consume hydrogen, including methane and ethylbenzene, remains constant although conversion increases, again due to the improved hydrogen permeation. However, the yields of the disproportionation products increase strongly, possibly due to the improved accessibility of toluene to the pores of ZSM-5 at high pressure [3, 124]. The combined benzene and xylenes yield increases from about 1.5 % to almost 8 %. Toluene disproportionation is the most dominant reaction at higher pressure. The activity of the catalyst for disproportionation may even be suppressing the dehydroalkylation reaction since the disproportionation reaction is very competitive for acid sites at higher pressures. During preliminary experiments with a used catalyst, the *WHSV* was varied in order to minimize the toluene disproportionation reaction, i.e., as in the case of Figure 4.7. However, at a higher *WHSV* the membrane reactor seemed ineffective, possibly as

Table 4.4: Activation energy and pre-exponential factor for hydrogen permeation in this work in relation to selected literature values.

| $Ea_{hydrogen}$ / kJ·mol$^{-1}$ | $Pe_{hydrogen}$ / $10^{-5}$ mol·s$^{-1}$·m$^{-1}$·Pa$^{-0.5}$ | Reference |
|---|---|---|
| 16.9 | 1.15 | this work |
| 33.3 | 1.66 | Basile *et al.* [51] |
| 15.7 | 6.33 | Shu *et al.* [133] |
| 20.4 | 1.07 | Iliuta *et al.* [55] |
| 12.5 | 0.38 | Itoh and Xu [134] |

a result of reduced hydrogen removal through the membrane (as it is swept out faster than it can permeate). Comparison of experimental yields of ethyltoluene, increasing from ca. 3 % at 2 bar to 5 % at 11 bar, with yields calculated from the same thermodynamic model described in Chapter 3.2, with an $\dot{n}_{ethane} / \dot{n}_{toluene} = 7$, which predicts an increase from ca. 3 % at 1 bar to ca. 16 % at 10 bar, indicates that the membrane reactor underperforms. This may be due to the power dependency of permeation kinetics (cf. equation (2.1)) or due to competing side reactions.

Hou and Hughes [77] observed an increase in conversion of propane in a membrane reactor from 30 % at 1 bar to 35 % at 3 bar, although there is a loss in the total number of moles during propane dehydrogenation. They assigned this increase to an increased rate in hydrogen permeation, which compensates for lowering of the equilibrium conversion. Lee *et al.* [88] studied the effect of pressure during the dry reforming of methane, from 1 to 20 bar, applying a $H_2$-selective silica-based membrane. The authors also reported increased hydrogen permeability through the membrane with increasing pressure. The yield of hydrogen first increased, and then decreased due to the unfavorable equilibrium at high pressure, ultimately resulting in severe losses in conversion with increasing pressure. During methane steam reforming, Mori *et al.* [48] observed a 25 % loss in methane conversion with increasing pressure up to 10 bar, even though hydrogen recovery improved.

### 4.5.4 Kinetic reaction/permeation model

In order to model the reaction/permeation process, the membrane was characterized for its permeation properties. Table 4.4 shows a comparison of the values for the activation energy and the pre-exponential factor as measured for the membrane (after reactions) as compared to some values found in literature. Both calculated parameters fall within the range of other

Table 4.5: Estimated parameters for rate constants of rate equations (3.25 and 3.29 to 3.31) and the corresponding linear variance from experimental data at 350 °C.

| | | $\sigma$ / - |
|---|---|---|
| $k_a$ / mol·g$^{-1}$·s$^{-1}$·Pa$^{-0.5}$ | $2.05 \cdot 10^{-4}$ | $6.20 \cdot 10^{-5}$ |
| $k_b$ / Pa$^{-0.5}$ | $8.89 \cdot 10^{-4}$ | $7.28 \cdot 10^{-4}$ |
| $k_c$ / mol·g$^{-1}$·s$^{-1}$·Pa$^{-2}$ | $1.35 \cdot 10^{-5}$ | $4.42 \cdot 10^{-6}$ |
| $k_d$ / Pa$^{-1}$ | $1.73 \cdot 10^{-2}$ | $1.59 \cdot 10^{+1}$ |
| $k_e$ / mol·g$^{-1}$·s$^{-1}$·Pa$^{-1.5}$ | $6.86 \cdot 10^{-4}$ | $1.05 \cdot 10^{-5}$ |
| $k_f$ / mol·g$^{-1}$·s$^{-1}$·Pa$^{-1.5}$ | $3.89 \cdot 10^{-4}$ | $8.72 \cdot 10^{-6}$ |

membrane reactors. Specifically, Iliuta *et al.* [55] used a similar membrane reactor and presented values very close to those measured in this work.

Table 4.5 shows estimated parameters for rate constants for rate equations (3.25, 3.29 to 3.31) and the corresponding linear variance from different product yields collected by changing the mass of catalyst. Rate factor terms $k_a$ and $k_c$, in the dehydroalkylation and disproportionation reactions, respectively, reflect the experimental selectivity towards the desired ethyltoluenes by the higher rate constant for the dehydroalkylation reaction. The inhibition factors $k_b$ and $k_d$ are higher than the rate factor, hence product/reactant inhibition may play an important role in determining the overall rate of reaction. However, whereas the variance for the rate factor terms are low, the calculated variance of the inhibition terms are not as good indicating that a good fit for these variables could not be achieved by the Levenberg-Marquadt algorithm, and these terms may be more redundant. The rate constants for the two hydrodealkylation reactions (ethyltoluenes: $k_e$ and toluene: $k_f$) are higher than those of the dehydroalkylation reaction. Again, this is due to a strong increase in methane yields at higher contact times which allows the secondary reactions to take place. The combination of the rate constants and hydrogen permeation constants were used to model the reaction/permeation process in the membrane reactor.

Figure 4.28 shows product selectivities from the kinetic model proposed by solving the coupled set of differential equations with appropriate rate equations and constants. Initially, the selectivity to hydrogen and ethyltoluenes is close to equimolar. Increasing the catalyst mass (or contact time), results in an increase in selectivity to ethyltoluenes, reaching a maximum of about 60 %. This is as a result of a hydrogen sink, either due to permeation

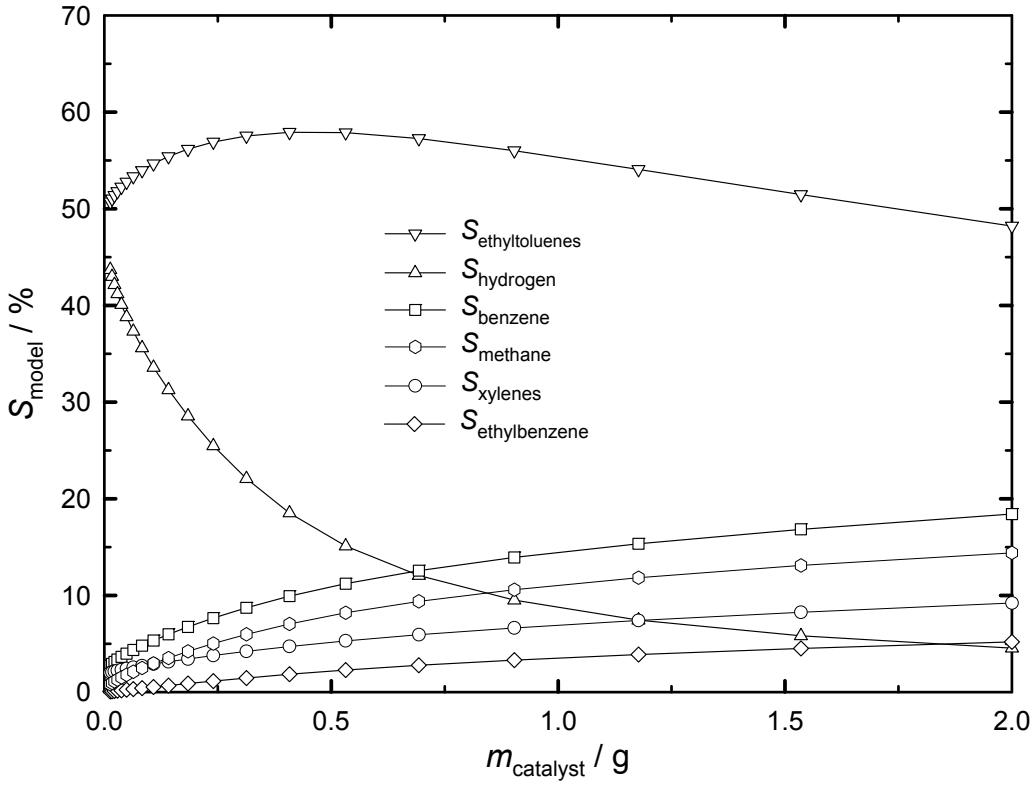


Fig. 4.28: Product selectivities for the kinetic reaction network as a function of catalyst mass in the membrane reactor at $\dot{n}_{\text{sweep gas}} / \dot{n}_{\text{ethane,0}} = 10$, 350 °C, with $\dot{n}_{\text{ethane}} / \dot{n}_{\text{toluene}} = 7$, $\dot{n}_{\text{nitrogen}} / \dot{n}_{\text{ethane}} = 5$.

(since the $\dot{n}_{\text{sweep gas}} / \dot{n}_{\text{ethane,0}}$ ratio is 10), at the lower contact times, or due to consumption of hydrogen during methane formation at higher contact times. As a result, hydrogen selectivity drops from about 45 % at low contact times to about 5 %. At higher contact times, the selectivity towards ethyltoluenes starts to drop, since the hydrodealkylation reactions start to consume ethyltoluenes, and compete with the membrane for hydrogen. Also the disproportionation reaction becomes more prominent at higher contact times. The selectivity trend quantitatively agrees with preliminary experimental results (with a used catalyst). With a catalyst mass of 0.2 g, the conversions are too low, however, with a catalyst mass of 1.0 g and higher conversions the toluene disproportionation reaction is highly dominant.

Figure 4.29 presents the product selectivities for the proposed kinetic reaction network as a function of the $\dot{n}_{\text{sweep gas}} / \dot{n}_{\text{ethane,0}}$ ratio as well as the corresponding experimental results (cf. Figure 4.24). At a low $\dot{n}_{\text{sweep gas}} / \dot{n}_{\text{ethane,0}}$ ratio selectivity to ethyltoluenes is about 40 %, increasing to about 60 % at a ratio of 30. This is due to a decrease in selectivity to hydrogen,

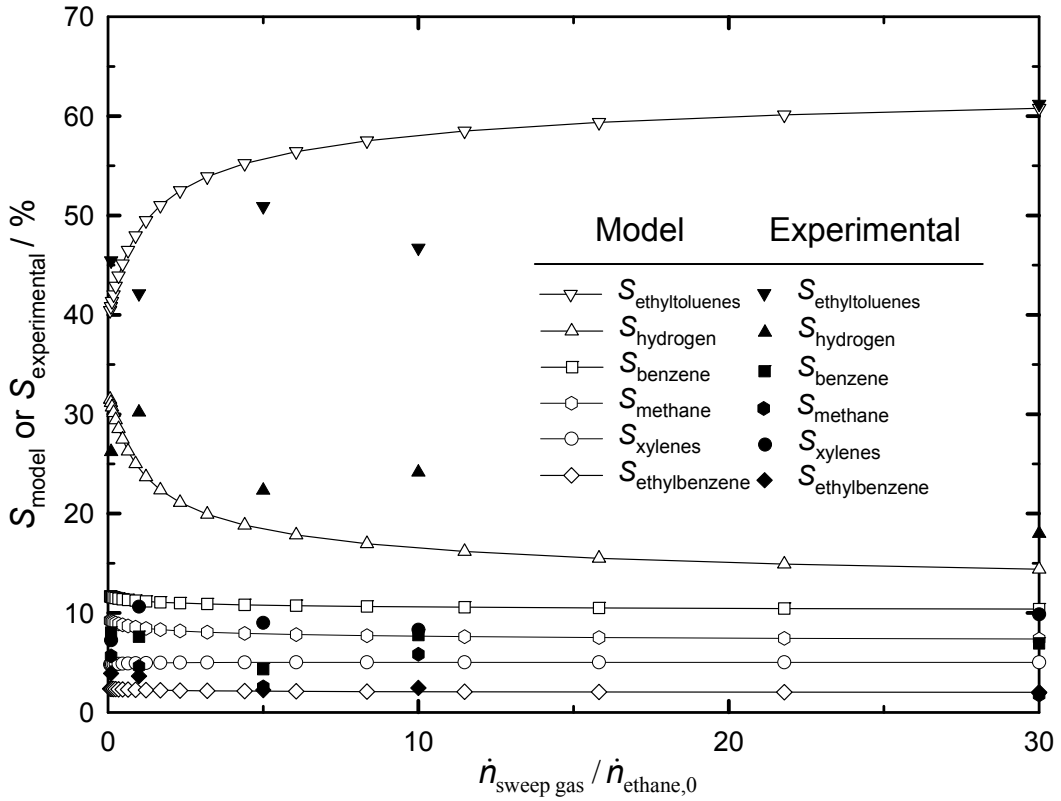


Fig. 4.29: Product selectivities for the kinetic reaction network as a function of the $\dot{n}_{sweep\ gas} / \dot{n}_{ethane,0}$ ratio at 350 °C and $\dot{n}_{ethane} / \dot{n}_{toluene} = 7$, $\dot{n}_{nitrogen} / \dot{n}_{ethane} = 5$ and $WHSV = 2.5\ h^{-1}$ (experimental results from Figure 4.24).

from about 30 % to 15 %, as a result of improved hydrogen removal. The modeling results are in good agreement with experimental results.

Selectivity to methane which competes for hydrogen drops from about 10 % to 7 %, since hydrogen recovery is better at higher $\dot{n}_{sweep\ gas} / \dot{n}_{ethane,0}$ ratios. The higher simulated methane selectivity from the model as compared to experimental results may be due to pre-coking of the catalyst. The controlled pre-coking ensures that metal particles on the surface, primarily responsible for hydrocracking reactions (cf. Chapters 3.1 and 4.2), are rendered inactive. Simulated xylenes selectivity is about 5 % and remains unaffected. Selectivity to benzene is over 10 %, dropping slightly (since the toluene dehydroalkylation reaction is also suppressed). The model predicts a benzene selectivity of over 10 %. However, experimentally less benzene is formed. This may, again, be due to the pre-coking of the catalyst, resulting in a reduced hydrodealkylation activity, producing less benzene. Furthermore, the experimental amounts of xylenes and benzene are similar, indicating that they are formed by disproportionation.

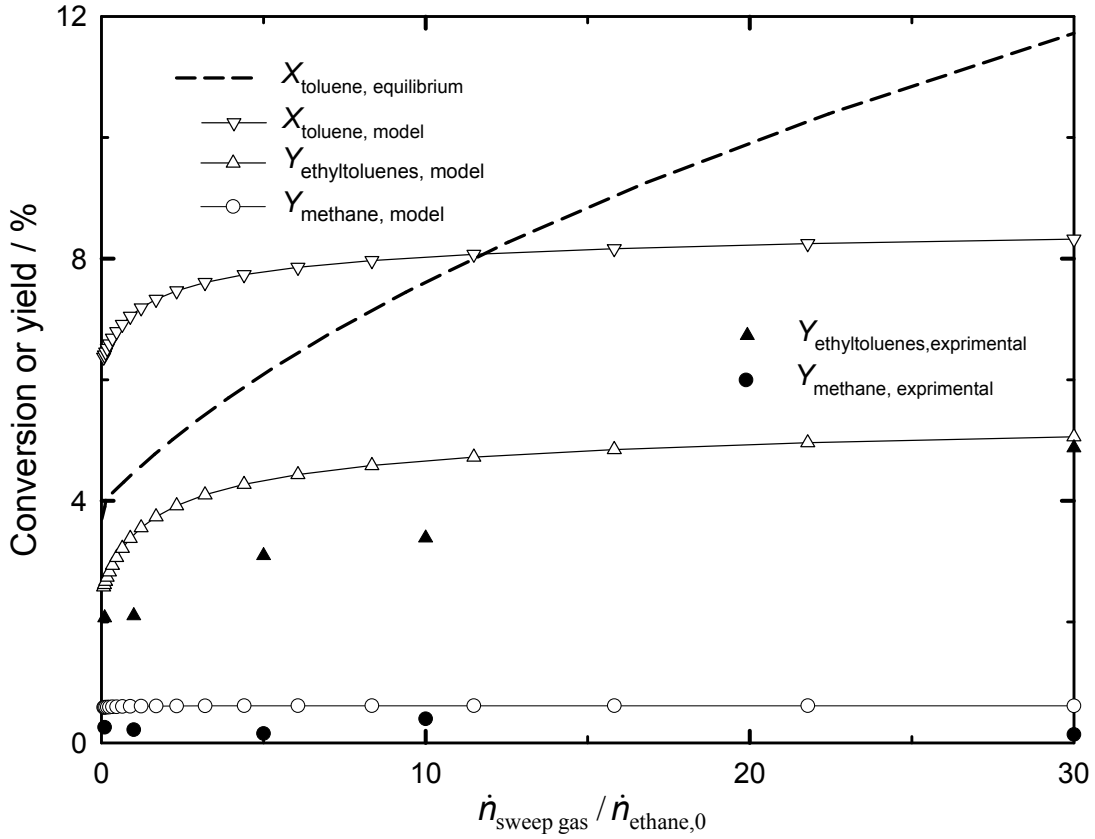


Fig. 4.30: Toluene conversion and yield of ethyltoluenes and methane for the kinetic reaction network in the membrane reactor as a function of the $\dot{n}_{\text{sweep gas}} / \dot{n}_{\text{ethane,0}}$ ratio at 350 °C and $\dot{n}_{\text{ethane}} / \dot{n}_{\text{toluene}} = 7$, ($\dot{n}_{\text{nitrogen}} / \dot{n}_{\text{ethane}} = 5$ and $WHSV = 2.5$ h$^{-1}$, not applicable to thermodynamic model. Experimental results from Table 4.3).

Figure 4.30 shows a comparison of toluene conversion and yield of ethyltoluenes and methane for the proposed kinetic reaction network models, toluene conversion for the single reaction thermodynamic model, as well as experimental results as a function of the $\dot{n}_{\text{sweep gas}} / \dot{n}_{\text{ethane,0}}$ ratio. Since the thermodynamic model is for the single reaction, comparison between the thermodynamic model and the kinetic model is possible only when comparing yield of ethyltoluenes from the kinetic model to the toluene conversion from the thermodynamic model.

Toluene conversion increases with increasing $\dot{n}_{\text{sweep gas}} / \dot{n}_{\text{ethane,0}}$, however, both simulated thermodynamic and kinetic conversions are higher than the experimentally observed conversion at low $\dot{n}_{\text{sweep gas}} / \dot{n}_{\text{ethane,0}}$ ratios (cf. Figure 4.23). This may be due to the fact that the activity of the catalysts was slightly reduced due to pre-coking, which is necessary to

minimize damage to the membrane as a result of catalyst coking. However, then model predicts a toluene conversion of over 8 % at an $\dot{n}_{\text{sweep gas}} / \dot{n}_{\text{ethane,0}}$ ratio of 30 which agrees well with the experimentally observed results (cf. Figure 4.23). Yet, whereas experimentally a steady increase in conversion is observed the model predicts a faster increase at low $\dot{n}_{\text{sweep gas}} / \dot{n}_{\text{ethane,0}}$ ratios.

The simulated yield of ethyltoluenes, from the kinetic model, increases from about 2.5 % to 5 %, again slightly higher than the experimentally observed yields. The stronger increase in the yield of ethyltoluenes is due to a coupled effect of increasing conversion, due to the shift in equilibrium by the membrane reactor and a simultaneous increase in selectivity to ethyltoluenes since the side reactions consuming methane are suppressed by scavenging of hydrogen. As a result, calculated methane yields remain almost unchanged (and even drop experimentally), although the conversion increases significantly. This is a significant advantage since in experiments carried out in a traditional packed-bed reactor an increase in conversion is accompanied by a strong increase in methane yield. Comparison of the thermodynamic and kinetic models ($Y_{\text{ethyltoluenes, model}} \equiv X_{\text{toluene, equilibrium}}$, since in the thermodynamic model ethyltoluenes formation is the only reaction considered) reveals flattening of the ethyltoluenes yield above an $\dot{n}_{\text{sweep gas}} / \dot{n}_{\text{ethane,0}}$ of 10 for the latter model. By contrast, the thermodynamic model predicts a further strong increase predicting an equivalent yield of almost 12 % at an $\dot{n}_{\text{sweep gas}} / \dot{n}_{\text{ethane,0}}$ ratio of 30 whereas the experimental (and kinetic model) $Y_{\text{ethyltoluenes}}$ is about 5 %. The models are in close agreement at low $\dot{n}_{\text{sweep gas}} / \dot{n}_{\text{ethane,0}}$ ratios. Therefore, it is likely that at high $\dot{n}_{\text{sweep gas}} / \dot{n}_{\text{ethane,0}}$ ratios permeation kinetics start playing a significant role.

### 4.5.5 Conclusions

In conclusion, the dehydroalkylation of toluene with ethane can be successfully achieved in a membrane reactor. Under mild conditions, the catalytic performance of the bifunctional zeolite in the membrane reactor is stable with time on stream (although severe deactivation is observed at higher temperatures and pressures). Experiments demonstrate large improvements with tripled conversion and almost tripled yield to the desired ethyltoluenes by increasing the sweep gas flow rate and the pressure on the reaction side. Selectivity to methane and ethylbenzene, formed from hydrodealkylation reactions that consume hydrogen, is reduced.

Increasing pressure has a positive effect on conversion since the net number of moles does not change during this reaction. Unfortunately, at high pressure, the toluene disproportionation reaction is dominant. Attempting to successfully eliminate the toluene disproportionation by decreasing contact time (cf. Chapter 4.2) is not possible here, since under these conditions the produced hydrogen is swept out of the reaction zone before it can permeate. Hence, a careful optimization of the catalyst and the reaction conditions is needed in order to further achieve industrially relevant yields.

The modeling results agree well with the experimental results and confirm the experimental observations that an optimum residence time exists, at which the hydrogen produced can be transported through the membrane reactor before it is transported out on the reaction side or is consumed by hydrodealkylation reactions. Furthermore, it can be confirmed from the model that the experimentally observed reduction of methane selectivity is a direct result of hydrogen permeation through the membrane reactor.

# 5 General conclusions and recommendations

### 5.1.1 General conclusions

Due to the high thermodynamic stability of ethane, the title reaction is strongly limited by equilibrium. Since the experimentally measured conversions are higher than the predicted thermodynamic values, assuming that the ideal gas law applies, a non-ideal reaction network model was used to investigate the effect of pressure. At 300 °C, the thermodynamic model is in agreement with the experimental results. However, at 350 °C conversions are well over the expected values calculated from the same model. The "supra-equilibrium" may be due to the formation of hydrogen-rich methane, acting as a hydrogen sink, hence shifting equilibrium towards the formation of ethyltoluenes. This was attributed to consumption of hydrogen as a result of methane formation. Since methane is mainly formed by consumption of hydrogen, i.e., it is a secondary reaction, the *WHSV* was varied to improve selectivity to the title reaction. At a high *WHSV*, the formation of methane can be entirely avoided. Furthermore, the disproportionation of toluene is also absent, resulting in 100 % selectivity to ethyltoluenes and hydrogen. Decreasing the *WHSV*, results in an increase in conversions as well as in the yield of ethyltoluenes. As conversion increases the selectivity to ethyltoluenes decreases, since the toluene disproportionation reaction can compete with the dehydroalkylation reaction. With increasing conversion, $C_1$ to $C_4$ alkanes are also formed to a larger extent, as well as other aromatics including benzene, xylenes, and ethylbenzene. A maximum yield of ethyltoluenes is observed at a conversion of 13 % at 90 h on stream. It is suggested that this maximum is a result of secondary reactions of ethyltoluenes. Hydrocracking experiments confirm that methane forms mainly from secondary reactions of the products or reactants. A noble metal is required for a dehydroalkylation catalyst with good activity. However, the metal can also promote undesired side reactions including hydrocracking/hydrogenolysis and, mainly, the hydrodealkylation of the reactants and products. Although Pt/H-ZSM-5 shows the highest toluene conversion, Pd/H-ZSM-5 has high activity for toluene dehydroalkylation and the highest yield to ethyltoluenes. This is a result of Pd being less active for hydrodealkylation. Hence, further experiments in the membrane reactor were carried out using a Pd/H-ZSM-5 catalyst.

Since high selectivity to the desired products can be achieved, the ultimate goal of increased yields can be achieved by improving conversion. This was attempted by application of a

membrane reactor, which may improve yields by selectively removing a product and hence shifting equilibrium. Prior to the catalytic experiments in the membrane reactor, a model was developed applying fundamental thermodynamics in order to gauge the maximum attainable shift in equilibrium by the selective removal of hydrogen in a membrane reactor. The model considers chemical reaction equilibrium and simultaneously the hydrogen equilibrium across the membrane. From the viewpoint of hydrogen recovery, the molar flow of the sweep gas must be about 10 times higher than the molar flow of the alkane to ensure that hydrogen recovery from the reactor is maximized. Under these conditions, an optimum shift in equilibrium can be achieved with a minimum dilution of the hydrogen on the sweep side.

Comparison of the dehydroalkylation reaction with, typically more widely studied, dehydrogenation reactions shows interesting advantages. Since dehydrogenation reactions typically result in a net increase in the number of moles, low pressure is favored. Removal of hydrogen, by means of a membrane, means that high conversions can still be maintained at high pressure. In contrast, for the dehydroalkylation of toluene with ethane, the number of moles does not change, thus, in a membrane reactor an increase in conversion can be achieved at higher pressures since more hydrogen can permeate at higher pressure. However, there is a limit to which the equilibrium can be shifted, depending on the thermodynamics of the given reaction. The model suggested here may be applied to simply estimate optimum conditions for specific reactions in order to achieve the highest attainable conversions when applying membrane reactors. The modeling results are confirmed by experimental results. The dehydroalkylation of toluene with ethane can be successfully performed in a membrane reactor. Since the reaction is taking place under mild conditions, the catalytic performance of the bifunctional zeolite in the membrane reactor is stable with time on stream. Experiments demonstrate large improvements with tripled conversion and almost tripled yield to the desired ethyltoluenes by increasing the sweep gas flow rate and the pressure on the reaction side. The selectivities to methane and ethylbenzene, formed from hydrodealkylation reactions that consume hydrogen, is reduced.

Increasing pressure has a positive effect on conversion since the net number of moles does not change during this reaction. However, at high pressure, the toluene disproportionation reaction is dominant. Unfortunately, choosing a low contact time to successfully eliminate the toluene disproportionation is not possible here, since under such conditions the produced hydrogen is swept out of the reaction zone before it can permeate. Hence, a careful

optimization of the catalyst and the reaction conditions is needed in order to further achieve industrially relevant yields. Modeling results confirm experimental observations that an optimum *WHSV* exists, at which the hydrogen produced can be transported through the membrane reactor before it can escape on the reaction side or is consumed during hydrodealkylation reactions. Furthermore, it can be confirmed from the model that the experimentally observed reduction of methane selectivity is as a direct result of hydrogen permeation through the membrane reactor. The proposed kinetic and thermodynamic models agree well at low $\dot{n}_{\text{sweep gas}} / \dot{n}_{\text{ethane,0}}$ ratios but deviate at higher ratios, possibly as permeation kinetics start to play a role at high $\dot{n}_{\text{sweep gas}} / \dot{n}_{\text{ethane,0}}$ ratios.

### 5.1.2 Recommendations

From the results of the work carried out here the following recommendations for future work can be made:

- Further optimization of the catalyst in order to avoid the toluene disproportionation reaction, especially at high pressure, temperature, and contact times. This can be achieved either by pore-size engineering of the zeolite, or by careful control of the strength and density of the acid sites of the zeolite.

- Improvement of the dehydrogenative component of the catalyst, in order to further reduce the hydrodealkylation activity and increase the hydrogen partial pressure, which would enhance hydrogen permeation during reaction in the membrane reactor.

- The alkylation of benzene with ethane seems very interesting taking into consideration the two above points. Using benzene instead of toluene would solve both problems, i.e., the disproportionation reaction can be entirely avoided, and hydrocracking reactions can be suppressed to a large extent.

- Faster, more effective removal of hydrogen on the sweep side can also lead to improvements. In this case, coupling a hydrogenative-type reaction on the sweep side would be beneficial. Coupling the dehydroalkylation reaction with, for example, direct phenol production from benzene and air in a membrane reactor, would be very interesting as one can simultaneously produce two intermediate bulk chemicals in a one-step process.

# 6 References

[1] S. Ernst, W. Petzny, in: Chemical Technology, Processes and Products, Energy Sources, Organic Raw Materials, R. Dittmeyer, W. Keim, G. Kreysa, and A. Oberholz (Eds.); Vol. 4, WILEY-VCH, Weinheim, 2005, p. 523-659.

[2] S. Sealy, Y. Traa, Appl. Catal. A: General 294 (2005) 273-278.

[3] D. Singer, S.A. Sadat Rezai, S. Sealy, Y. Traa, Ind. Eng. Chem. Res. 46 (2007) 395-399.

[4] A.V. Smirnov, E.V. Mazin, V.V. Yuschenko, E.E. Knyazeva, S.N. Nesterenko, I.I. Ivanova, L. Galperin, R. Jensen, S. Bradley, J. Catal. 194 (2000) 266-277.

[5] S. Todorova, B.L. Su, J. Mol. Catal. A: Chemical 201 (2003) 223-235.

[6] X.Q. Huang, X.D. Sun, S.K. Zhu, Z.M. Liu, Catal. Lett. 119 (2007) 332-338.

[7] S. Sealy, D. Singer, Y. Traa, in: Oxidation and Functionalization: Classical and Alternative Routes and Sources, S. Ernst, E. Gallei, J.A. Lercher, S. Rossini, and E. Santacesaria (Eds.); DGMK, Hamburg, Milan, 2005, p. 245-251.

[8] S. Kato, K. Nakagawa, N. Ikenaga, T. Suzuki, Catal. Lett. 73 (2001) 175-180.

[9] S. Kato, K. Nakagawa, N. Ikenaga, T. Suzuki, Chem. Lett. (1999) 207-208.

[10] D.B. Lukyanov, T. Vazhnova, J. Mol. Catal. A: Chemical 279 (2008) 128-132.

[11] J.A. Labinger, J.E. Bercaw, Nature 417 (2002) 507-514.

[12] N. Mizuno, M. Misono, in: Catalytic Activation and Functionalisation of Light Alkanes, E.G. Derouane, J. Haber, F. Lemos, F. Ramôa Ribeiro, and M. Guisnet (Eds.); Kluwer Academic Publishers, Dordrecht, 1998, p. 311-331.

[13] D.R. Stull, E.F. Westrum Jr., G.C. Sinke, The Chemical Thermodynamics of Organic Compounds, John Wiley & Sons, New York, 1969, 875 pp.

[14] J. Weitkamp, personal communication, 2008.

[15] W.W. Kaeding, L.B. Young, A.G. Prapas, CHEMTECH 12 (1982) 556-562.

[16] J.S. Beck, W.O. Haag, in: Handbook of Heterogeneous Catalysis, G. Ertl, H. Knözinger, and J. Weitkamp (Eds.); Vol. 5, WILEY-VCH, Weinheim, 1997, p. 2123-2136.

[17] D.S. Coombs, A. Alberti, T. Armbruster, G. Artioli, C. Colella, W. Galli, J.D. Grice, F. Liebau, J.A. Mandarino, H. Minato, E.H. Nickel, E.H. E. Passaglia, D.R. Peacor, S. Quartieri, R. Rinaldi, M. Ross, R.A. Sheppard, E. Tillmanns, G. Vezzalini, Can. Mineral. 35 (1997) 1571-1606.

[18] O.D. Friedrichs, A.W.M. Dress, D.H. Huson, J. Klinowski, A.L. Mackay, Nature 400 (1999) 644-647.

[19] http://www.iza-structure.org/default.htm, accessed on 18.09.2008.

[20] J. Weitkamp, Solid State Ionics 131 (2000) 175-188.

[21] T. Maesen, in: Introduction to Zeolite Science and Practice, J. Čejka, H. van Bekkum, A. Corma, and F. Schüth (Eds.); Studies in Surface Science and Catalysis, Vol. 168, Elsevier, Amsterdam, 2007, p. 1-12.

[22] A. Corma, J. Catal. 216 (2003) 298-312.

[23] M. Stöcker, Microporous Mesoporous Mater. 82 (2005) 257-292.

[24] US Patent 3702886, 14 November 1977, Mobil Oil Corp. (Inv.: R.J. Argauer, G.R. Landolt).

[25] T.C. Bowen, R.D. Noble, J.L. Falconer, J. Membr. Sci. 245 (2004) 1-33.

[26] C. Perego, P. Ingallina, Catal. Today 73 (2002) 3-22.

[27] T.F. Degnan Jr., C.M. Smith, C.R. Venkat, Appl. Catal. A: General 221 (2001) 283-294.

[28] US Patent 6031143, 29 February 2000, Snamprogetti S.p.A. (Inv.: F. Buonomo, G. Donati, E. Micheli, L. Tagliabue).

[29] I.I. Ivanova, N. Blom, E.G. Derouane, J. Mol. Catal. A: Chemical 109 (1996) 157-168.

[30] E. Derouane, H. He, S. Derouane-Abd Hamid, I. Ivanova, Catal. Lett. 58 (1999) 1-19.

[31] P. Mériaudeau, J.F. Dutel, J. Mol. Catal. A: Chemical 108 (1996) L1-L3.

[32] G. Caeiro, R.H. Carvalho, X. Wang, M.A.N.D.A. Lemos, F. Lemos, M. Guisnet, F. Ramôa Ribeiro, J. Mol. Catal. A: Chemical 255 (2006) 131-158.

[33] S.I. Abasov, F.A. Babayeva, R.R. Zarbaliyev, G.G. Abbasova, D.B. Tagiyev, M.I. Rustamov, Appl. Catal. A: General 251 (2003) 267-274.

[34] I.I. Ivanova, D. Brunel, J.B. Nagy, E.G. Derouane, J. Mol. Catal. A: Chemical 95 (1995) 243-258.

[35] M. Adebajo, R. Howe, M. Long, Catal. Lett. 72 (2001) 221-224.

[36] M.O. Adebajo, R.F. Howe, M.A. Long, Energy Fuels 15 (2001) 671-674.

[37] L.S.K. Pang, M.A. Wilson, R.A. Quezada, J.L. Prochazka, M.A. Long, S.J.X. He, M.L. Gorbaty, P.S. Maa, Fuel 76 (1997) 1091-1104.

[38] S. Todorova, B.L. Su, Catal. Today 93-95 (2004) 417-424.

[39] A. Bressel, T. Donauer, S. Sealy, Y. Traa, Microporous Mesoporous Mater. 109 (2008) 278-286.

[40] J.N. Armor, Catal. Today 25 (1995) 199-207.

[41] J.N. Armor, J. Membr. Sci. 147 (1998) 217-233.

[42] G. Saracco, H.W.J.P. Neomagus, G.F. Versteeg, W.P.M. van Swaaij, Chem. Eng. Sci. 54 (1999) 1997-2017.

[43] S. Adhikari, S. Fernando, Ind. Eng. Chem. Res. 45 (2006) 875-881.

[44] J. Zaman, A. Chakma, J. Membr. Sci. 92 (1994) 1-28.

[45] S.N. Paglieri, J.D. Way, Sep. Purif. Methods 31 (2002) 1-169.

[46] J. Tong, Y. Matsumura, Appl. Catal. A: General 286 (2005) 226-231.

[47] J. Tong, Y. Matsumura, Catal. Today 111 (2006) 147-152.

[48] N. Mori, T. Nakamura, K. Noda, O. Sakai, A. Takahashi, N. Ogawa, H. Sakai, Y. Iwamoto, T. Hattori, Ind. Eng. Chem. Res. 46 (2007) 1952-1958.

[49] F. Gallucci, L. Paturzo, A. Basile, Ind. Eng. Chem. Res. 43 (2004) 2420-2432.

[50] N. Itoh, Y. Kaneko, A. Igarashi, Ind. Eng. Chem. Res. 41 (2002) 4702-4706.

[51] A. Basile, F. Gallucci, L. Paturzo, Catal. Today 104 (2005) 244-250.

[52] S. Irusta, J. Munera, C. Carrara, E.A. Lombardo, L.M. Cornaglia, Appl. Catal. A: General 287 (2005) 147-158.

[53] L. Paturzo, F. Gallucci, A. Basile, G. Vitulli, P. Pertici, Catal. Today 82 (2003) 57-65.

[54] B. Faroldi, C. Carrara, E.A. Lombardo, L.M. Cornaglia, Appl. Catal. A: General 319 (2007) 38-46.

[55] M.C. Iliuta, F. Larachi, B.P.A. Grandjean, I. Iliuta, A. Sayari, Ind. Eng. Chem. Res. 41 (2002) 2371-2378.

[56] M.C. Iliuta, B.P.A. Grandjean, F. Larachi, Ind. Eng. Chem. Res. 42 (2003) 323-330.

[57] F. Larachi, H. Oudghiri-Hassani, M.C. Iliuta, B.P.A. Grandjean, P.H. McBreen, Catal. Lett. 84 (2002) 183-192.

[58] S. Tosti, A. Basile, G. Chiappetta, C. Rizzello, V. Violante, Chem. Eng. J. 93 (2003) 23-30.

[59] S. Uemiya, N. Sato, H. Ando, E. Kikuchi, Ind. Eng. Chem. Res. 30 (1991) 585-589.

[60] G. Barbieri, A. Brunetti, T. Granato, P. Bernardo, E. Drioli, Ind. Eng. Chem. Res. 44 (2005) 7676-7683.

[61] A. Basile, E. Drioli, F. Santell, V. Violante, G. Capannelli, G. Vitulli, Gas Sep. Purif. 10 (1996) 53-61.

[62] S. Niwa, M. Eswaramoorthy, J. Nair, A. Raj, N. Itoh, H. Shoji, T. Namba, F. Mizukami, Science 295 (2002) 105-107.

[63] K. Sato, T. Hanaoka, S. Hamakawa, M. Nishioka, K. Kobayashi, T. Inoue, T. Namba, F. Mizukami, Catal. Today 118 (2006) 57-62.

[64] K. Sato, T. Hanaoka, S. Niwa, C. Stefan, T. Namba, F. Mizukami, Catal. Today 104 (2005) 260-266.

[65] E. Gobina, K. Hou, R. Hughes, Chem. Eng. Sci. 50 (1995) 2311-2319.

[66] N. Itoh, T. Wu, J. Membr. Sci. 124 (1997) 213-222.

[67] R.E. Buxbaum, T.L. Marker, J. Membr. Sci. 85 (1993) 29-38.

[68] S. Uemiya, T. Matsuda, E. Kikuchi, J. Membr. Sci. 56 (1991) 315-325.

[69] US Patent 3350845, 7 November 1967, Union Int. (Inv.: D.L. McKinley).

[70] US Patent 3439474, 22 April 1969, Union Int. (Inv.: D.L. McKinley).

[71] A. Kulprathipanja, G.O. Alptekin, J.L. Falconer, J.D. Way, J. Membr. Sci. 254 (2005) 49-62.

[72] E. Gobina, R. Hughes, J. Membr. Sci. 90 (1994) 11-19.

[73] L. Wang, K. Murata, M. Inaba, Catal. Today 82 (2003) 99-104.

[74] Y. Yildirim, E. Gobina, R. Hughes, J. Membr. Sci. 135 (1997) 107-115.

[75] H. Weyten, J. Luyten, K. Keizer, L. Willems, R. Leysen, Catal. Today 56 (2000) 3-11.

[76] P. Quicker, V. Hollein, R. Dittmeyer, Catal. Today 56 (2000) 21-34.

[77] K. Hou, R. Hughes, J. Chem. Technol. Biotechnol. 78 (2003) 35-41.

[78] E. Gobina, R. Hughes, Appl. Catal. A: General 137 (1996) 119-127.

[79] L. van Dyk, S. Miachon, L. Lorenzen, M. Torres, K. Fiaty, J.A. Dalmon, Catal. Today 82 (2003) 167-177.

[80] W. Liang, R. Hughes, Catal. Today 104 (2005) 238-243.

[81] T. Matsuda, I. Koike, N. Kubo, E. Kikuchi, Appl. Catal. A: General 96 (1993) 3-13.

[82] N. Itoh, W. Xu, K. Haraya, J. Membr. Sci. 66 (1992) 149-155.

[83] N. Itoh, AIChE J. 33 (1987) 1576-1578.

[84] A. Gora, D.A.P. Tanaka, F. Mizukami, T.M. Suzuki, Chem. Lett. 35 (2006) 1372-1373.

[85] H. Amandusson, L.G. Ekedahl, H. Dannetun, Appl. Catal. A: General 217 (2001) 157-164.

[86] W.-H. Lin, H.-F. Chang, Catal. Today 97 (2004) 181-188.

[87] Y. She, J. Han, Y.H. Ma, Catal. Today 67 (2001) 43-53.

[88] D. Lee, P. Hacarlioglu, S.T. Oyama, Top. Catal. 29 (2004) 45-57.

[89] L. Li, R.W. Borry, E. Iglesia, Chem. Eng. Sci. 57 (2002) 4595-4604.

[90] G. Barbieri, G. Marigliano, G. Perri, E. Drioli, Ind. Eng. Chem. Res. 40 (2001) 2017-2026.

[91] M.R. Rahimpour, S. Ghader, Chem. Eng. Proc. 43 (2004) 1181-1188.

[92] E. Gobina, K. Hou, R. Hughes, Catal. Today 25 (1995) 365-370.

[93] M. Harold, B. Nair, G. Kolios, Chem. Eng. Sci. 58 (2003) 2551-2571.

[94] E. Gobina, K. Hou, R. Hughes, J. Membr. Sci. 105 (1995) 163-176.

[95] C. Hermann, P. Quicker, R. Dittmeyer, J. Membr. Sci. 136 (1997) 161-172.

[96] M.E.E. Abashar, A.A. Al-Rabiah, Chem. Eng. Proc. 44 (2005) 1188-1196.

[97] F. Kapteijn, J. Moulijn, in: Handbook of Heterogeneous Catalysis, G. Ertl, H. Knözinger, and J. Weitkamp (Eds.); Vol. 3, WILEY-VCH, Weinheim, 1997, p. 1190-1209.

[98] D.W. Marquardt, J. Soc. Ind. Appl. Math. 11 (1963) 431-441.

[99] G. Marigliano, G. Barbieri, E. Drioli, Chem. Eng. Proc. 42 (2003) 231-236.

[100] N. Itoh, J. Chem. Eng. Jpn. 24 (1991) 664-666.

[101] N. Itoh, Catal. Today 25 (1995) 351-356.

[102] N. Itoh, J. Chem. Eng. Jpn. 23 (1990) 420-426.

[103] S. Ernst, J. Weitkamp, Chem. Ing. Tech. 63 (1991) 748-750.

[104] F. Bauer, W. Chen, H. Ernst, S. Huang, A. Freyer, S. Liu, Microporous Mesoporous Mater. 72 (2004) 81-89.

[105] T.E. Daubert, R.P. Danner, Physical and Thermodynamic Properties of Pure Chemicals: Data Compilation, Taylor and Francis, London, 1989, p.1-736.

[106] http://www.rebresearch.com/newsite/membranes.html, accessed on 07.02.2008.

[107] A. Raichle, Ph.D. Thesis, University of Stuttgart, 2002, p. 57.

[108] W.A. Dietz, J. Gas Chromatogr. 5 (1967) 68-71.

[109] D.Y. Peng, D.B. Robinson, Ind. Eng. Chem. Fundam. 15 (1976) 59.

[110] M.J.D. Powell, Comput. J. 7 (1964) 155-162.

[111] M.A. Uguina, J.L. Sotelo, D.P. Serrano, Ind. Eng. Chem. Res. 32 (1993) 49-55.

[112] L.C. Doelp, W. Brenner, A.H. Weiss, Ind. Eng. Chem. Proc. Des. Dev. 4 (1965) 92-96.

[113] A. Corma, M.J. Díaz-Cabañas, J.L. Jordá, C. Martínez, M. Moliner, Nature 443 (2006) 842-845.

[114] F. Xiao, L. Wang, C. Yin, K. Lin, Y. Di, J. Li, R. Xu, D.S. Su, R. Schlögl, T. Yokoi, T. Tatsumi, Angew. Chem. Int. Ed. 45 (2006) 3090-3093.

[115] W.W. Kaeding, L.B. Young, C.C. Chu, J. Catal. 89 (1984) 267-273.

[116] C. Bigey, B.L. Su, J. Mol. Catal. A: Chemical 209 (2004) 179-187.

[117] D.C. Grenoble, J. Catal. 56 (1979) 32-39.

[118] D.C. Grenoble, J. Catal. 56 (1979) 40-46.

[119] C. Hoang-Van, B.L. Villemin, S.J. Teichner, J. Catal. 105 (1987) 469-477.

[120] J.H. Sinfelt, Catal. Rev. - Sci. Eng. 3 (1970) 175.

[121] H.C. Brown, H. Jungk, J. Am. Chem. Soc. 78 (1956) 2182-2184.

[122] S.A. Sadat Rezai, Y. Traa, Catal. Lett. 122 (2008) 91-97.

[123] J. Weitkamp, A. Raichle, Y. Traa, Appl. Catal. A: General 222 (2001) 277-297.

[124] N.R. Meshram, S.G. Hegde, S.B. Kulkarni, P. Ratnasamy, Appl. Catal. 8 (1983) 359-367.

[125] J. Engelhardt, D. Kalló, I. Zsinka, J. Catal. 135 (1992) 321-324.

[126] F. Lónyi, J. Engelhardt, D. Kalló, Zeolites 11 (1991) 169-177.

[127] J. Engelhardt, M. Szabó, D. Kalló, Zeolites 12 (1992) 916-924.

[128] J. Čejka, B. Wichterlovà, S. Bednarova, Appl. Catal. A: General 79 (1991) 215-226.

[129] J. de Graaf, A.J. van Dillen, K.P. de Jong, D.C. Koningsberger, J. Catal. 203 (2001) 307-321.

[130] S.A. Sadat Rezai, Y. Traa, J. Membr. Sci. 319 (2008) 279-285.

[131] N. Itoh, W.C. Xu, S. Hara, K. Kakehida, Y. Kaneko, A. Igarashi, Ind. Eng. Chem. Res. 42 (2003) 6576-6581.

[132] S.A. Sadat Rezai, Y. Traa, Chem. Commun. (2008) 2382-2384.

[133] J. Shu, B.P.A. Grandjean, S. Kaliaguine, Appl. Catal. A: General 119 (1994) 305-325.

[134] N. Itoh, W.C. Xu, Appl. Catal. A: General 107 (1993) 83-100.

[135] E.W. Thiele, Ind. Eng. Chem. 31 (1939) 916-920.

[136] J.G. Knudsen, H.C. Hottel, A.F. Sarofim, P.C. Wankat, K.S. Knaebel, in: Perry's Chemical Engineers' Handbook, R.H. Perry, and D.W. Green (Eds.); 7th Edn., McGraw Hill, New York, 1997, Section 5, p. 1-79.

# 7 Appendix

## 7.1 Mass flow controller and saturator settings

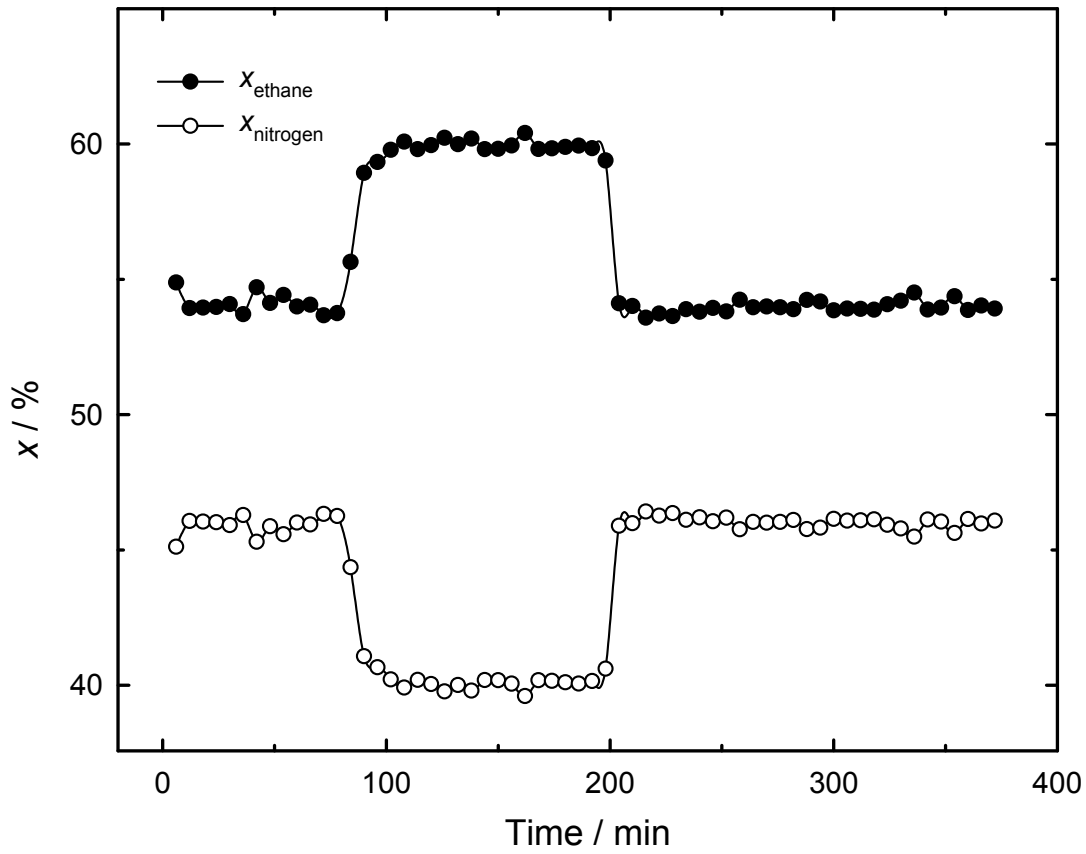


Fig. 7.1: Ethane and nitrogen molar fraction as a function of time. The step changes in composition correspond to mass flow controller set point changes.

Table 7.1: Parameters for vapor pressure calculation [105].

| Species | Toluene | *m*-Xylene | *p*-Ethyltoluene |
|---|---|---|---|
| $B_i$ / - | $8.336 \cdot 10^{1}$ | $1.432 \cdot 10^{2}$ | $1.129 \cdot 10^{2}$ |
| $C_i$ / K | $-6.995 \cdot 10^{3}$ | $-9.247 \cdot 10^{3}$ | $-8.838 \cdot 10^{3}$ |
| $D_i$ / - | $-9.164 \cdot 10^{0}$ | $-1.944 \cdot 10^{1}$ | $-1.415 \cdot 10^{1}$ |
| $E_i$ / - | $6.225 \cdot 10^{-6}$ | $1.908 \cdot 10^{-2}$ | $1.135 \cdot 10^{-2}$ |
| $F_i$ / - | $2.000 \cdot 10^{0}$ | $1.000 \cdot 10^{0}$ | $1.000 \cdot 10^{0}$ |

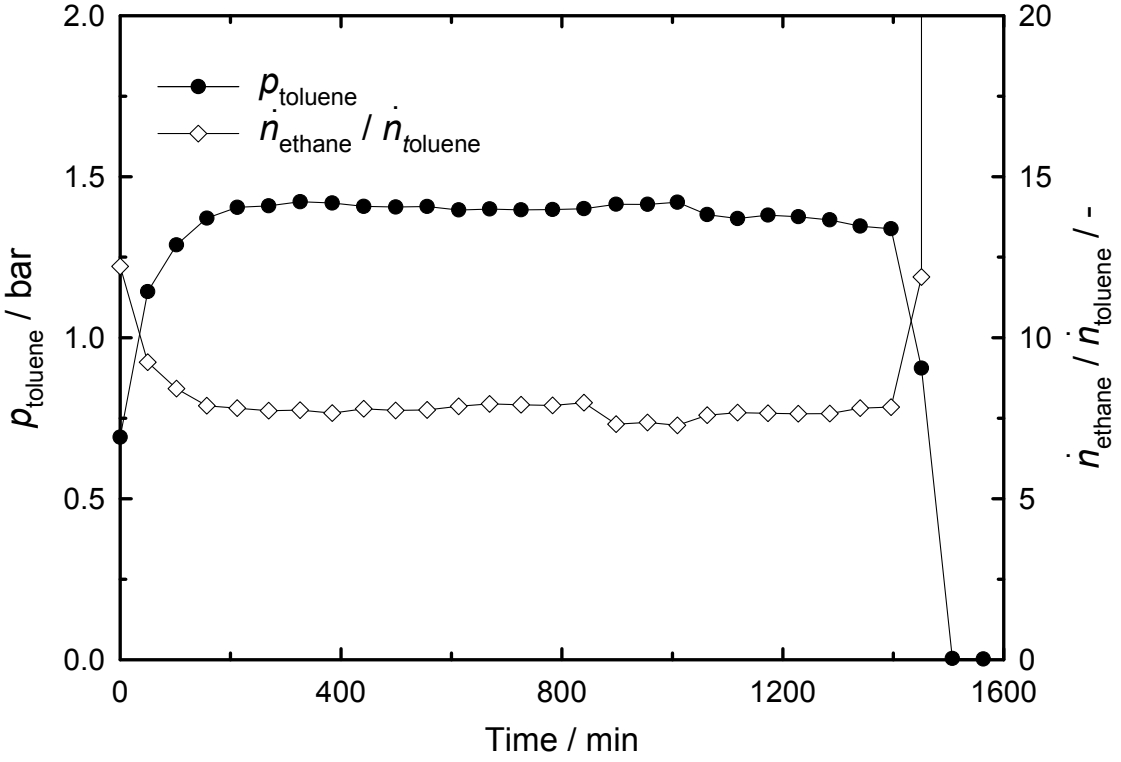


Fig. 7.2: Partial pressure of toluene and $\dot{n}_{ethane} / \dot{n}_{toluene}$ feed ratio as a function of time, the saturator is at 110 °C and loaded with about 12 g of toluene.

Figure 7.1 shows the short-term stability of the mass flow controllers as well as the response time to a set point change in the reactor exit stream. The molar fractions of ethane and nitrogen are constant in the absence of a set point change. Once a set point change is introduced, about 10 minutes elapse before the molar fractions are constant again. Figure 7.2 represents the long-term stability of the saturator and the corresponding $\dot{n}_{ethane} / \dot{n}_{toluene}$ feed ratio. Once the saturator is heated, a period of about 300 minutes is required to reach a constant toluene feed flow rate. The toluene partial pressure is constant thereafter until 1400 minutes, resulting in a constant $\dot{n}_{ethane} / \dot{n}_{toluene}$ feed ratio of about 7. After about 1400 minutes the toluene in the saturator is depleted, and hence, the partial pressure of toluene goes down and the $\dot{n}_{ethane} / \dot{n}_{toluene}$ feed ratio increases.

## 7.2 Membrane reactor scheme

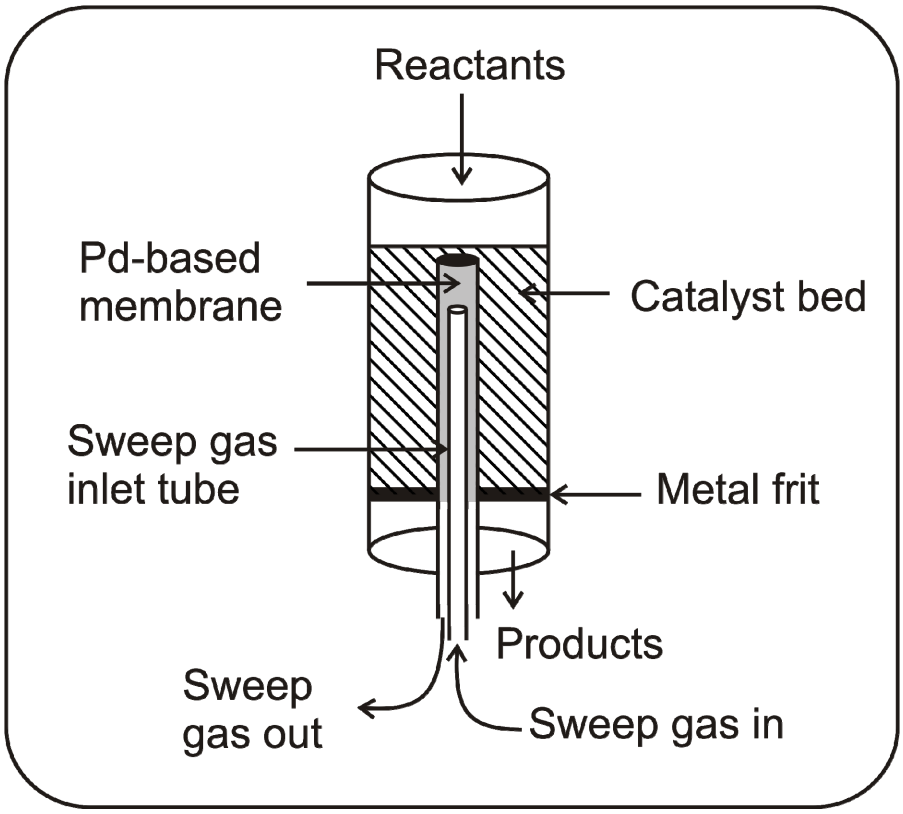


Fig. 7.3: Schematic representation of the membrane reactor set up.

Figure 7.3 represents the set up of the membrane reactor that was applied experimentally. The reactant is fed in a flow-down manner, with a metal frit holding the catalyst in place. Sweep gas was fed into the sweep side at the seal via an inlet tube. The top part of the membrane was sealed. Therefore, the sweep gas is co-current to the feed. The membrane was ca. 5 mm in diameter and 10 cm long, with the sweep gas line running inside the membrane in a 1.5 mm line. Catalyst was placed outside the membrane in a ca. 10 mm line. Typically, ca. 50 ml/min (under standard conditions) were used on the reaction side. The amount of nitrogen sweep gas was varied in order to achieve the desired sweep gas / feed ratio.

## 7.3 Evaluation of mass-transfer limitations

Since ethane is relatively inert, the inherent rate of reaction is low, hence mass transfer limitations may be negligible. In order to ensure that under experimental conditions external mass transfer is not limiting, two mass-transfer correlations, to and from the catalyst particles, were used to estimate the mass-transfer coefficient, $k_{mt}$. The Thiele modulus [135], $\phi$, was used to estimate significance of internal mass transfer. The rate of reaction per unit surface area of the catalyst was estimated from experimental results, assuming first order rate law. The rate of reaction is the ratio of conversion and catalyst mass per unit surface area.

The Sherwood number, $N_{Sh}$, the particle diameter, $d_p$, and diffusivity, $\wp$, were used to calculate the mass-transfer coefficients and then compared to an estimated maximum rate constant of reaction in order to judge the significance of film diffusion.

The mass-transfer coefficient can be calculated from equation (7.1) for both equations.

$$N_{Sh} = \frac{k_{mt} \cdot d_p}{\wp} \tag{7.1}$$

The Sherwood number can be calculated from equation (7.2) using the Chilton-Colburn factor, $j_{D,i}$, the Reynold number, $N_{Re}$, and the Schmidt number, $N_{Sc}$.

$$j_{D,i} = \frac{N_{Sh}}{N_{Re} \cdot (N_{Sc})^{0.33}} \tag{7.2}$$

The Schmidt number can be calculated from equation (7.3), with $\mu$ and $\rho$ representing dynamic viscosity and density, respectively. In the case of the Wilson-Geankoplis correlation, the Schmidt number is given as 2.57.

$$N_{Sc} = \frac{\mu}{\rho \cdot \wp} \tag{7.3}$$

Given that in this case the particle Reynold number is about 0.07, the Yoshida-Ramaswami-Hougen correlation, $j_{D,a}$, (Table 5.27, part A in [136]), equation (7.4) for $0.01 < N_{Re} < 50$ was chosen along with the Wilson-Geankoplis correlation, $j_{D,b}$, (Table 5.27 part F in [136]), for $0.0016 < N_{Re} < 55$, equation (7.5) to calculate the Chilton-Colburn factor, with an assumed bed porosity, $\varepsilon$, of 0.3.

$$j_{D,a} = 0.91 \cdot (N_{Re})^{-0.55} \tag{7.4}$$

Table 7.2: Intermediate figures for evaluation of the mass-transfer coefficients.

| $P$ / bar | $\dot{V}_{super}$ / m·s$^{-1}$ | $\rho$ / kg·m$^3$ | $\mu$ / Pa·s | $\wp$ / m$^2$·s$^{-1}$ | $N_{Re}$ / - | $N_{Sc}$ / - |
|---|---|---|---|---|---|---|
| 1 | $8.7\cdot10^{-2}$ | 0.64 | $1.75\cdot10^{-4}$ | $4.62\cdot10^{-6}$ | 0.095 | 59.4 |
| 2 | $4.3\cdot10^{-2}$ | 1.28 | $1.80\cdot10^{-4}$ | $2.31\cdot10^{-6}$ | 0.092 | 61.1 |
| 4 | $2.2\cdot10^{-2}$ | 2.55 | $1.85\cdot10^{-4}$ | $1.15\cdot10^{-6}$ | 0.090 | 62.7 |
| 6 | $1.4\cdot10^{-2}$ | 3.83 | $1.90\cdot10^{-4}$ | $7.70\cdot10^{-7}$ | 0.087 | 64.4 |
| 8 | $1.1\cdot10^{-2}$ | 5.10 | $1.95\cdot10^{-4}$ | $5.77\cdot10^{-7}$ | 0.085 | 66.1 |
| 10 | $8.7\cdot10^{-3}$ | 6.38 | $2.00\cdot10^{-4}$ | $4.62\cdot10^{-7}$ | 0.083 | 67.8 |
| 20 | $4.3\cdot10^{-3}$ | 12.8 | $2.05\cdot10^{-4}$ | $2.31\cdot10^{-7}$ | 0.081 | 69.5 |
| 30 | $2.9\cdot10^{-3}$ | 19.1 | $2.10\cdot10^{-4}$ | $1.54\cdot10^{-7}$ | 0.079 | 71.2 |
| 40 | $2.2\cdot10^{-3}$ | 25.5 | $2.15\cdot10^{-4}$ | $1.15\cdot10^{-7}$ | 0.077 | 72.9 |
| 50 | $1.7\cdot10^{-3}$ | 31.9 | $2.20\cdot10^{-4}$ | $9.24\cdot10^{-8}$ | 0.075 | 74.6 |
| 60 | $1.4\cdot10^{-3}$ | 38.3 | $2.25\cdot10^{-4}$ | $7.70\cdot10^{-8}$ | 0.074 | 76.3 |
| 70 | $1.2\cdot10^{-3}$ | 44.7 | $2.30\cdot10^{-4}$ | $6.60\cdot10^{-8}$ | 0.072 | 78.0 |
| 80 | $1.1\cdot10^{-3}$ | 51.0 | $2.35\cdot10^{-4}$ | $5.77\cdot10^{-8}$ | 0.071 | 79.7 |
| 90 | $9.6\cdot10^{-3}$ | 57.4 | $2.40\cdot10^{-4}$ | $5.13\cdot10^{-8}$ | 0.069 | 81.4 |
| 100 | $8.7\cdot10^{-3}$ | 63.8 | $2.45\cdot10^{-4}$ | $4.62\cdot10^{-8}$ | 0.068 | 83.1 |

$$j_{D,b} = \frac{1.09}{\varepsilon \cdot (N_{\mathrm{Re}})^{0.66}} \tag{7.5}$$

The Reynolds number was calculated according to equations (7.6) and (7.7) in each case from the particle diameter, superficial velocity, $\dot{V}_{super}$, gas density, gas viscosity and bed porosity.

$$N_{\mathrm{Re},a} = \frac{d_p \cdot \dot{V}_{super} \cdot \rho}{\mu \cdot (6 \cdot \varepsilon)} \tag{7.6}$$

$$N_{\mathrm{Re},b} = \frac{d_p \cdot \dot{V}_{super} \cdot \rho}{\mu} \tag{7.7}$$

Table 7.2 shows intermediate numbers for the evaluation of the mass-transfer coefficient. Figure 7.4 shows the mass-transfer coefficients and the estimated rate of reaction. Since the mass-transfer coefficients from both models are much larger than the estimated rate constant of the reaction, species can be transported across the external film of the catalyst particles. Therefore, external mass transfer is not limiting.

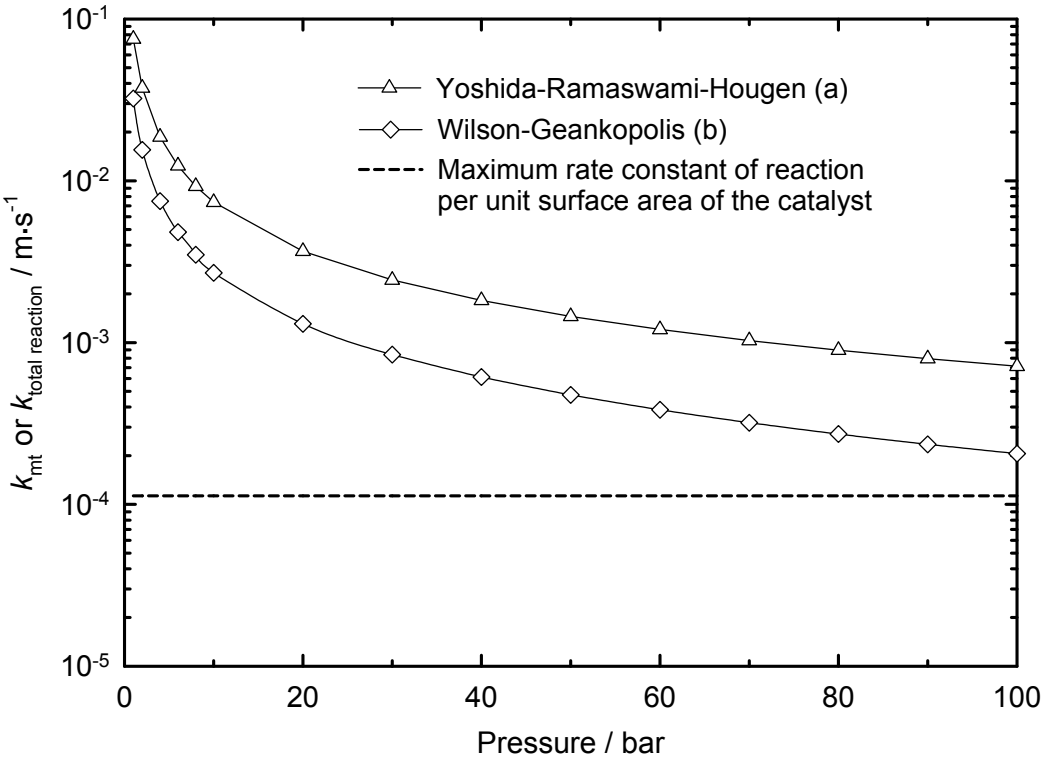


Fig. 7.4: Mass-transfer coefficients ($k_{mt}$) from the Yoshida-Ramaswami-Hougen and the Wilson-Geankopolis correlation and the estimated maximum rate constant of reaction per unit surface area of catalyst ($k_{total\ reaction}$) as a function of pressure.

The maximum Thiele modulus, assuming first order kinetics [135], was estimated to be approximately 0.23, corresponding to an effectiveness factor for spherical particles of 0.99. Therefore internal mass transfer can also be neglected.

## 7.4 FID and TCD response factors

Table 7.3: Retention times, $t_{ret}$, and correction factors, $f_{i,j}$ [108], for FID and TCD detectors.

| Species | $f_{i,j}$ (FID) | $t_{ret}$ (FID)/ min | $f_{i,j}$ (TCD)† | $t_{ret}$ (TCD)/ min |
|---|---|---|---|---|
| Hydrogen | - | - | 0.01 | 1.7 |
| Nitrogen | - | - | 1.00 | 1.8 |
| Methane | 1.03 | 2.0 | - | - |
| Ethene | 0.98 | 4.1 | - | - |
| Ethane | 1.03 | 5.1 | 0.23 | 5.1 |
| Propane | 1.02 | 10.9 | - | - |
| Benzene | 0.89 | 19.7 | - | - |
| Toluene | 0.93 | 22.0 | - | - |
| Ethylbenzene | 0.97 | 25.1 | - | - |
| *p*-/*m*-Xylene | 1.00 | 25.3 | - | - |
| *o*-Xylene | 0.98 | 26.1 | - | - |
| *m*-Ethyltoluene | 0.99 | 29.8 | - | - |
| *p*-Ethyltoluene | 1.00 | 30.2 | - | - |
| *o*-Ethyltoluene | 0.98 | 30.7 | - | - |

†measured using ethane/hydrogen mixtures of various compositions

TCD response factors were measured using 6 gas samples. Gas samples with different, unknown, compositions were prepared. The peak areas of each unknown mixture were compared to pure nitrogen (response factor for nitrogen was set to be 1.00) at the same total flowrate. This results in a set of linear equations, evaluation of which gives response factors.

TCD response factors were measured in mole%, however, converted to wt.-% for easy comparison with FID response factors. The hydrogen response factor is much lower due to its lower molecular weight. The response factor for hydrogen was measured at 0.013±0.002. The response factor for ethane was measured using the same gas samples as for hydrogen. The response factor for ethane was 0.233±0.003.

## 7.5 Peng-Robinson equation of state

The Peng-Robinson equation of state was used for calculation of non-ideal gas behavior [109], by finding the roots of equation (7.8) at various pressures, $P$, at a specific temperature, $T$, and with the ideal gas law constant, $R$, attraction coefficient, $a(T)$, volume coefficient, $b$, calculated accordingly.

$$P = \frac{R \cdot T}{V - b} - \frac{a(T)}{V \cdot (V + b) + b \cdot (V - b)} \tag{7.8}$$

The attraction coefficient, $a\ (T)$ is calculated from equation (7.9), from the reduced temperature, $T_C$, reduced pressure, $P_C$, and the scaling factor, $\alpha(T)$.

$$a(T) = \frac{0.45724 \cdot R^2 \cdot T_C^2 \cdot \alpha(T)}{P_C} \tag{7.9}$$

The volumetric coefficient, $b$, is evaluated by equation (7.10).

$$b = \frac{0.07780 \cdot R \cdot T_C}{P_C} \tag{7.10}$$

The scaling factor in equation (7.9) is evaluated from equation (7.11) based on the reduced temperature, $T_R$, and the characteristic constant, $\kappa$.

$$\alpha^{1/2} = 1 + \kappa \cdot \left(1 - T_R^{1/2}\right) \tag{7.11}$$

The characteristic constant, $\kappa$, can be calculated from equation (7.12), with the acentric factor, $\omega$, defined in Table 7.3.

$$\kappa = 0.37464 + 1.54226 \cdot \omega - 0.26992 \cdot \omega^2 \tag{7.12}$$

The reduced temperature and pressure, $P_R$, are calculated according to equations (7.13) and (7.14) with critical parameters from Table 7.3.

$$T_R = \frac{T}{T_C} \tag{7.13}$$

$$P_R = \frac{P}{P_C} \tag{7.14}$$

Table 7.4: Parameters for evaluation of the Peng-Robinson equation of state [105].

| Species | $T_C$ / K | $P_C$ / bar | $\omega$ / – |
|---|---|---|---|
| Toluene | 591.7 | 41.1 | 0.264 |
| Ethane | 305.4 | 48.8 | 0.099 |
| *m*-Ethyltoluene | 637.0 | 28.4 | 0.360 |
| *p*-Ethyltoluene | 640.0 | 29.4 | 0.322 |
| *o*-Ethyltoluene | 651.0 | 30.4 | 0.294 |
| Hydrogen | 33.2 | 13.0 | -0.220 |
| Benzene | 562.1 | 48.9 | 0.212 |
| *m*-Xylene | 617.1 | 35.4 | 0.320 |
| *p*-Xylene | 616.2 | 35.1 | 0.320 |
| *o*-Xylene | 630.3 | 37.3 | 0.310 |
| Ethylbenzene | 617.2 | 36.0 | 0.302 |

Fugacity coefficients, $f$, can then be calculated from equation (7.15)

$$\ln\left(\frac{f}{P}\right) = (Z-1) - \ln(Z-B) - \frac{A}{2\cdot\sqrt{2}\cdot B}\cdot\ln\left[\frac{Z+(1+\sqrt{2})\cdot B}{Z+(1-\sqrt{2})\cdot B}\right] \tag{7.15}$$

with the compressibility factor, $Z$, dimensionless attraction coefficient, $A$, and the dimensionless volumetric coefficient, $B$, given by equations (7.16 to 7.18),

$$Z = \frac{n\cdot P\cdot V}{R\cdot T} \tag{7.16}$$

$$A = \frac{a\cdot P}{(R\cdot T)^2} \tag{7.17}$$

$$B = \frac{b\cdot P}{R\cdot T} \tag{7.18}$$

## 7.6 Kinetic rate law derivation

Assuming that equation (3.20) is rate-limiting and all other assumptions mentioned in Chapter 3 hold, the rate of reaction can be described by equation (7.19),

$$-r_{\mathrm{To},1} = k_{f,2}\theta_{\mathrm{C_2H_5^*}} - k_{r,2}p_{\mathrm{C_2H_4}}\theta_{\mathrm{H^*}} \tag{7.19}$$

The rate of toluene consumption in reaction 1 (cf. Figure 3.9), $-r_{\mathrm{To},1}$, is given as a function of $k_{f,2}$ and $k_{r,2}$, the rate constants for the forward and reverse reactions, respectively, of equation 3.20, $p_{\mathrm{i}}$, the partial pressure of species i, with $\theta_{\mathrm{i}}$ representing the surface coverage of species i. The first part of equation (7.19) can be evaluated by rearranging and substituting equation (3.19) into equation (3.21). This yields equation (7.20), the surface coverage of the adsorbed ethane intermediate as a function of the measurable partial pressures, $p_{\mathrm{i}}$, of ethane and hydrogen, $K_{\mathrm{j}}$, the equilibrium constant of reaction j, and the free metal sites, $\theta_*$.

$$\theta_{\mathrm{C_2H_5^*}} = \frac{K_1 K_3^{0.5} p_{\mathrm{C_2H_6}} \theta_*}{p_{\mathrm{H_2}}^{0.5}} \tag{7.20}$$

According to the mechanism, ethene is an intermediate and it must also be written in terms of measurable species. Rearrangement of equations (3.22 to 3.24) then gives an expression for the partial pressure of ethene as a function of partial pressure of ethyltoluene and toluene, equation (7.21) with the equation (7.22) giving last part of equation (7.19).

$$p_{\mathrm{C_2H_4}} = \frac{p_{\mathrm{E}}}{K_4 K_5 K_6 p_{\mathrm{To}}} \tag{7.21}$$

$$\theta_{\mathrm{H^*}} = \frac{p_{\mathrm{H_2}}^{0.5}\theta_*}{K_3^{0.5}} \tag{7.22}$$

Substitution of equations (7.21) and (7.22) into equation (7.19) gives the rate law, equation (7.23).

$$-r_{\mathrm{To},1} = k_{f,2} \cdot \frac{K_1 K_3^{0.5} p_{\mathrm{C_2H_6}} \theta_*}{p_{\mathrm{H_2}}^{0.5}} - k_{r,2} \cdot \frac{p_{\mathrm{E\text{-}To}} p_{\mathrm{H_2}}^{0.5} \theta_*}{K_3^{0.5} K_4 K_5 K_6 p_{\mathrm{To}}} \tag{7.23}$$

Carrying out a total metal site balance, equation (7.24), and assuming that the concentration of adsorbed hydrogen is much less than that of the ethene intermediate, since hydrogen can be desorbed more easily, equation (7.24) yields an expression for the free metal site concentration, equation (7.26).

$$\theta_* + \theta_{\mathrm{H^*}} + \theta_{\mathrm{C_2H_5^*}} = 1 \tag{7.24}$$

$$\theta_{\mathrm{H}^*} \approx 0 \tag{7.25}$$

$$\theta_* = \left(1 + \frac{K_1 K_3^{0.5} p_{\mathrm{C_2H_6}}}{p_{\mathrm{H_2}}^{0.5}}\right)^{-1} \tag{7.26}$$

Substitution of equation (7.26) into equation (7.23) yields equation (7.27), rearrangement and simplification of which gives equations (3.25 to 3.28).

$$-r_{\mathrm{To},1} = \frac{k_{f,2} K_1 K_3^{0.5} p_{\mathrm{C_2H_6}} \left(1 + \frac{K_1 K_3^{0.5} p_{\mathrm{C_2H_6}}}{p_{\mathrm{H_2}}^{0.5}}\right)^{-1}}{p_{\mathrm{H_2}}^{0.5}} - \frac{k_{r,2} p_{\mathrm{E\text{-}To}} p_{\mathrm{H_2}}^{0.5} \left(1 + \frac{K_1 K_3^{0.5} p_{\mathrm{C_2H_6}}}{p_{\mathrm{H_2}}^{0.5}}\right)^{-1}}{K_3^{0.5} K_4 K_5 K_6 p_{\mathrm{To}}} \tag{7.27}$$

$$-r_{\mathrm{To},1} = \frac{k_a p_{\mathrm{C_2H_6}}}{p_{\mathrm{H_2}}^{0.5} + k_b p_{\mathrm{C_2H_6}}} \left(1 - \frac{p_{\mathrm{E\text{-}To}} p_{\mathrm{H_2}}}{K_{\mathrm{DHA}} p_{\mathrm{To}} p_{\mathrm{C_2H_6}}}\right) \tag{3.25}$$

$$k_a = k_{f,2} K_1 K_3^{0.5} \tag{3.26}$$

$$k_b = K_1 K_3^{0.5} \tag{3.27}$$

$$K_{\mathrm{DHA}} = K_1 K_2 K_3 K_4 K_5 K_6 \tag{3.28}$$